

**THE EFFECTS OF CHANGING DEPOSITION CONDITIONS ON
THE SIMILARITY OF SPUTTER-DEPOSITED FLUOROCARBON
THIN FILMS TO BULK PTFE**

by

Philip Zandona

A thesis submitted to the Faculty of the University of Delaware in partial
fulfillment of the requirements for the degree of Master of Science in
Mechanical Engineering

Summer 2014

© 2014 Philip Zandona
All Rights Reserved

UMI Number: 1567835

All rights reserved

INFORMATION TO ALL USERS

The quality of this reproduction is dependent upon the quality of the copy submitted.

In the unlikely event that the author did not send a complete manuscript and there are missing pages, these will be noted. Also, if material had to be removed, a note will indicate the deletion.



UMI 1567835

Published by ProQuest LLC (2014). Copyright in the Dissertation held by the Author.

Microform Edition © ProQuest LLC.

All rights reserved. This work is protected against unauthorized copying under Title 17, United States Code



ProQuest LLC.
789 East Eisenhower Parkway
P.O. Box 1346
Ann Arbor, MI 48106 - 1346

**THE EFFECTS OF CHANGING DEPOSITION CONDITIONS ON
THE SIMILARITY OF SPUTTER-DEPOSITED FLUOROCARBON
THIN FILMS TO BULK PTFE**

by

Philip Zandona

Approved: _____
David L. Burris, Ph. D.
Professor in charge of thesis on behalf of the Advisory Committee

Approved: _____
Joshua L. Hertz, Ph. D.
Professor in charge of thesis on behalf of the Advisory Committee

Approved: _____
Dr. Suresh G. Advani, Ph. D.
Chair of the Department of Mechanical Engineering

Approved: _____
Babatunde A. Ogunnaike, Ph.D.
Dean of the College of Engineering

Approved: _____
James G. Richards, Ph.D.
Vice Provost for Graduate and Professional Education

ACKNOWLEDGMENTS

First and foremost I would like to extend my heartfelt gratitude to my advisors, Dr. David Burris and Dr. Joshua Hertz, for their guidance, support, and infinite patience through preparing this document for submission. Without their ongoing support, starting from my time as an undergraduate up through the completion of this work, graduate school would not have been possible for me.

I would like to thank Dr. John Rabolt for his guidance and for granting access to the FTIR equipment in his lab. I am extremely appreciative of my fellow lab mates, especially Weida Shen, Jun Jiang, Andrew Baker, and Eric Fischer for their assistance in keeping the sputtering machine running through all the issues and malfunctions, and Harman Khare for his clear and patient explanations of how to operate the AFM.

I would also like to thank Joe Cabush, Shari Oley, and Tom Cender: their time, concern, and mentorship through difficult times have been invaluable to me. Finally I would like to thank my parents, Oliver and Paulette Zandona, for their support in helping me through the last year, and most of the years before that.

TABLE OF CONTENTS

LIST OF TABLES	vii
LIST OF FIGURES	viii
ABSTRACT	xv
Chapter	
1. INTRODUCTION	1
1.1 Background and Introduction	1
1.2 Sputter Deposition	6
1.2.1 Sputtering Dynamics	8
1.2.2 Radio Frequency Magnetron Sputtering	12
1.3 Characterization of Sputter-Prepared Fluorocarbon Films	14
1.3.1 Chemical Characterization	15
1.3.2 Mechanical Characterization	20
1.4 Effects of Changing Deposition Parameters on Sputter-Prepared Fluorocarbon Films	22
1.5 Motivation for Research	28
2. METHODS	30
2.1 Sample Preparation	30
2.1.1 Sputtering System Overview	30
2.1.2 Deposition Process	34
2.1.3 Deposition Parameters	35
2.2 Sputtering Target Preparation and Characterization	36
2.3 Sample Characterization	37
2.3.1 Interferometry and Film Thickness	37
2.4 Chemical Characterization	41

2.4.1	Fourier Transform Infrared Spectroscopy	41
2.4.2	X-Ray Photoelectron Spectroscopy	43
2.5	Mechanical Characterization	46
2.5.1	Nanoindentation.....	46
2.5.2	Contact Angle Measurements.....	51
3.	RESULTS.....	52
3.1	Sputtering Targets	52
3.2	Sputtering Deposition Rates.....	53
3.3	Chemical Characterization	57
3.3.1	Fourier Transform Infrared Spectroscopy	57
3.3.2	X-Ray Photoelectron Spectroscopy	68
3.4	Mechanical Characterization	76
3.4.1	Nanoindentation.....	76
3.4.2	Contact Angle Measurements.....	78
4.	DISCUSSION.....	83
4.1	The Effects of Changing Film Preparation Parameters.....	83
4.1.1	The Effects of Sputtering Power.....	83
4.1.2	The Effects of Deposition Temperature.....	88
4.1.3	The Effects of Post-Deposition Annealing.....	91
4.1.4	The Effects of Film Thickness.....	92
5.	CONCLUSION	93
5.1	Summary and Conclusions.....	93
5.2	Recommendations	94
	REFERENCES.....	96
Appendix		
A	SUPPLEMENTAL CHEMICAL CHARACTERIZATION DATA.....	102
A.1	FTIR Bond Group Assignment References.....	102
A.2	XPS Bond Group Assignment References.....	104

B	PTFE TARGET SOURCES	107
B.1	Compressed Powder vs. Extruded Stock Targets.....	107
C	PERMISSION LETTERS	113
C.1	Permission Letters	113

LIST OF TABLES

Table 1.1.	Sampling depth of XPS analysis by core level, take-off angle [35].	18
Table 3.1.	Post-deposition target pictures and initial / final masses for the targets used in the bulk of this study. Each target was used for a 2 hour, 50 W deposition and a 1 hour, 100 W deposition.	52
Table 3.2.	Peak appearances and associations found in the IR spectra outside of the CF ₂ stretching region produced from sputtered fluorocarbon films. “(Noisy)” indicates a region where the signal / noise ratio was too low to clearly indicate the presence or absence of a peak in that region.	60
Table 3.3.	Bond types assigned to Gaussian curves fit to XPS spectra.....	68
Table A.1.	Bond group / binding energy assignments compiled from the literature. Sorted by wavenumber.....	102
Table A.2.	Bond group / binding energy assignments compiled from the literature. Sorted by binding energy.....	104
Table B.1.	Post-deposition target pictures and initial / final masses for both compressed, 7C PTFE powder targets and extruded PTFE targets used in the bulk of this study. Each target was used for a 2 hour, 50 W deposition and a 1 hour, 100 W deposition	108
Table C.1.	Permission letters obtained by the author for usage of select figures.	113

LIST OF FIGURES

Figure 1.1.	a) The structure of bulk PTFE: long, continuous chains of fluorinated carbon twisted into a helix.	3
Figure 1.2.	The structure of sputtered fluorocarbon film structure proposed by Biederman [25]; structure is substantially different from that of the parent bulk material (Figure 1.1). Figure reprinted with permission.....	5
Figure 1.3.	A simplified schematic of the DC sputtering process. Figure shows a single instance of argon atom ionization and subsequent collision with the surface of the sputtering target. Labeled events are: 1) Argon is introduced into the chamber at a controlled rate, maintaining the specified chamber pressure. 2) A voltage difference is established between the target gun (-) and the rest of the chamber (+), causing any free electrons (-) in the chamber to move away from the target gun. 3) Electrons (-) moving away from the target ionize any argon atoms that are in their path. 4) Argon ions (+) travel towards and collide with the surface of the target, ejecting the target material. 5) Sputtered off target material sticks to and coats all areas of the chamber that lie within line-of-site of the target.	8
Figure 1.4.	A schematic of how sputtering chamber geometry (specifically, the target – substrate separation distance) affects both the film deposition rate and the range of arrival angles of the sputtered target material.	10
Figure 1.5.	The deposition rate vs. pressure relationship reported for the sputtering of PTFE [26]. Figure reprinted with permission.	12
Figure 1.6.	Example sputtering target polarity vs. time for an RF sputtering system.	14
Figure 1.7.	An example FTIR spectrum generated from untreated bulk PTFE [21]. The two peaks located between approximately 1300 cm^{-1} and 1100 cm^{-1} are typically the dominating spectral feature of	

	bulk PTFE, representing both asymmetric and parallel asymmetric CF ₂ bonds. Figure reprinted with permission.	15
Figure 1.8.	An example FTIR spectrum generated from a sample of sputtered PTFE [12]. The single, broad, prominent peak at 1186 cm ⁻¹ is associated with CF ₂ bond groups and is characteristic of sputtered PTFE films. Figure adapted from source with permission.....	16
Figure 1.9.	An example XPS spectrum generated from a bulk PTFE sample [21]. C1s region shown. The peak found at 292.5 eV is assigned to –[CF ₂ –CF ₂] _n bonds which form the long fluorocarbon chains found in bulk PTFE. The peak found at 293.5 eV is assigned to the CF ₃ bonds that form the terminating ends of the chains. Figure reprinted with permission.....	19
Figure 1.10.	An example XPS spectrum generated from a sputtered fluorocarbon film sample [38]. C1s region shown. Figure reprinted with permission.	20
Figure 1.11.	A general schematic overview of atomic force microscopy, shown with and without stage movement. Figure is not drawn to scale.	21
Figure 1.12.	Carbon-fluorine bond types (as a percentage of total bonds in C1s region) present in sputter deposited fluorocarbon films, prepared over increasing deposition pressures [26]. Figure reprinted with permission.	24
Figure 1.13.	Hardness and elastic modulus values for fluorocarbon films prepared with increasing sputtering power [11]. Bulk values were found to be 0.05 GPa for hardness and 1 GPa for modulus. Figure reprinted with permission.....	25
Figure 1.14.	Hardness and elastic modulus values for fluorocarbon films prepared with increasing sputtering power [15]. Figure reprinted with permission.	25
Figure 1.15.	FTIR spectra of a) the bulk PTFE material and b) the sputtered fluorocarbon films under increasing sputtering powers [12]. Figure reprinted with permission.....	26

Figure 1.16.	Critical load of sputter deposited fluorocarbon films prepared under increasing deposition temperatures [41]. Figure reprinted with permission.	27
Figure 2.1.	A cross sectional view of the sputtering chamber used for this study. System components are: a) substrate holder (blue) and rotating stage, b) target (red) + target gun assembly, c) vacuum chamber, d) loadlock, e) chamber / loadlock isolation valve, and f) chamber / loadlock transfer arm. Approximate target / stage geometry is shown in the inset; with the distance between the two components being approximately equal to 15 cm. Figure is not to scale.	31
Figure 2.2.	a) Stainless steel substrate holder for use in sputtering machine, with inset showing b) the effective sputtering area (8 mm x 8 mm) on each silicon wafer. Figure is drawn to scale.	32
Figure 2.3.	A cross-sectional view of the step-height sample preparation process. Vertical scale of the diagram is greatly exaggerated for clarity.	38
Figure 2.4.	Sample topographical plot (top) and resultant histogram with calculated step height (bottom) produced from interferometry of sputtered film.	40
Figure 2.5.	Sample straight-line curve-leveling performed on spectrum obtained via FTIR. Raw and processed spectra shown.	42
Figure 2.6.	A sample XPS spectra showing the $-\text{[CF}_2\text{-CF}_2\text{]}_n-$ bond peak area (in red) / CF_3 bond peak area (grey) ratio.	44
Figure 2.7.	A sample XPS spectra showing the $-\text{[CF}_2\text{-CF}_2\text{]}_n-$ bond peak area (in red) as a percentage of the entire C1s region (grey).	45
Figure 2.8.	A sample XPS spectra showing the C1s (in red, right) / F1s (grey, left) areas. Fluorocarbon film atomic ratios calculated from this data.	45
Figure 2.9.	Unprocessed nanoindentation curves (loading, unloading). Data produced from nanoindentation of sputtered, 223 nm thick fluorocarbon film on silicon substrate (50 W sputtering power and deposition temperature of 36 °C used in film preparation).	46

Figure 2.10.	Processed nanoindentation curves (loading, unloading). Data produced from nanoindentation of sputtered, 223 nm thick fluorocarbon film on silicon substrate (50 W sputtering power and deposition temperature of 36 °C used in film preparation).	48
Figure 2.11.	Regions used in calculating the hardness and elastic modulus of the films. Data produced from nanoindentation of sputtered, 223 nm thick fluorocarbon film on silicon substrate (50 W sputtering power and deposition temperature of 36 °C used in film preparation).....	50
Figure 3.1.	Target used for deposition of films using a sputtering power of 150 W. Dark areas on the target surface at a) are extremely thin and close to failure due to erosion through to the copper backing mesh.....	53
Figure 3.2.	Deposition rate data measured from three films prepared under nominally identical sputtering and deposition conditions: sputtering power of 50 W and deposition temperature of 36 °C used. Error bars indicate the standard deviation calculated from averaging the film thickness over three samples within the same deposition, three measurements on three samples each.	54
Figure 3.3.	Deposition rate vs. RF sputtering power for sputtered fluorocarbon films. Deposition temperature for these films was 36 °C. Linear regression fit shown.	55
Figure 3.4.	Deposition rate vs. RF sputtering power for sputtered fluorocarbon films. Films sputtered at similar temperature were prepared from the same sputtered targets. Connecting lines are not from curve fitting and are meant only as a visual guide.	56
Figure 3.5.	Percent change in thickness for three films prepared under nominally identical deposition conditions (50 W sputtering power at 36 °C) after post-deposition annealing.	57
Figure 3.6.	An FTIR spectrum generated from a sample of bulk 7C PTFE.	58
Figure 3.7.	A representative FTIR spectrum from a sputtered (100 W at 36 °C) PTFE film. Spectrum from corresponding bulk parent target material (see Figure 3.6, above) underlaid for comparison.....	59
Figure 3.8.	FTIR spectra in the CF ₂ stretching region for films sputtered at increasing RF sputtering powers. Spectra of 50 W, 100 W, and	

	150 W power levels are shown; all produced at a deposition temperature of 36 °C. Spectrum produced from bulk PTFE given as a reference (bottom). The location of the fit peak maxima [1/cm] are indicated above each peak.....	62
Figure 3.9.	FTIR spectra in the CF ₂ stretching region for films sputtered at increasing deposition temperatures. Spectra for film prepared at temperatures of 36 °C, 68 °C, and 100 °C are shown; all produced using a sputtering power of 50 W. Spectrum produced from bulk PTFE given as a reference (bottom). The location of the fit peak maxima [cm ⁻¹] are indicated above each peak.....	64
Figure 3.10.	FTIR spectra in the CF ₂ stretching region for pre-anneal and post-anneal films; both produced using deposition temperature of 36 °C. Spectrum produced from bulk PTFE given as a reference (bottom). The location of the fit peak maxima [cm ⁻¹] are indicated above each peak.....	65
Figure 3.11.	FTIR spectra of thick and thin fluorocarbon films prepared using the same deposition conditions (deposition temperature measured at approximately 36 °C). Spectrum produced from bulk PTFE given as a reference (bottom). The location of the fit peak maxima [cm ⁻¹] are indicated above each peak. Emergence of secondary peak at ‘a.’ is noted (middle).....	67
Figure 3.12.	XPS spectra and curve fitting for sputtered PTFE films prepared using 50 W sputtering power (top) and 100 W sputtering power (bottom). Both films prepared using deposition temperature of 36 °C.....	69
Figure 3.13.	XPS spectra and curve fitting for sputtered PTFE films prepared using deposition temperatures of 36 °C (top) 68 °C (bottom). Both films prepared using sputtering powers of 100 W.....	70
Figure 3.14.	-[CF ₂ -CF ₂] _n peak area / CF ₃ peak area ratio of the C1s spectrum for sputtered fluorocarbon films prepared at two different sputtering powers (50 W, 100 W, both at 36 °C), and using like sputtering powers (100 W) with two different deposition temperatures (36 °C and 68 °C).....	72
Figure 3.15.	-[CF ₂ -CF ₂] _n peak area percentage of total peak area of the C1s spectrum for sputtered fluorocarbon films prepared using two different sputtering powers (50 W and 100 W, both at 36 °C),	

	and using like sputtering powers (100 W) with two different deposition temperatures (36 °C and 68 °C).....	74
Figure 3.16.	F1s / C1s ratio for sputtered fluorocarbon films prepared using two different sputtering powers (50 W and 100 W, both at 36 °C), and using like sputtering powers (100 W) with two different deposition temperatures (36 °C and 68 °C).....	76
Figure 3.17.	Hardness and elastic modulus values produced from nanoindentation on the fluorocarbon thin films prepared using differing sputtering powers. Film thicknesses were 223 nm for the film prepared using a sputtering power of 50 W and and 452 nm for the film prepared using 100 W. Error bars represent standard deviation produced from an average of five indentations across the surface of each of the films.....	78
Figure 3.18.	Contact angle of DI water droplets on sputtered fluorocarbon films prepared under increasing RF sputtering powers at a deposition temperature of 36 °C. Contact angle range for unsputtered silicon wafer substrate and bulk PTFE material included for reference.....	79
Figure 3.19.	Contact angle of DI water droplets on sputtered fluorocarbon films prepared under increasing deposition temperatures for RF sputtering powers of 50 W and 100 W. Contact angle range for bulk PTFE material included for reference. Y-axis is truncated for clarity.	80
Figure 3.20.	Contact angle of DI water droplets on sputtered fluorocarbon films prepared under increasing RF sputtering powers for both unannealed and annealed films. Deposition temperature remained 36 °C. Y-axis is truncated for clarity.....	81
Figure 3.21.	Contact angle of DI water droplets on sputtered fluorocarbon films prepared under increasing deposition temperatures for both unannealed and annealed films. Data shown is from depositions using sputtering powers of 100 W. Y-axis is truncated for clarity.....	82
Figure 4.1.	Estimated 7C PTFE powder target mass loss as a function of sputtering power. Data point at 150 W is measured directly from target weights before and after sputtering. Data points at 50 W and 100 W are estimated using deposition rates compiled from 50 W, 100 W, and 150 W fluorocarbon film depositions.	

	Connecting lines are not generated from curve fitting and are intended to serve as a visual guide.	88
Figure B.1.	Deposition rate vs. RF sputtering power for sputtered fluorocarbon films prepared from the compressed powder targets (red) and the extruded targets (blue). Deposition temperature for these films was 36°C. Linear regression fits shown for each set of data.	110
Figure B.2.	XPS spectra of two films prepared under nominally identical depositions (100 W sputtering power, deposition temperature of 36 °C) using two different PTFE target sources: compressed powder (top), and extruded powder (bottom).....	111

ABSTRACT

Solid lubrication of space-borne mechanical components is essential to their survival and the continued human exploration of space. Recent discoveries have shown that PTFE when blended with alumina nanofillers exhibits greatly improved physical performance properties, with wear rates being reduced by several orders of magnitude. The bulk processes used to produce the PTFE-alumina blends are limiting. Co-sputter deposition of PTFE and a filler material overcomes several of these limitations by enabling the reduction of particle size to the atomic level and also by allowing for the even coating of the solid lubricant on relatively large areas and components. The goal of this study was to establish a baseline performance of the sputtered PTFE films as compared to the bulk material, and to establish deposition conditions that would result in the most bulk-like film possible. In order to coax change in the structure of the sputtered films, sputtering power and deposition temperature were increased independently. Further, post-deposition annealing was applied to half of the deposited film in an attempt to affect change in the film structure. Complications in the characterization process due to increasing film thickness were also examined. Bulk-like metrics for characterization processes the included Fourier transform infrared spectroscopy (FTIR), X-ray spectroscopy (XPS), nanoindentation via atomic force microscopy, and contact angle of water on surface measurements were established. The results of the study revealed that increasing sputtering power and deposition temperature resulted in an increase in the similarity between the fluorocarbon films and the bulk PTFE, at a cost of affecting the potential

of the film thicknesses, either by affecting the deposition process directly, or by decreasing the longevity of the sputtering targets.

Chapter 1

INTRODUCTION

1.1 Background and Introduction

The lubrication of the moving components in any mechanical system is essential to its survival and functionality throughout its lifespan. Without sufficient lubrication, adhesion, friction, and wear often reduce system lifespan by several orders of magnitude. In many of the more common mechanical systems (automotive engines, for example), liquid lubricants are used. There are, however, many existing applications where the use of liquids for lubrication is undesirable, impractical, or impossible. Applications in space are one example. The ultra-high vacuum encourages strong adhesion between contacting mechanical surfaces, and the vacuum, coupled with intense UV irradiation, atomic oxygen, and large thermal range (-50 °C to 80 °C) of low Earth orbit (LEO), evaporates liquids and degrades even robust solids.

Despite the lubrication challenges of LEO, communication satellites and space exploration systems have heavy tribological demands. Mission launch volume is limited by the inner diameter of the payload fairing envelope attached to the delivery rocket. Larger rockets, such as the Atlas V and Delta IV currently used by NASA, support envelopes with inner diameters ranging up to 4.5 meters [1]. Missions using smaller rockets, such as the Taurus® and the Pegasus® also currently used by NASA, support envelopes with inner diameter ranging from approximately 1 to 2 meters [2, 3]. System function often scales with surface area (for data transmission antennas and solar power collection); as a result, most spacecraft enter space in a folded

configuration, and upon reaching orbit begin a complex unfolding process involving large numbers of bearings, gears, and motors. These systems often cost billions of dollars and the opportunity for mission success depends on the engineer's ability to lubricate components without the aid of liquid lubricants in an extreme environment.

Molybdenum disulfide (MoS_2) is unique in its ability to provide extremely low friction coefficients in vacuum; as a result, it is in a class of materials known as 'solid lubricants'. MoS_2 has served as the standard for solid lubrication in space applications since the first mission into orbit. Unfortunately, its favorable lubrication properties degrade in the humid terrestrial environment [4]. Since these systems must be assembled, tested, and transported on Earth, the tribological coatings are susceptible to damage or failure prior to launch. One or more MoS_2 coating failures are suspected to have contributed to the deployment failure of the Galileo spacecraft's high-gain antenna [5]. The inability of MoS_2 to provide effective lubrication in air has motivated efforts to develop environmentally insensitive solid lubricant materials. Polytetrafluoroethylene (PTFE) has attracted attention for this application due to its ability to provide low friction in both humid and dry environments.

PTFE, more colloquially referred to by its trade name of Teflon®, was created by Roy J. Plunkett in 1938 and patented in 1941 [6]. Since its discovery, the use of PTFE has become widespread, with the rapid adoption of the material attributed to its excellent material properties across a variety of metrics, including: low friction coefficient, high corrosion resistance, high hydrophobicity, high thermal stability, high chemical inertness, low dielectric constant, low surface energy, and biocompatibility [7–15]. Practical applications of PTFE and its derivatives can be found in almost all branches of science and industry: non-stick coatings for home cookware, thermal

insulation material, pipe sealant in plumbing, low friction and non-reactive lab equipment, computer hard drives, microelectromechanical systems, and coatings to ensure the biocompatibility of medical equipment, amongst many more. However, its use in bearings applications has been limited by its unusually high wear rates.

PTFE (structural formula: $-\text{[CF}_2\text{-CF}_2\text{]}_n-$) is characterized by long chains of fluorinated carbon (Figure 1.1) and has a highly oriented crystal structure [16]. The low friction ($\mu < 0.07$) exhibited by PTFE has been attributed to the easy shear of the crystalline structure when the CF_2 chains are reoriented parallel to the direction of sliding, during which a transfer film is formed on both contacting surfaces [16]. The long chains of CF_2 are essential to the formation of the transfer film, and the formation and adhesion of this transfer film on the contacting surface is essential to the low friction properties of the PTFE coating.

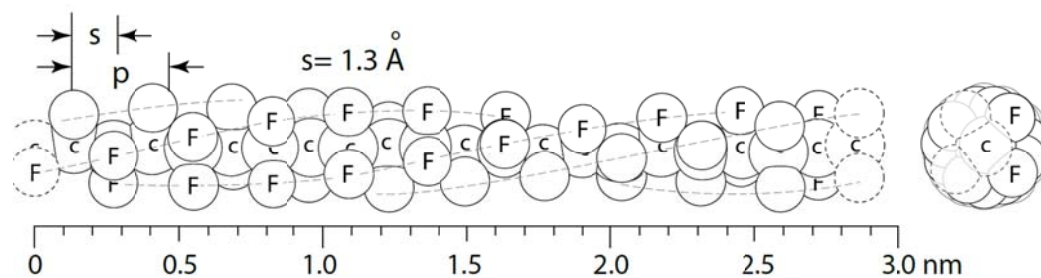


Figure 1.1. a) The structure of bulk PTFE: long, continuous chains of fluorinated carbon twisted into a helix.

The need of an improved version of either MoS_2 or PTFE has led to an interest in composite materials containing either (or both) parent material. The Air Force Research Laboratory has been developing MoS_2 nanocomposites to deal with the sensitivity to humidity, while some studies [17, 18] have been focused on composite blends utilizing both parent materials; materials of this type have found direct

application on systems launched by the Japan Aerospace Exploration Agency (JAXA). Composite blends that combine PTFE and a filler material have been studied as a potential solution for the rapid wear rate of virgin PTFE with varying degrees of success. Lancaster [19] first showed that wear rate present in PTFE could be reduced orders of magnitude with reinforcement using 30% carbon fibers. Fillers of varying composition, shape, and size have since been studied, most of which interfere with crack propagation, the predominant wear mode of PTFE. However, at the 10-50% loading necessary to prevent crack propagation, hard microscale fillers abrade the counterface and increase the coefficient of friction.

Li et al. (1998) [20], Chen et al. [21], and Sawyer et al [22] showed that nanofillers can reduce wear by 100X with filler loading remaining relatively low (on the order of 5-10%). In 2006, Burris and Sawyer found that an alpha-phase alumina nanoparticle reduced wear rates by 5,000X with only 1% filler loading [23]. In 2009, Burris et al. showed that particle fluorination could retain the low wear behavior down to 0.13% filler, and it was suggested that improved dispersibility of the fluorinate particles was responsible for the wear improvements. The reinforcement efficiency of this material remains unprecedented in the field of tribological composites and nanocomposites. The bulk processing methods used by Burris et al. are limiting. For example, in all cases, the standard PTFE 7C resin has a particle size of 20 μm . Consequently, dispersed powder ensembles consist of 20 μm PTFE particles decorated by nanoparticles [22]. These ensembles are compressed and sintered to produce a nanocomposite with microscale domains of unreinforced PTFE; these unreinforced domains are likely the weak mechanical link in the nanocomposite. Additionally, most applications require coatings rather than bulk parts.

The physical vapor deposition (PVD) family of thin film preparation methods allow for composite films of much smaller length scales to be prepared. Sputtering, a form of PVD, is commonly used to deposit thin films or coatings of ceramic, metallic, and polymeric source materials. In comparison to other forms of PVD, such as pulsed laser deposition (PLD), when all other conditions are held constant films prepared via sputtering have been shown to contain a better quality crystalline structure while having comparatively fewer defects [24]. Co-deposition of materials (PTFE and a filler of graphite, alumina, bronze, etc.) is possible using sputtering, and the length scale between the co-deposited materials in these nanocomposite blends is several orders of magnitude less than the 20 μm length scale offered by more traditional methods due to the mechanism of deposition, where the target material is vaporized and re-condensed to form the resultant film. Sputtering provides the potential to prepare nanocomposite films that practically eliminate the microscale domain of unreinforced PTFE found in the compressed and sintered bulk PTFE, removing the weak mechanical link in the structure of the material.

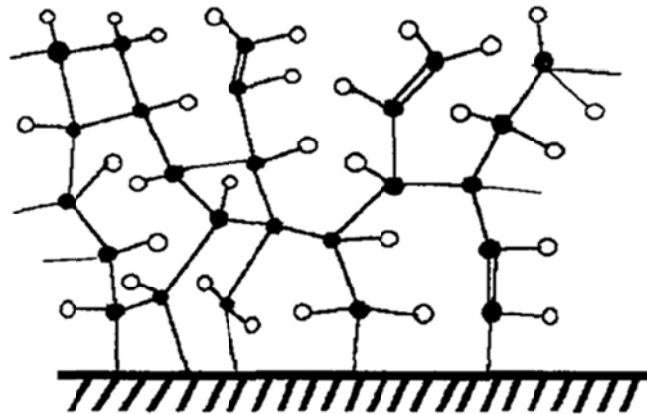


Figure 1.2. The structure of sputtered fluorocarbon film structure proposed by Biederman [25]; structure is substantially different from that of the parent bulk material (Figure 1.1). Figure reprinted with permission.

Unfortunately the mechanics of the sputtering process (overviewed in section 1.2 below) result in a drastic change to the structure of the sputtered fluorocarbon film relative to the parent bulk PTFE. Although reports on the exact structure of the resultant fluorocarbon thin films sputtered from PTFE targets have been conflicting [11], a proposed structure by Biederman et. al. [25] and Li et al. (2011) [15] presents one possibility. Illustrated in Figure 1.2, the film structure bears little resemblance to that of the bulk PTFE (Figure 1.1), with cross-linking carbon bonds and some of the “tangled” qualities of amorphous fluorocarbon structures. Data gathered from films in numerous studies support the presence of bonds not associated with bulk PTFE (non – $[\text{CF}_2\text{-CF}_2]_n$ and CF_3 bonds) [9–13, 15, 26], and of a non-bulk-like PTFE structure [7, 12, 13, 25] being present in the sputtered fluorocarbon films. Sputtering processes that result in a more bulk-PTFE-like chemical structure would be desirable due to a potential retention of the superior mechanical properties that are a product of the fluorocarbon chain- structure of bulk PTFE. If the ultimate goal is to use sputtering as a method of controlled PTFE nanocomposite coating design, a process that produces a bulk-like material should be established; therefore the specific goal of this study is to produce a baseline sputtered PTFE film that is as similar structurally, mechanically, and chemically to the bulk PTFE material as possible.

1.2 Sputter Deposition

When using sputtering as a method of film preparation, the material being sputtered is referred to as the “target”, while the surface being coated with the target material is referred to as the “substrate”. Taking place in a vacuum chamber of a range of sizes, sputtering involves a target material that is situated in line-of-sight with

a substrate some relatively small distance away, typically less than 10 cm. A sputtering gas (typically an inert gas, and most often, as in our case, argon) is pumped into the chamber at a controlled rate to achieve the desired deposition pressure. A voltage difference is established between the target, acting as the cathode, and the substrate, acting as the anode. The sputtering gas atoms are ionized and collide with the target surface, and the resulting momentum transfer causes the target material to eject outward as allowed by the chamber geometry. Any areas of the chamber “in-sight” of the target, including the substrate, are coated by the target material. A simplified schematic of the sputtering mechanism is given in Figure 1.3.

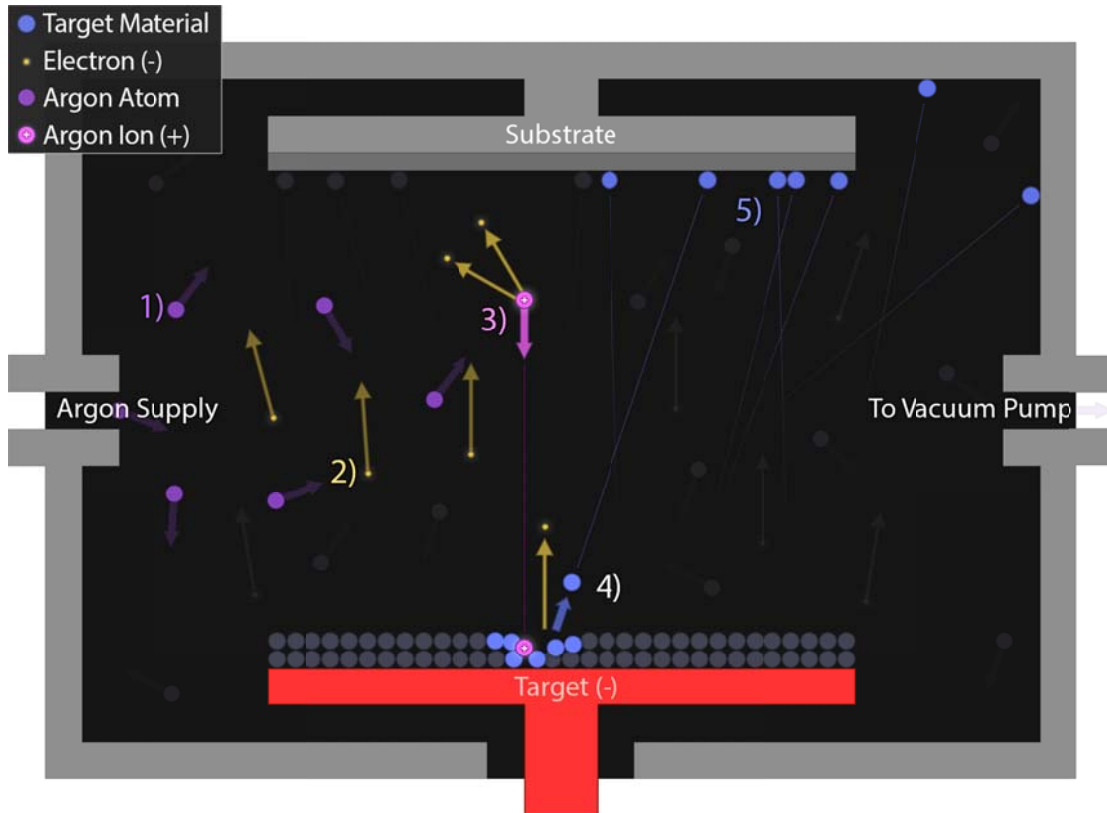


Figure 1.3. A simplified schematic of the DC sputtering process. Figure shows a single instance of argon atom ionization and subsequent collision with the surface of the sputtering target. Labeled events are: 1) Argon is introduced into the chamber at a controlled rate, maintaining the specified chamber pressure. 2) A voltage difference is established between the target gun (-) and the rest of the chamber (+), causing any free electrons (-) in the chamber to move away from the target gun. 3) Electrons (-) moving away from the target ionize any argon atoms that are in their path. 4) Argon ions (+) travel towards and collide with the surface of the target, ejecting the target material. 5) Sputtered off target material sticks to and coats all areas of the chamber that lie within line-of-site of the target.

1.2.1 Sputtering Dynamics

The quality of the sputter deposition is a function of a number of different factors, all of which affect the quality of the resultant sputtered film. The rate at which the target is sputtered is referred to as the “sputter yield” (measured in target atoms ejected per ion collision) In order to break the molecular and atomic bonds

present and eject the target material, a minimum energy level is required for each impacting ion. Once this threshold is reached, sputter yield increases rapidly with increasing ion energy. When sputtering using argon gas, sputter yield is not highly dependent on target material, and typically lies in the range of 0.1 to 10 ejected atoms per impacting argon ion [27]. Additionally, increasing the impacting ion energy causes an increase in the energy flux towards the substrate (an increase in the kinetic energy of the ejected target material). This increase can have an effect on the resultant sputtered film deposition [28].

When the target – substrate separation distance is increased, the number of sputtered target molecules that arrive at the surface of the substrate decreases due to increased scattering of the sputtered material; the trade-off is a decrease in the average incident angle, seen in Figure 1.4. The incident angle is important as it is a major factor affecting the “sticking coefficient” of the sputtering setup. The sticking coefficient is the number of atoms that adhere to the surface of the substrate per striking target molecule. The sticking coefficient is itself a function of the chamber geometry (including the incident angle of the arriving sputtered material), the target and substrate material utilized, and the deposition temperature (the temperature of the surface of the substrate), among other factors. Halving the target – substrate separation distance has been shown by Mahieu et al. [28] to decrease the sticking coefficient by more than 30%. To further complicate matters, decreasing the target – substrate separation distance increases the energy flux towards the substrate [29], which means that substrate temperature increases as the target and substrate are moved closer together. This increase in substrate temperature causes the desorption rate to increase, thereby further decreasing the sticking coefficient [28]. Substrate

temperature has additionally been shown to dramatically alter a range of qualities such as film crystallinity [30], electrical properties [31], and mechanical properties [32] across a variety of target types (the effects of substrate temperature with respect to fluorocarbon film structure will be examined further in section 1.4).

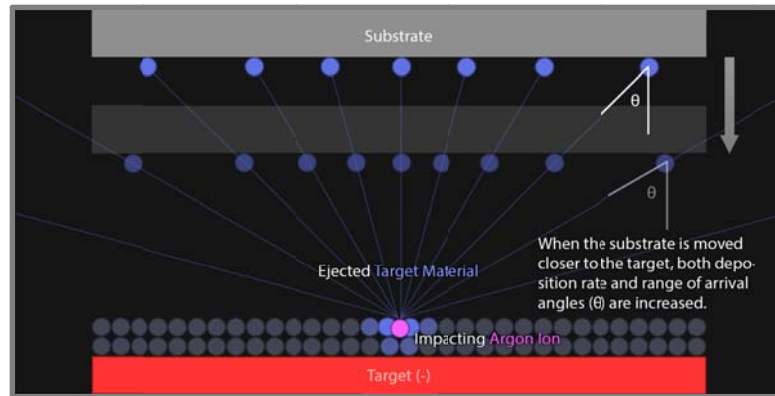


Figure 1.4. A schematic of how sputtering chamber geometry (specifically, the target – substrate separation distance) affects both the film deposition rate and the range of arrival angles of the sputtered target material.

The rate at which the arriving sputtered material adheres to the surface of the substrate is referred to as the “deposition rate” (measured by deposition thickness per time). The deposition rate of a material, when all other factors are held constant, is proportional to the discharge voltage and the supplied current, seen in Eqn. 1.1 below,

$$\text{Deposition Rate} = \text{const.} * V * I [24] \quad (1.1)$$

where “const.” takes into consideration the sputtering material, chamber geometry, and sticking coefficient of the experimental setup, and “V * I” is sputtering power which is proportional to ion energy. Examining Eqn. 1.1, and holding all other variables constant, an increase in sputtering power should result in a linear increase in deposition rate, which is verified experimentally for PTFE in results reported by

Lawson & Nicholls [33]. Unfortunately holding all other variables constant is difficult across multiple studies where sputtering chambers are of a different (sometimes radically) configuration. Changing chamber geometry is often a time consuming process and is only possible up to a point in each chamber, while upgrading equipment can be prohibitively expensive. It can be expected, therefore, that deposition rates (and possibly more film properties) for materials will differ greatly between studies even after a reasonable amount of data normalization.

When no sputtering is occurring, the sputtering chamber is held at a base pressure, typically 10^{-7} Torr or lower. For any sputtering at all to take place, gas must be introduced into the chamber to allow atoms to ionize at and collide with the surface of the target; this causes the need for an increase from base pressure. Typically during sputtering, the chamber pressure is held between 5- 40 mTorr. As the pressure increases – as more argon atoms are introduced into the chamber – the mean free path of both the argon ions and the target fragments decreases, increasing the chances of the sputtered atoms colliding with additional argon ions while en route to the substrate. The relationship between pressure and deposition rate is nonlinear, and has been investigated by Stelmashuk et al. [26]. Results from that study are presented in Figure 1.5.

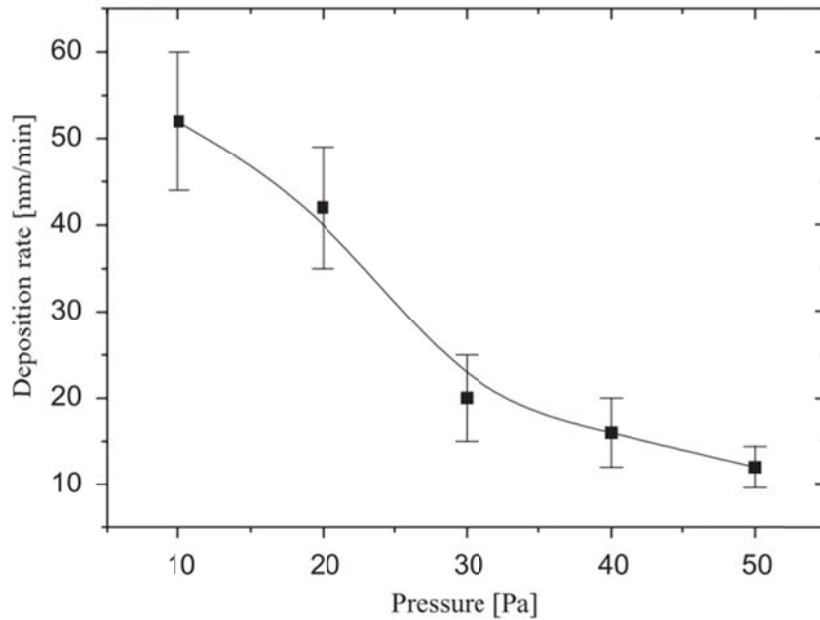


Figure 1.5. The deposition rate vs. pressure relationship reported for the sputtering of PTFE [26]. Figure reprinted with permission.

1.2.2 Radio Frequency Magnetron Sputtering

In “magnetron” sputtering, magnets are arranged on the backside of the sputtering targets in order to condition the plasma geometry for improved process efficiency. In the sputtering system used for this study, and in most other systems, the magnets are arranged in a circular pattern of like polarity around the outer diameter of the backside of the target, with a magnet of opposite polarity in the center. This causes the free electrons to follow a helical path towards the target, which improves the collision rate with the sputtering gas and increases the sputtering rate of the target. This arrangement of magnets creates a toroidal-shaped plasma, which causes a distinct erosion ring to form on the surface of the target, as the sputtering gas ions are more likely to collide with the target in this region. Due to the high powers used to form the plasma at the target surface, the magnets and target surface can heat up appreciably,

which can become an issue with the lifespan of the magnets and the integrity of the target. To counter this issue, cooling water may be flushed through copper water lines behind the magnets in the target assembly, and the target itself may be fitted with a copper mesh or backing plate to facilitate heat dissipation.

There are two primary sub-families of magnetron sputtering: direct current (DC) and radio frequency (RF). DC sputtering is the simpler of the two (described in this study previously and pictured in Figure 1.3 above); however the types of materials that can be used as sputtering targets are more limited. The polarity between the target and the substrate surfaces remains constant, which quickly results in a charge buildup on the surface of any electrically insulating targets. The surface eventually discharges; sparking between the target and the insulated components of the target “gun,” which extinguishes the plasma and halts further material deposition. Therefore, only conductive materials may be used in DC sputtering systems.

RF sputtering (which, along with DC, is present on our system and is used for most of the sample preparation in this study) overcomes the charge buildup issues present in DC sputtering by rapidly alternating the electric field polarity between the target and the substrate (Figure 1.6). This brief change in polarity allows for the neutralization of the charge buildup present on the target surface, and does not last long enough for the much more massive argon ions to significantly reverse their path and begin sputtering the surface of the substrate and/or chamber. This type of system allows for the sputtering of insulating targets, including PTFE and other polymers.

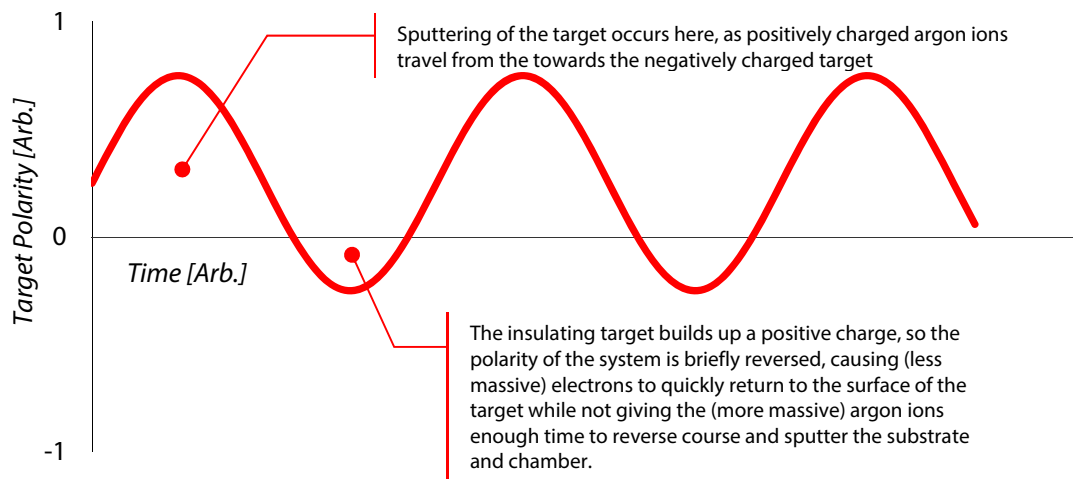


Figure 1.6. Example sputtering target polarity vs. time for an RF sputtering system.

1.3 Characterization of Sputter-Prepared Fluorocarbon Films

In sputtering, due to the vaporization, transportation, and deposition of the target material on an atomic scale, films prepared from polymer targets cannot be reasonably expected to retain the chemical structure or material properties held by their parent, bulk materials. Fluorocarbon films prepared from sputtering bulk PTFE are no exception. Due to the range of sputter yield using argon as a sputtering gas (0.1 – 10 [27]), the deposited films will most likely not resemble the long fluorocarbon chains that form the bulk PTFE structure. How the sputtered PTFE molecules recombine on the surface of the substrate is a factor of several parameters, including sputtering power (sputter yield, energy flux), chamber geometry (incident angle, target – substrate separation distance), substrate temperature, and choice of substrate material. Due to the (aforementioned) differences in structure of the sputtered fluorocarbon films and the bulk PTFE equivalent, the sputtered fluorocarbon films can be characterized by their relative similarities to the bulk parent material, or “bulk-likeness”, across a variety of characterization techniques.

1.3.1 Chemical Characterization

There are several techniques available to ascertain the molecular structure of the sputtered fluorocarbon thin films. Two of the most common techniques used in previous studies (and this study) are Fourier transform infrared spectroscopy (FTIR) and X-ray photoelectron spectroscopy (XPS). FTIR is used to provide information about the sample chemical groups through the analysis of molecular vibrations. The sample to be analyzed is bombarded with excitation radiation and the sample absorbance of the radiation excites the vibrational states to a higher energy level. The radiation used typically lies within the 4000 cm^{-1} - 200 cm^{-1} infrared range. The transmittance vs. absorbance relationship is used in conjunction with the corresponding wavenumber (cm^{-1}) to form the FTIR spectrum for the sample [34].

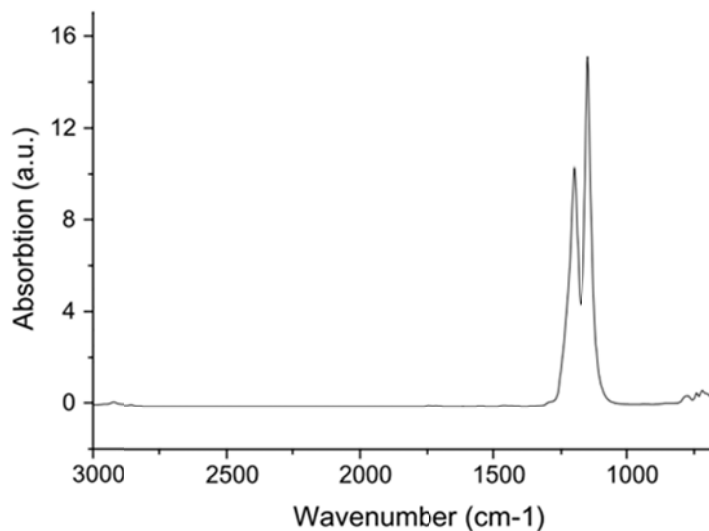


Figure 1.7. An example FTIR spectrum generated from untreated bulk PTFE [21]. The two peaks located between approximately 1300 cm^{-1} and 1100 cm^{-1} are typically the dominating spectral feature of bulk PTFE, representing both asymmetric and parallel asymmetric CF_2 bonds. Figure reprinted with permission.

Because FTIR involves the transmission of radiation through the entirety of the sample film and substrate, the resultant spectra is generated from the entirety of the film up to the substrate. A representative FTIR spectrum for bulk (non-sputtered) PTFE is presented in Figure 1.7. Characteristic of untreated, bulk PTFE, there are two prominent peaks located between approximately 1300 cm^{-1} and 1100 cm^{-1} , with no other major features along the spectrum. In contrast to the bulk film, an example FTIR spectrum produced from sputtered PTFE (Figure 1.8) shows a single, broad, prominent peak at approximately 1200 cm^{-1} . This change from the prominent, dual peak spectrum to the broad, single peak spectrum is indicative of a shift from the bulk-like, $-\text{[CF}_2\text{-CF}_2\text{]}_n$ chain structure present in the bulk PTFE to a more amorphous fluorocarbon structure present in the sputtered films.

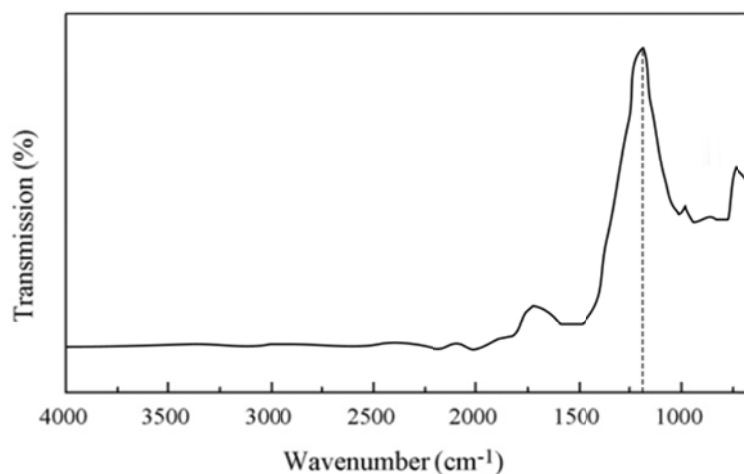


Figure 1.8. An example FTIR spectrum generated from a sample of sputtered PTFE [12]. The single, broad, prominent peak at 1186 cm^{-1} is associated with CF_2 bond groups and is characteristic of sputtered PTFE films. Figure adapted from source with permission.

Another technique commonly used for characterization is XPS. XPS has been used as a method of material characterization for over a century, and the use of the technique on polymers was first reported by Clark & Kilcast, in 1971 [35] while analyzing a sample of PTFE. XPS is complimentary to FTIR with regards to the general type of information it can provide (i.e. indicators of various bonds and elements), however it is more surface sensitive and specific in the bond types that it can identify. During XPS, the sample to be analyzed is bombarded with monochromatic X-rays, which ionize atoms at the sample surface, causing photoelectrons to be released at the core-level of the ions. The released photoelectrons can then be collected and analyzed for both binding energy and emission intensity, and the resulting data, when plotted, forms a spectrum of electron intensity as a function of wavenumber.

One drawback of the XPS process is that the photoelectrons that are released have a chance of being resorbed before being collected. This means that the resulting spectrum is produced from the topmost layers of the thin films; the structure of the film closer to the substrate is not represented in the resultant spectrum. The exact depth of photoelectron origin is a function of both the type of X-ray source used by the system, the angle at which the X-ray source is mounted relative to the sample surface (or which way the sample surface has been rotated relative to the X-ray source), and also the core level that the photoelectrons emerge from [35]. This relationship between XPS instrument setup and sampling depth is summarized in the scope of this study in Table 1.1.

Table 1.1. Sampling depth of XPS analysis by core level, take-off angle [35].

Core Level	Binding Energy [eV]	Sampling depth (95% signal) [nm]		
		X-ray Source: Al $K\alpha$		
		10°	45°	90°
F1s	686	1.1	4.5	6.3
C1s	287	1.5	6.2	8.5

A representative XPS spectrum for the C1s region of bulk PTFE is given in Figure 1.9. Characteristic of the XPS spectrum of PTFE, the binding energies lying between 290 eV and 295 eV represent the carbon chemical groups (C1s). The structure of bulk PTFE (as shown in Figure 1.2) is comprised of long chains of $-\text{CF}_2-\text{CF}_2-\text{CF}_2-\text{CF}_2-\text{CF}_2-$ which are terminated by CF_3 bonds. This chain structure is represented in the XPS spectrum, with the dominant peak at approximately 292.5 eV being associated with the presence of $-\text{CF}_2-\text{CF}_2-$ bonds, and the smaller peak at approximately 294.5 eV being associated with the lesser presence of CF_3 bonds [21].

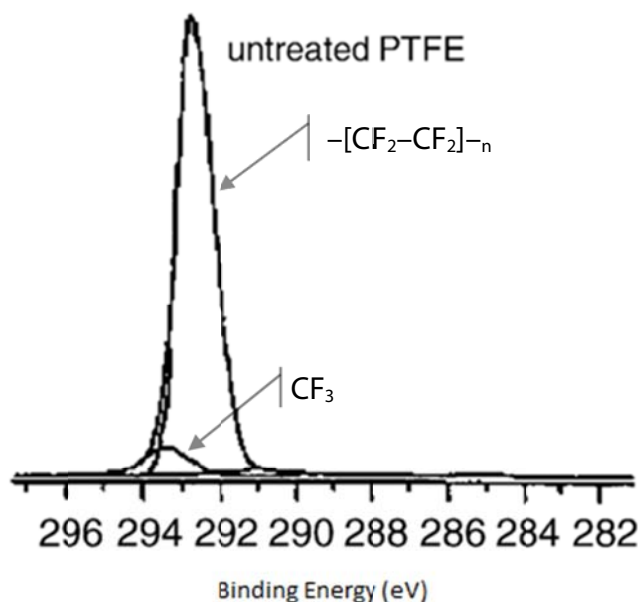


Figure 1.9. An example XPS spectrum generated from a bulk PTFE sample [21]. C1s region shown. The peak found at 292.5 eV is assigned to $-\text{[CF}_2\text{-CF}_2\text{]}_n$ bonds which form the long fluorocarbon chains found in bulk PTFE. The peak found at 293.5 eV is assigned to the CF_3 bonds that form the terminating ends of the chains. Figure reprinted with permission.

A representative XPS spectrum for the C1s region of a sputtered fluorocarbon film is given in Figure 1.10. The bond assignments of the five peaks are similar to those assignments found in other studies [7, 9–15, 21, 26, 36–38]. Typically, the most prominent peak located around approximately 292 eV is assigned $-\text{[CF}_2\text{-CF}_2\text{]}_n$ bond, with the remaining four peaks being assigned (from high to low) CF_3 , CF , C-CF_x , and C-C or C=C bond types.

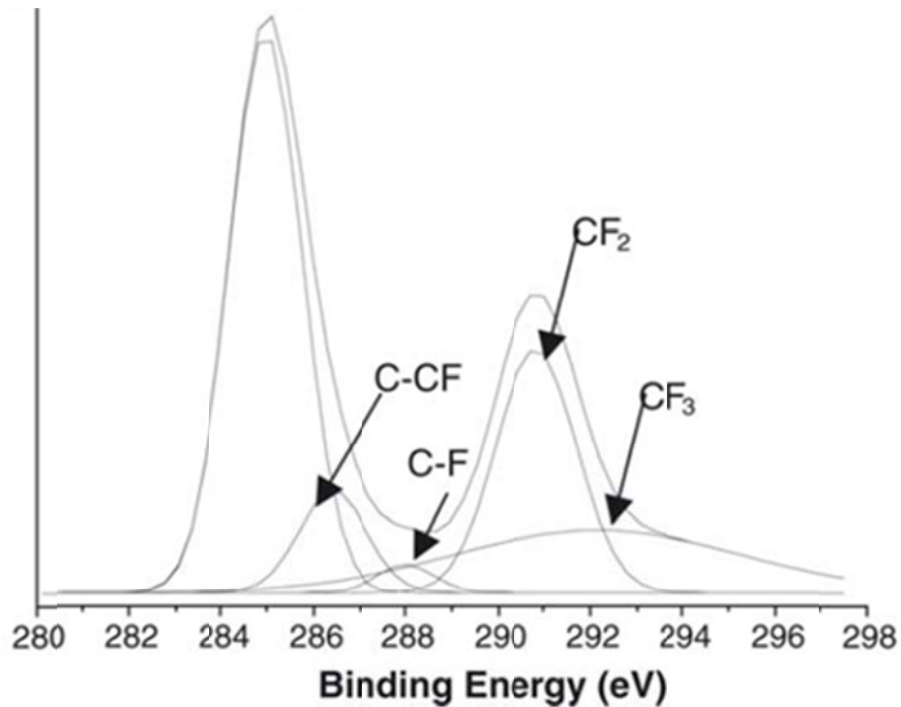


Figure 1.10. An example XPS spectrum generated from a sputtered fluorocarbon film sample [38]. C1s region shown. Figure reprinted with permission.

1.3.2 Mechanical Characterization

To mechanically characterize thin fluorocarbon films, nanoindentation is commonly employed to ascertain the hardness and elastic modulus properties of the deposited material. In nanoindentation via atomic force microscopy (instrument/process: AFM), a laser is reflected off a microscale AFM tip, and is then received by a detector. The AFM piezo stage (where the tip, laser, and detector assembly are all mounted and fixed relative to one another) is slowly lowered towards the surface of the sample. As contact between the tip and the surface is made, the tip deflects as a function of piezo movement, cantilever stiffness, sample mechanical properties, and sample/tip adhesion. This tip deflection moves the reflected laser across the detector, and a change in voltage is registered by the controlling program

(Figure 1.11). The stage movement is stopped and reversed, yielding a loading curve (or “trace”) and an unloading curve (or “retrace”). Using these curves and the known properties of the AFM tip, hardness and elastic modulus can then be calculated for the given thin film. This processing is expanded upon in section 2.5.1. Annotated sample loading and unloading curves are shown in Figure 2.9.

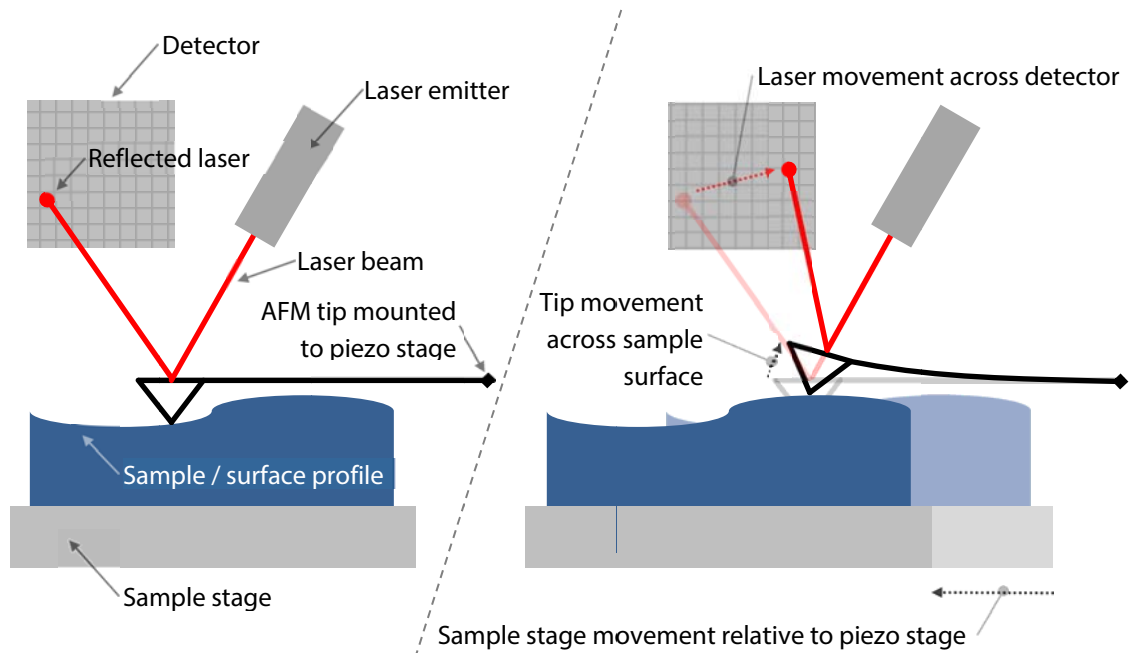


Figure 1.11. A general schematic overview of atomic force microscopy, shown with and without stage movement. Figure is not drawn to scale.

The deposition rates and film thicknesses that result from the mechanics of sputtering present an additional set of challenges when characterizing the produced films. Deposition rates of films on the order of 10 to 100 nm/hr practically limit how thick the films can be. In these thin films, substrate effects and film-substrate adhesion must be taken into consideration when characterizing films. Sputtered fluorocarbon films on the order of (and well below) 1 micron in thickness are not as well

understood as their thicker equivalents [15], both in terms of their physical performance (where substrate effects and surface adhesion are major obstacles), and also in terms of their chemical structure (where the low film thickness / substrate thickness ratio decreases the signal / noise ratio in many characterization techniques) [11]. The resemblance of the fluorocarbon films to that of the bulk PTFE in terms of physical performance breaks down in films of this thickness. Harop [39] found that the friction coefficient of the sputtered fluorocarbon films rose to that of the underlying substrate (in that case, metal) when film thickness fell below 500 nm, while film hardness increased by a factor of 2.5 when compared to the bulk material. Tang et al. [11] reported that hardness and elastic modulus increased by factors of 20 and 15 respectively in the thin (~100 nm thick) fluorocarbon films when compared to those values of the bulk PTFE. Likewise, a study by Li et al. (2011) [15] found that fluorocarbon films of nanometer thickness exhibited hardness and elastic modulus values at 24X and 18X that of the bulk PTFE. Properties of the substrate in such films are very likely an influencing factor on these physical values, especially at the 1 to 10 nm range. However, Kuster et al. [40] have shown that even for relatively thick (1.5 μm) sputtered films there are substantial differences between the properties of the films and the bulk materials, with hardness increasing 8X and the elastic modulus increasing 6X when compared to the bulk PTFE.

1.4 Effects of Changing Deposition Parameters on Sputter-Prepared Fluorocarbon Films

The numerous deposition parameters available in sputtering systems can have a major impact on the resultant film characteristics; available parameters commonly

include chamber deposition pressure, sputtering power, and deposition temperature. Several studies have been carried out measuring the effects of these parameters on the structure and performance of the sputtered fluorocarbon films. A study by Stelmashuk et al. [26] found that, aside from dramatically affecting the film deposition rate (Figure 1.5), increasing sputtering pressure has been shown to increase surface roughness of the fluorocarbon films, which increases the water/surface static contact angle [26]. The same study found that as deposition pressure was increased from 10 to 70 Pa static contact angle rose from approximately 105° to 145° . Using chemical characterization techniques, otherwise identically deposited films sputtered at increasing sputtering pressures were shown to exhibit increases in the percentage of CF_2 bonds present in the films, which is seen as an increase in similarity to the bulk material (as seen in Figure 1.2, XPS indicates CF_2 bonds comprise the majority of those found in bulk PTFE). CF_2 bond percentage increased from 20% to over 35%, a trend which continued up until sputtering pressure reached 40 Pa, after which the trend reversed. By comparison, in bulk PTFE CF_2 bonds make up of 95.7% of the total bonds present in the structure [21].

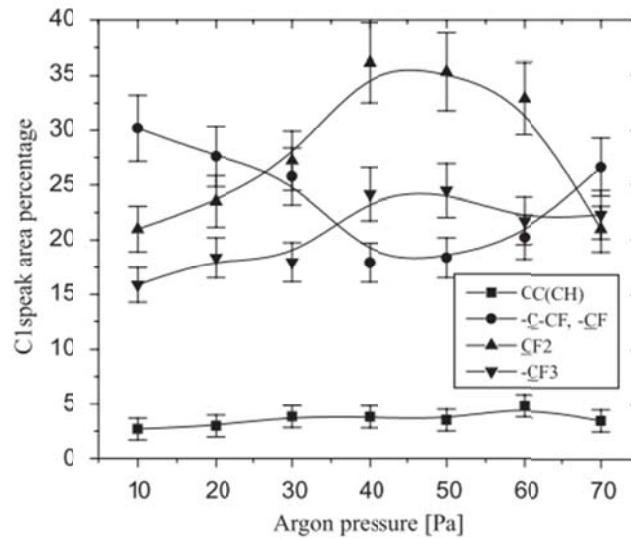


Figure 1.12. Carbon-fluorine bond types (as a percentage of total bonds in C1s region) present in sputter deposited fluorocarbon films, prepared over increasing deposition pressures [26]. Figure reprinted with permission.

Several studies have examined the relationship between sputtering power and fluorocarbon film structure [7, 11, 12, 15] with the general trend of fluorocarbon film bulk-likeness increasing with increasing sputtering power. Tang et al. [11] reported that as sputtering power increased from 200 W to 400 W, fluorine content increased from 33% to 43%; that increase can be attributed to an increase in the percentage of CF₂ bonds shown in the study. By comparison, in bulk PTFE the fluorine has been measured to make up 66.8% of the structure [21]. The same study showed that values for both hardness and elastic modulus decreased towards those of the bulk PTFE (Figure 1.13) as sputtering power was increased. Bulk values were measured to be 0.05 GPa for hardness and 1 GPa for modulus. Similar results were also reported by Li et al. (2011) [15], as shown in Figure 1.14, with bulk values for elastic modulus and hardness reported at 1.0 GPa and 0.05 GPa, respectively.

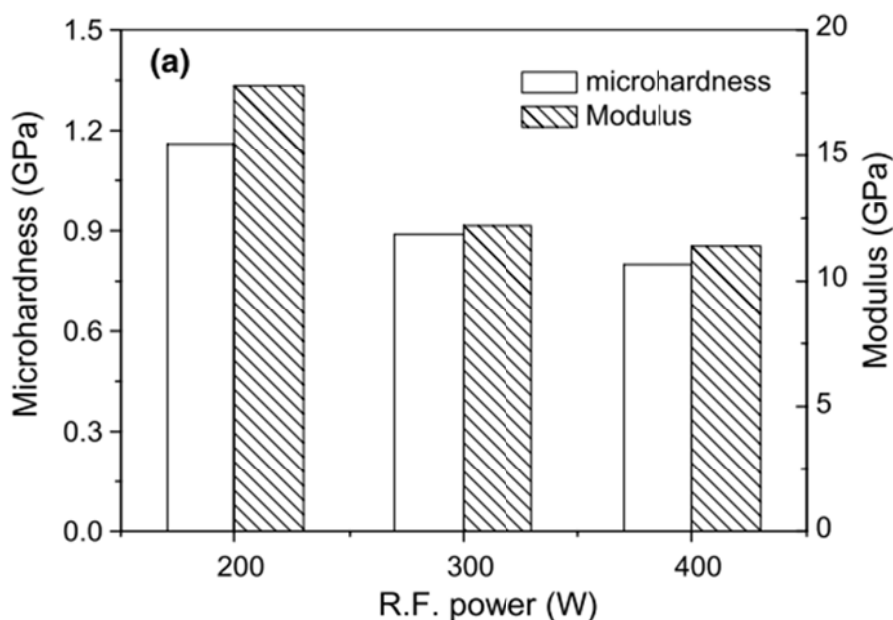


Figure 1.13. Hardness and elastic modulus values for fluorocarbon films prepared with increasing sputtering power [11]. Bulk values were found to be 0.05 GPa for hardness and 1 GPa for modulus. Figure reprinted with permission.

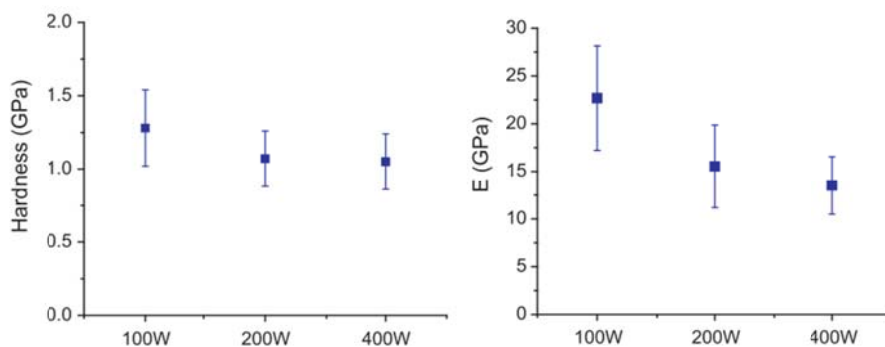


Figure 1.14. Hardness and elastic modulus values for fluorocarbon films prepared with increasing sputtering power [15]. Figure reprinted with permission.

FTIR results from Li et al. (2008) [12] (Figure 1.15) show that as sputtering power is increased, there is a decrease in the intensity of the strong peak found at approximately 1220 cm^{-1} that the authors have associated with a decrease in CF, CF_2 , and CF_3 groups. Two peaks, located at 1202 cm^{-1} and 1146 cm^{-1} , are the primary spectral features found in the spectrum of the bulk PTFE. The reduction in height of

the strong peak at 1220 cm^{-1} of the sputtered films with an increase in sputtering power suggests that the films become less bulk-like with increasing sputtering power. However, as sputtering power is increased, there is a smoothing and disappearance of non-bulk PTFE peaks on the resultant spectra presented by Li et al (2008); specifically, a peak present at 1720 cm^{-1} , which is associated with $\text{C}=\text{CF}_2$ bonds and a more complex, cross-linking structure unlike that of bulk PTFE, disappears completely as sputtering power is increased from 80 W to 110 W (Figure 1.15).

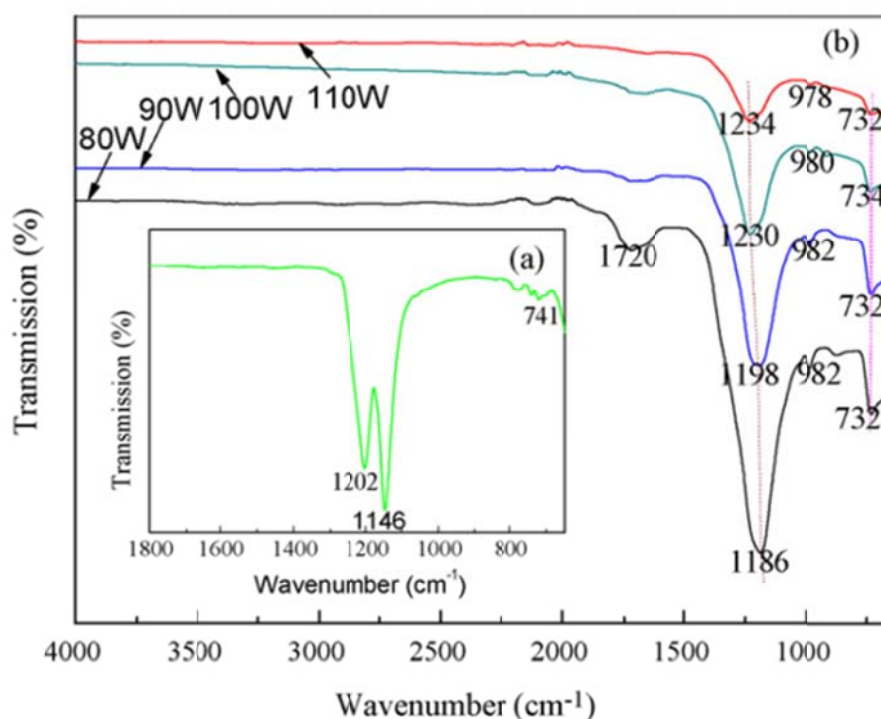


Figure 1.15. FTIR spectra of a) the bulk PTFE material and b) the sputtered fluorocarbon films under increasing sputtering powers [12]. Figure reprinted with permission.

Increasing deposition temperature (i.e. temperature of the substrate during sputter deposition) has been shown by Oya & Kusano [13] to affect the quality of the resultant fluorocarbon films. The surface energy (a function of the contact angle of

H₂O) on the deposited films increased from 15.5 mJ/m² (0.8X that of bulk PTFE) to 26.3 mJ/m² (1.4X bulk PTFE) when deposition temperature was increased from 150 °C to 230 °C. Additionally, the percentage of the bulk-like CF₂ bonds present in the fluorocarbon films decreased by 50% with increasing deposition temperature. However, a similar study carried out by Suzuki et al. [41] showed that the percentage of CF₂ bonds present in the fluorocarbon films decreases by only 3% when increasing deposition temperature from 20 °C to 150 °C, while the critical load of the same films increased from approximately 35 mN to 62 mN (Figure 1.16). The authors hypothesize that this increase in critical load is an indicator of an increase in polymer chains grafted to the surface of the substrate, which yield better film-substrate adhesion.

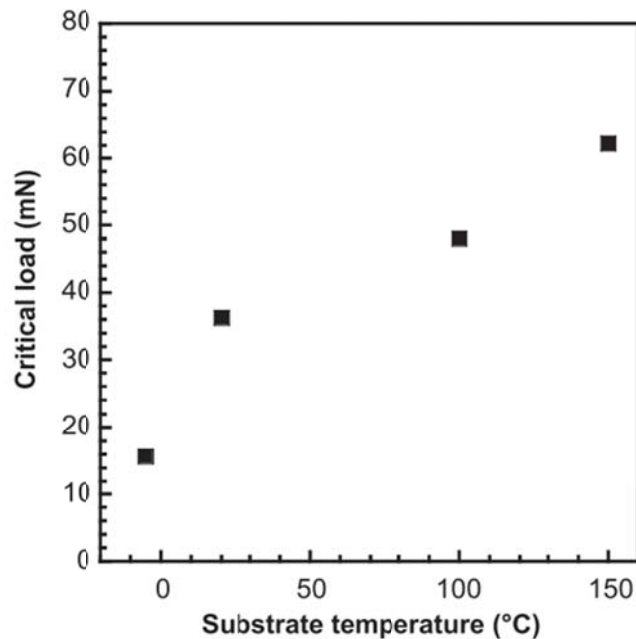


Figure 1.16. Critical load of sputter deposited fluorocarbon films prepared under increasing deposition temperatures [41]. Figure reprinted with permission.

The effects of post-deposition annealing on the crystallinity of sputter deposited fluorocarbon films have been studied to some degree. Sun et al. [42] found using X-Ray Diffraction (XRD) that when annealing a fluorocarbon film at a temperature of 290 °C, below the melting point of PTFE (327 °C [42]), the film exhibited a minor increase in crystallinity from 43.6% to 45.1%. When anneal temperature was increased beyond the melting point of PTFE in a pressurized CO₂ atmosphere (34.5 MPa, 330 °C), the crystallinity of the films increased from 43.6% to 52.6%. Films were annealed for 3 hours each; increasing the anneal time to 6 hours caused less than 1% difference in crystallinity for a majority of the reported tests. In the same study, annealing at 330 °C and ambient pressure was shown to decrease creep by 35%. Performance improvements are thought to be due to increased cross linking caused by the anneal process.

1.5 Motivation for Research

Several groups have found success in improving the wear resistance of bulk PTFE through the use of nanofiller reinforcements. These composite PTFE-blends can exhibit wear rates orders of magnitude less than the unfilled materials. However, there are limitations on how small the length scale between filler material can be, caused by the size of the PTFE particles, which are on the order of tens of microns in diameter. It is hypothesized that as the regimes of unfilled PTFE are reduced, material performance of the composite materials will improve. Co-depositional sputtering of both virgin-grade PTFE and the filler materials will grant greater control over this nanofiller length scale, down to an atomic level. However, a better working understanding of the thin films produced from sputtered PTFE must first be

established. Similarities between the properties of the sputter-prepared thin films and the properties of the bulk PTFE material are taken as a measure of the “bulk-likeness” of the thin film. It is this bulk-likeness that will be used as a way to relatively compare the effects of changing parameters during film preparation.

The processing parameters found in the sputtering machine used in this study are chamber deposition pressure, sputtering power, and substrate deposition temperature; modifying these parameters in other studies has been shown to change the structure and performance of the resultant films. The results reported in the literature indicate that: as chamber deposition pressure is increased, the bulk-likeness of the films increases until reaching a critical pressure, after which it decreases. As sputtering power is increased, there is an increase in the bulk-likeness of the fluorocarbon films, although there are instrumental limitations to how high the sputtering power can reach; and as substrate deposition temperature is increased, the bulk-likeness of the film structure decreases slightly, while the mechanical properties of the film become much less bulk-like, but yield better adhesion to the substrate.

The primary aim of this thesis is thus to further establish the relationship between sputtering parameters and fluorocarbon film structural and mechanical properties for films prepared in the sputtering chamber, with the hope of establishing effective processing procedures for the most bulk-like fluorocarbon film possible. Additionally, the creation of bulk-like thin fluorocarbon films, while in and of itself a desirable goal, would form a logical starting point for the introduction of co-deposited material that would build off of previous successes with composite PTFE blends.

Chapter 2

METHODS

2.1 Sample Preparation

2.1.1 Sputtering System Overview

All fluorocarbon films prepared in this study (excluding any bulk PTFE samples) were prepared using radio frequency (RF) magnetron sputtering. The sputtering system used for sample preparation was manufactured and assembled by PVD Products Inc. A basic schematic of the system used in this study is given in Figure 2.1. The chamber was setup in the “sputter-up” configuration, where the target materials faced upwards and the substrates were held facing downwards by the “substrate holder” (Figure 2.2.a), which in-turn was held by the stage. The stage was capable of rotation in order to give each substrate surface a radially uniform coating of the target material during depositions. The chamber was equipped with four target “guns”, three of which were powered by an RF power supply and one of which was powered by a DC power supply. Although capability existed in the system for co-depositions, wherein sputtering occurs from multiple target sources simultaneously, for this study only one target source was utilized at any one time.

The approximate substrate / target gun geometry inside the sputtering chamber is given in the inset of Figure 2.1. The distance between the target and the substrate was approximately 15 cm, which is relatively large compared to the distances reported in similar studies (7 cm [10], 4 cm [11], 5 cm [26], 8 cm [12], 7.5 cm [13], 3.2 cm [15]). All targets, and the stage itself, were equipped with shutters that could be

toggled open and closed, allowing for the precise control of deposition times and the prevention of target contamination during deposition of other materials.

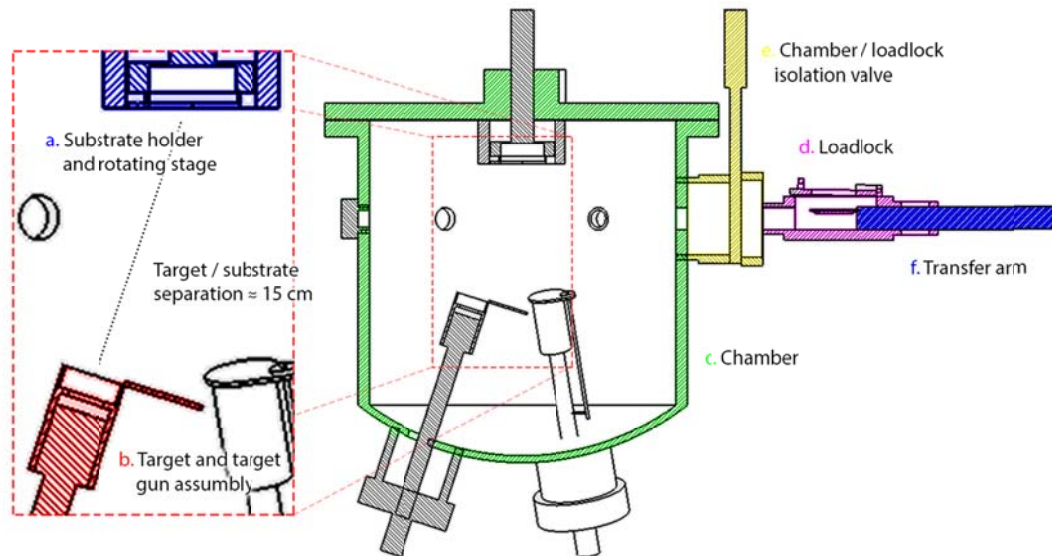


Figure 2.1. A cross sectional view of the sputtering chamber used for this study. System components are: a) substrate holder (blue) and rotating stage, b) target (red) + target gun assembly, c) vacuum chamber, d) loadlock, e) chamber / loadlock isolation valve, and f) chamber / loadlock transfer arm. Approximate target / stage geometry is shown in the inset; with the distance between the two components being approximately equal to 15 cm. Figure is not to scale.

The loading and unloading of substrates into and out of the chamber and stage were accomplished with the aid of a loadlock and transfer arm, as seen in Figure 2.1.d. This allowed for the quick transfer of substrates without a significant increase in the base pressure of the chamber. Target loading and unloading, however, required venting the chamber to atmospheric pressure. The pressure in the chamber was pumped down by means of an Onboard-8 cryopump manufactured by CTI Cryogenics, which held the base pressure of the chamber to below 10^{-7} Torr before each deposition. The pressure in the loadlock was pumped down (again to 10^{-7} Torr)

by means of a HiPace 300 turbopump manufactured by Pfeiffer Vacuum. Both the chamber and the loadlock were “roughed” from atmosphere (approximately 760 Torr) to 250 mTorr by means of an EDX-10 dry pump manufactured by Edwards Vacuum.

A diagram of the substrate holder is presented in Figure 2.2.a. Using this holder, the capability exists for eight 1 cm x 1 cm wafers to be sputtered upon at one time. The recessed edge seen in each of the eight slots prevents the wafers from falling to the bottom of the chamber, but reduces the effective sputtering area of each wafer to 8 mm x 8 mm (Figure 2.2.b). To ensure a uniform coating of film sputtered upon each substrate the substrate holder was rotated at a constant rate of 30 rpm during every deposition.

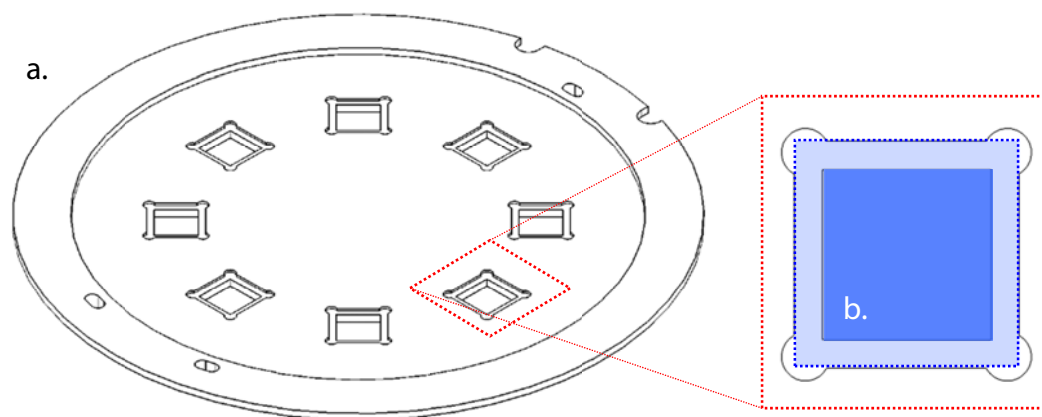


Figure 2.2. a) Stainless steel substrate holder for use in sputtering machine, with inset showing b) the effective sputtering area (8 mm x 8 mm) on each silicon wafer. Figure is drawn to scale.

Prior to loading into the chamber, all materials, including substrates, parts of the target assembly, and target materials, were cleaned of potential contaminants using successive rinses of: acetone, isopropyl alcohol, and deionized (DI) water. The clean components, including the Si wafers, were then blown dry with compressed, filtered,

and desiccated air. The amount of time between the “triple-rinse” of the components and their loading into the sputtering system was kept to a minimum. Due to the (approximately) line-of-sight nature of sputtering, chamber components in-view of the target are “contaminated” with target material whenever a deposition is made. Chamber walls and substrate stage were not thoroughly cleaned in between depositions of like-materials. Due to the high-use nature of the lab sputtering machine for other projects, an effort was made to schedule depositions into like-material time blocks in order to reduce the risk of cross-contamination between depositions of differing materials. All depositions referenced in this study were made in these blocks of like-deposition-materials, with light cleaning (wiping with acetone and isopropyl alcohol soaked cloths) of the chamber occurring in between blocks.

When increased substrate temperature was called for during sputtering, heating of the substrates was achieved through a halogen lamp heater located directly above the stage. Although the capability existed to increase stage temperature to approximately 800 °C during depositions, in this study the maximum deposition temperature was approximately 200 °C. Sputtering temperature of the stage was monitored using a thermocouple mounted in contact with the rotating stage axis, approximately 1.5 inches (3.81 cm) above the back surface of the substrate holder. Target and stage cooling were achieved through the use of a closed-loop water circulation system attached to a heat exchanger. The temperature of the water was monitored but not controlled directly, and ranged from approximately 17 °C when idle to approximately 36 °C during depositions.

2.1.2 Deposition Process

Silicon wafers, measuring 470 μm thick and of $\langle 1\ 0\ 0 \rangle$ orientation, were used as substrates for all depositions in this study. The stock 3 inch (7.62 cm) diameter silicon wafers were sprayed with a film of photoresist to prevent chipping and fracture, and then cut using a dicing saw into 1 cm x 1 cm squares for use in the sputtering system substrate holder. The silicon squares were cleaned of the photoresist coating by a bath of 3 parts sulfuric acid, 1 part hydrogen peroxide for a minimum of one hour, then thoroughly rinsed with deionized water and set out to dry in lab air in the lab fume hood.

During depositions for the majority of this study, pressure was held constant at 10 mTorr, which is typical of similar studies of sputtered PTFE (4.95 mTorr [10], 5.25 mTorr [11]). For all depositions in this study, the sputtering gas used was research grade argon, above 99.999% purity, purchased from Keene Compressed Gas Co. Argon flow rate through the chamber was kept at a constant rate of 20 sccm.

While sputtering power during depositions was varied throughout this study, RF frequency supplied to the targets was held constant at 13.56 MHz. Prior to each deposition from a new (unsputtered) target, the target was “pre-sputtered” (sputter-cleaned) with all chamber shutters closed (shielding substrates from deposition) for a period of 30 minutes. This pre-sputtering allowed any surface irregularities to be minimized, therefore ensuring a purer and more consistent coating on the substrates. Pre-sputtering was not performed before depositions from previously used targets.

2.1.3 Deposition Parameters

The main sputtering parameters that were varied in this study were the power supplied to the RF sputtering gun and the temperature of the stage during deposition. Power levels of 50 W and 100 W were used in all sample sets; a power level of 150 W was used for select sample sets. Deposition time was linked to sputtering power for each of the samples, with 2 hours allotted for the 50 W depositions, 1 hour allotted for the 100 W depositions, and 30 minutes allotted for the 150 W depositions. The deposition time was decreased with increasing sputtering power to ensure that the targets would not erode through to the surface of the target gun, invalidating the samples and exposing the target gun to the argon plasma, which could potentially damage the system. To prevent such damage to the targets, supplied power was slowly ramped up over a period of 2 minutes at the beginning of each deposition, and, upon deposition completion, ramped down to 0 W over the same amount of time. This power ramping was carried out on every deposition.

For those samples not temperature controlled, the measured deposition temperature remained at approximately 36 °C for all depositions (temperature of the stage when depositions were not occurring was measured at approximately 27 °C). The controlled deposition temperatures used in this study were 68 °C, 100 °C, and 200 °C. Temperature control was enabled after loading the samples into the chamber, and allowed to settle at temperature for five minutes before flowing argon into the chamber and beginning deposition. A heating and cooling rate for the halogen lamps was held constant at 2 °C per second across all heated depositions; while this value corresponded closely with the heating rate of the substrate, the cooling rate of the stage and substrates was much lower than this value. After heated depositions,

substrates were allowed to cool to room temperature in the chamber before their removal from the system. Significant time (more than 1 hour) was allowed for cooling at the two higher temperature settings.

On half of the resultant films, post-deposition annealing was performed in lab atmosphere using a small box furnace. The anneal temperature remained constant at 200 °C for all sample sets that underwent the annealing process. Samples were loaded from room temperature into the furnace, which was then set to 200 °C. Temperature ramp-up time was approximately 5 minutes. Total anneal time was 3 hours.

2.2 Sputtering Target Preparation and Characterization

Targets for use in the sputtering machine were constrained to 2 inches (5.08 cm) in diameter and approximately 0.25 inches (0.635 cm) in thickness. Sputtering target thicknesses, on average, were equal to approximately 0.2794 cm +/- 0.0254 cm. The target material used was virgin-grade 7C PTFE molding resin (~30µm diameter particles on average) purchased from E. I. du Pont de Nemours and Company. The 7C PTFE powder was compressed in a two inch diameter mold using a machine press at a pressure of 20,000 psi for approximately five minutes at room temperature. Targets were sputtered for only one 50 W deposition and one 100 W deposition each. Target geometry and mass were recorded – both before undergoing any sputtering, and after all depositions using the target had been performed – with the intention of establishing limits on the amount of sputtering each individual target could endure before eroding through to the surface of the target gun, exposing it to the argon plasma and damaging the sputtering system.

2.3 Sample Characterization

A digital camera was used to record the appearance of each coated substrate. The coating thickness was also recorded, using a process outlined in the following section. According to sputtering system manufacturer specifications, normalized film uniformity across a 4 inch (10.16 cm) silicon substrate (effectively the entire sputtering surface of the substrate holder) was +/- 1.25 % (PVD Products).

2.3.1 Interferometry and Film Thickness

Optical interferometry (Veeco Wyko NT9100) was used to characterize thickness of the deposited coatings because it has excellent height resolution (height uncertainty of ± 5 nm) and large spatial range (up to 1 mm for high statistical confidence). However, the technique requires both a reflective surface and a step height across which to take a measurement. The PTFE coatings prepared in this study were translucent, and therefore their thicknesses could not be measured directly using this technique. Deposited film thicknesses were measured using a “key” wafer which loaded into the substrate holder, and which was partially covered during deposition with a piece of Kapton vacuum tape. Following film deposition and anneal (if any) the step height was created by removing the tape and standard triple rinsing the wafer to remove any leftover adhesive residue. Titanium was then sputtered from the DC target location in the chamber to make the surface of the wafer reflective for use with the interferometer. Assuming a uniform Ti-film thickness, the step height of the original PTFE coating was preserved in this process, which is represented in Figure 2.3.

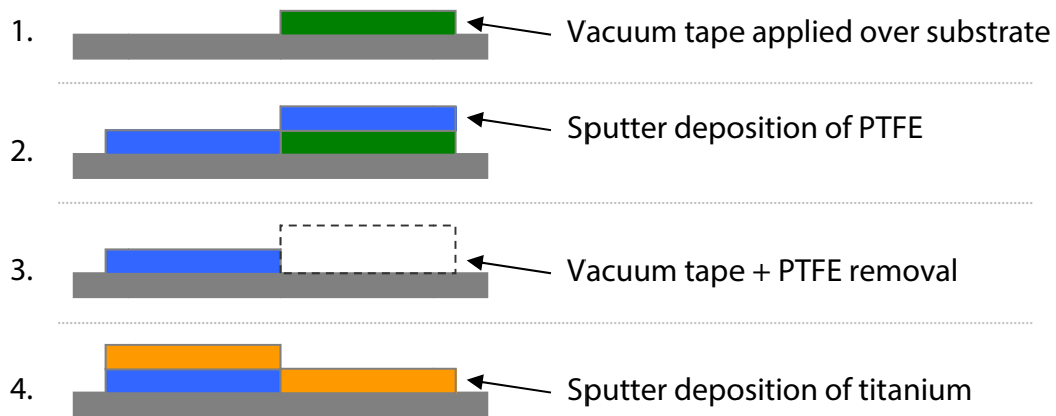


Figure 2.3. A cross-sectional view of the step-height sample preparation process. Vertical scale of the diagram is greatly exaggerated for clarity.

A Wyko NT9100 interferometer from Veeco was used to measure the thickness of each of the Ti-coated “key” wafers. In optical interferometry, the interference of light is used to measure the relative surface heights across a field of view. Briefly, light of variable wavelength hits a beam splitter whereby half the incident light continues toward the surface of interest while the other half is redirected to a reference mirror at a fixed location on the interferometer head. The light rays reflected by the sample and reference mirror interfere across a CCD sensor. As the head moves toward the sample, the instrument uses the vertical location of maximum light intensity (constructive interference) at every pixel to create a 3-D height map of the surface.

For this study, the sample was loaded onto the instrument, the surface brought into focus by manually adjusting head height, the stage angle was adjusted to minimize tilt of the sample (by ‘spreading’ the interference bands). The measurement consisted of a 5 μm backscan and a 25 μm forward scan. An example topographical plot obtained from interferometry is shown in Figure 2.4. Defects on the surface of

the sample (dust particles, scratches) were masked out by the software, and the stage angle was compensated for by specifying a flat area of the sample (the substrate side of the step-height was used for this). A histogram of pixel heights was then created; in the case of a clean step-height, the histogram was bimodal. The height difference between the two peaks on the histogram provided the film thickness in that region of the wafer.

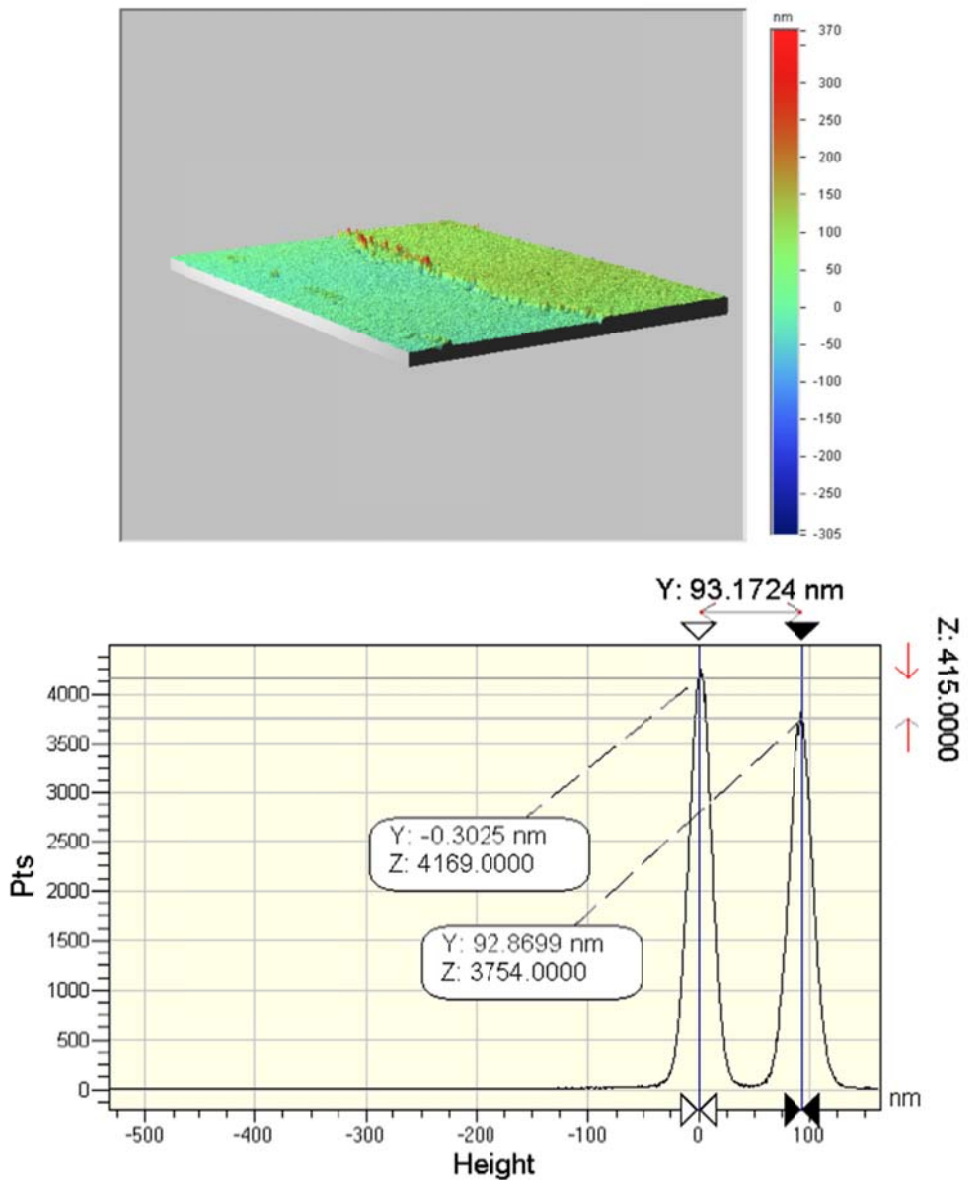


Figure 2.4. Sample topographical plot (top) and resultant histogram with calculated step height (bottom) produced from interferometry of sputtered film.

For this study, three areas on each sample were measured to account for any substrate holder masking effects at the sample edges, as well as any inherent lack of uniformity. Each area measured by the interferometer was 640 x 480 pixels, which

corresponded to 238 μm x 315 μm on the sample surface (10X objective, 2X field of view). This method of assigning thickness measurements to an entire sample set from one “key” wafer assumed that, due to both the stage rotation during sputtering and the nature of the sputtering process itself, each wafer in a given sample set (from the same deposition) had approximately the same thickness. This assumption had to be made, as the Ti coating required for this method of thickness measurement prevented the sample from being used with any of the other characterization techniques used in this study.

2.4 Chemical Characterization

2.4.1 Fourier Transform Infrared Spectroscopy

FTIR was used to provide information about the chemical structure of the sputtered fluorocarbon films, in addition to the structure of the bulk 7C PTFE material. All spectra (with the exception of the bulk PTFE powder target) were taken with the instrument in transmission mode, and were acquired between 3950 cm^{-1} and 450 cm^{-1} . Because the transmission mode also acquired absorbance from the silicon wafer, some additional steps had to be taken to acquire the spectrum of just the PTFE film. First, a background spectrum was acquired using a blank silicon wafer. Then the sample spectrum was acquired, and the background spectrum was subtracted in real time, resulting in only the film spectrum. This background re-calibration was performed every four samples to correct for any gradual change in the machine performance or atmosphere of the lab environment. Additionally, all samples were given the standard triple-rinse before spectra were acquired in an effort to minimize contamination.

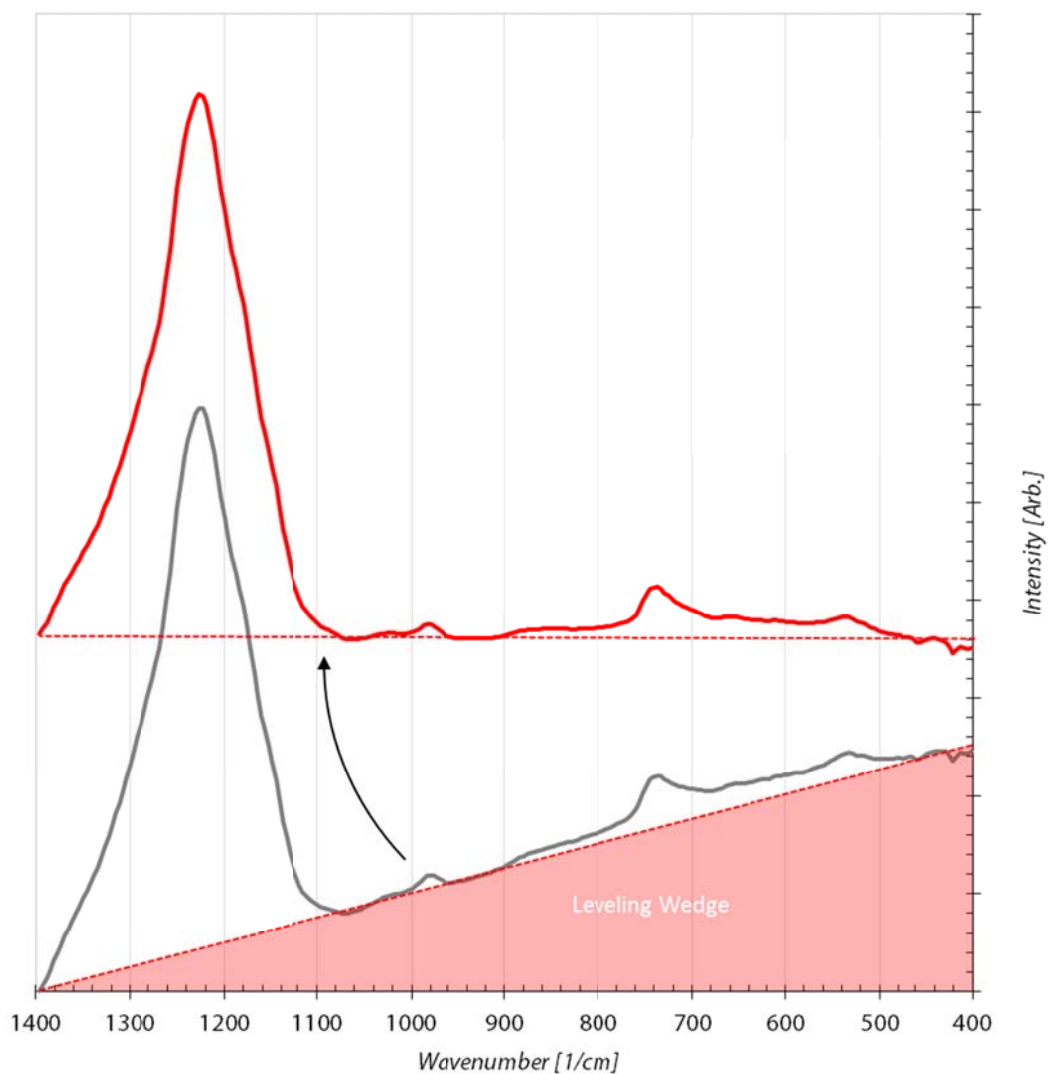


Figure 2.5. Sample straight-line curve-leveling performed on spectrum obtained via FTIR. Raw and processed spectra shown.

For the comparison between spectra of different samples, some degree of background subtraction was required due to differing background noise caused by the substrate. A “wedge” method was employed between like-points on all spectra, with anchor-point location depending upon the area of interest. This type of basic curve-leveling (as seen in Figure 2.5) attempts to remove any operator bias that might be

present with more complex polynomial curve-fittings [43, p. 54]. Wavenumbers of 950 cm^{-1} and 1400 cm^{-1} were used as these leveling-points in spectra acquired for samples in this study. In addition to curve-leveling, curves were then normalized based upon area under the curve, in order to compensate for the differences in intensities due to varying film thickness. A fit was made to the data ($R^2 > 0.99$) using Gaussian functions. Film bulk-likeness was established by comparing the spectra and corresponding fit Gaussian curves of the sputtered fluorocarbon films to those of the bulk PTFE. Specific metrics of bulk-likeness included any emergence of a “two peak” spectrum, as seen in the bulk PTFE (see Figure 1.7), any shift in peak position or intensity towards that of the bulk PTFE spectrum, and the minimization of peaks commonly associated with non-PTFE-like bonds.

2.4.2 X-Ray Photoelectron Spectroscopy

XPS analysis was performed using a VG Scientific 220i-XL imaging multitechnique surface analysis system equipped with a monochromatic high-flux microfocused Al X-ray source. After acquisition of the XPS spectra for each sample set, peak flattening and peak fitting was performed in the C1s region. The C1s region was fit with five Gaussian peaks, similar to other sputtered PTFE films reported in the literature [7, 9–15, 21, 26, 36–38] (see Table A.2). The five peak assignments and locations used in this study were CF_3 assigned to 293.5 eV, $-\text{[CF}_2\text{-CF}_2\text{]}_n-$ assigned to 292.5 eV, CF assigned to 287 eV, C- CF_x assigned to 291.5 eV, and C-C or C=C assigned to 284.5 eV. Bulk materials are typically fit with one to three peaks [13, 21], with the dominant peak at 292.5 eV assigned to $-\text{[CF}_2\text{-CF}_2\text{]}_n-$ bond types. The area under each peak corresponded to the relative quantity of the assigned bond type. For

comparison between different spectra, peak normalization was performed using total C1s area for each sample spectrum.

Three metrics of bulk-likeness were considered for the spectra: 1) the ratio between the $-\text{[CF}_2\text{-CF}_2\text{]}_n-$ bond peak area to the CF_3 bond peak area (Figure 2.6), 2) the percentage of the $-\text{[CF}_2\text{-CF}_2\text{]}_n-$ bond peak area of the entire C1s region of the spectrum (Figure 2.7), and 3) the ratio of the F1s region of the spectrum to the C1s region of the spectrum (Figure 2.8), which yields the atomic percentage of carbon and fluorine for the film. All three metrics were compared with their bulk equivalents to establish a measure of bulk-likeness for the film spectra.

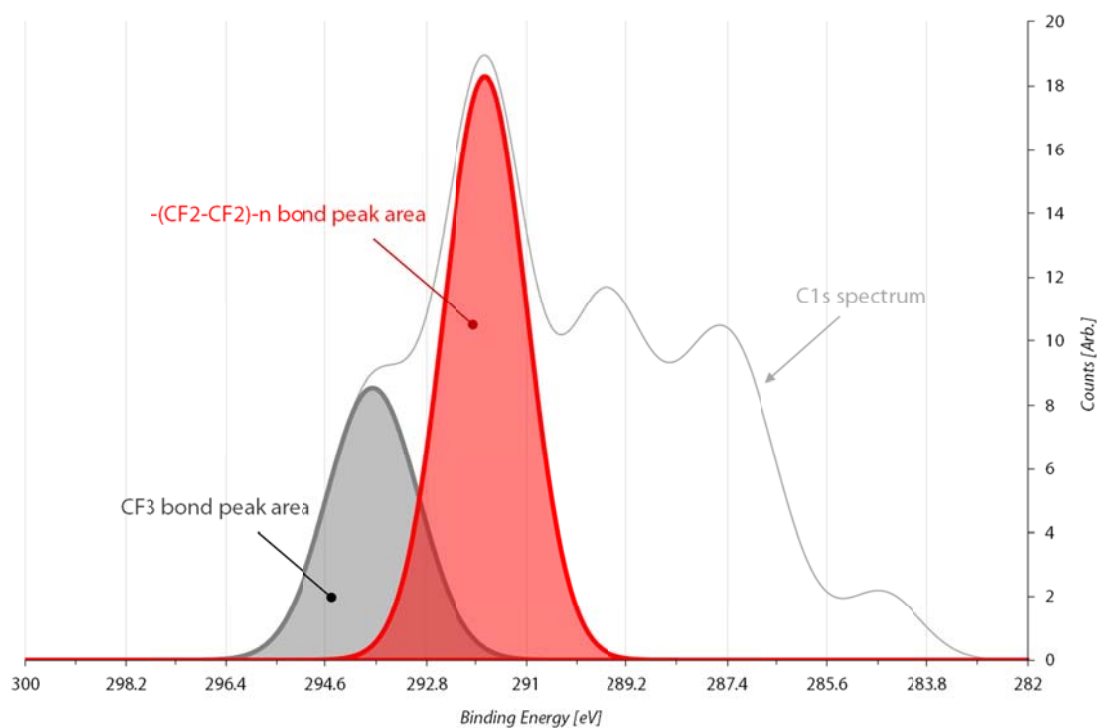


Figure 2.6. A sample XPS spectra showing the $-\text{[CF}_2\text{-CF}_2\text{]}_n-$ bond peak area (in red) / CF_3 bond peak area (grey) ratio.

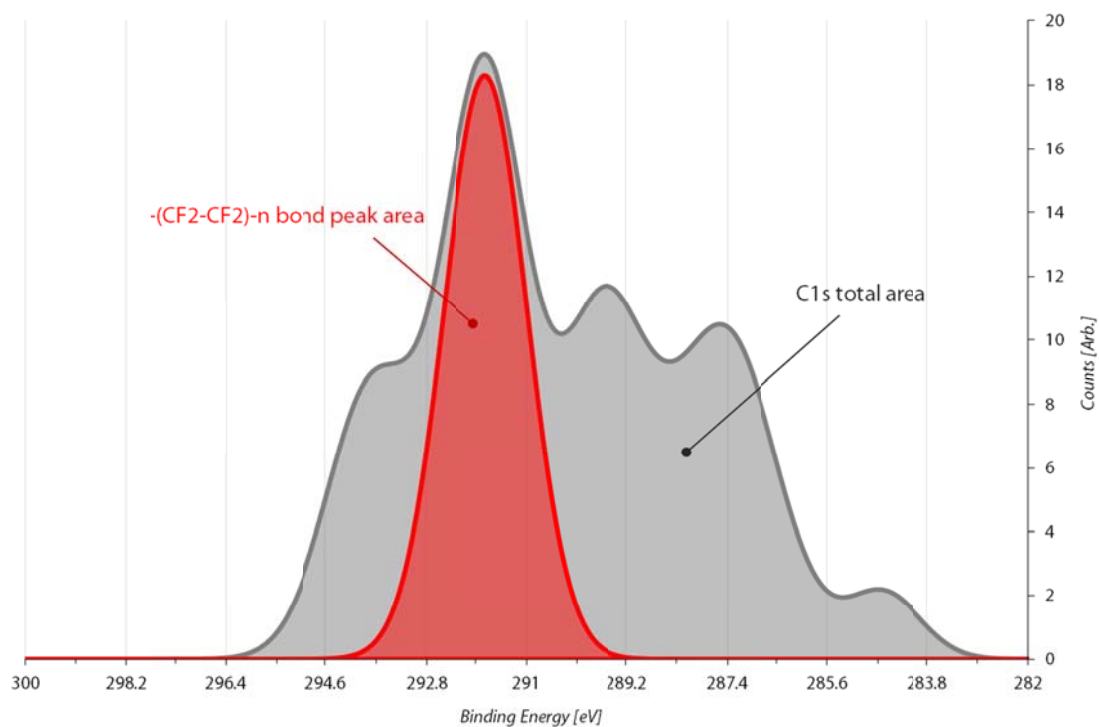


Figure 2.7. A sample XPS spectra showing the $-(CF_2-CF_2)_n-$ bond peak area (in red) as a percentage of the entire C1s region (grey).

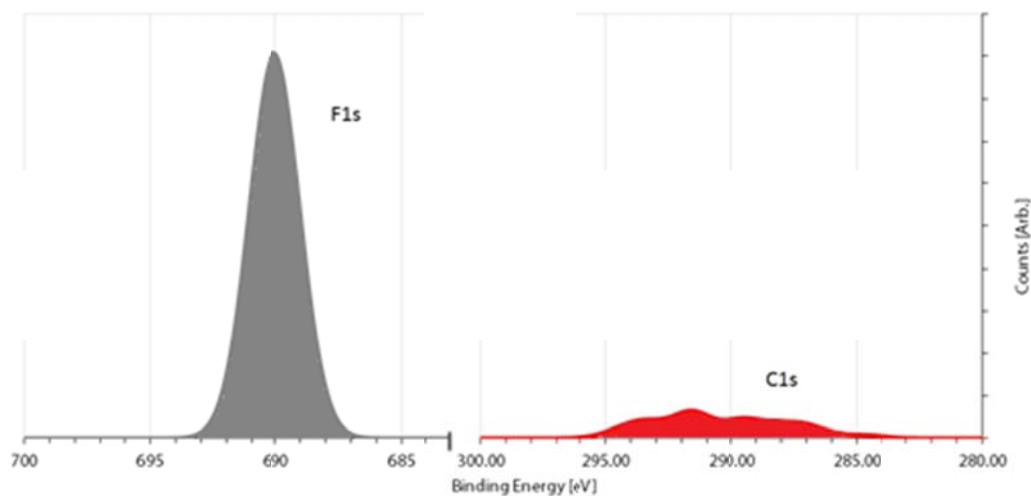


Figure 2.8. A sample XPS spectra showing the C1s (in red, right) / F1s (grey, left) areas. Fluorocarbon film atomic ratios calculated from this data.

2.5 Mechanical Characterization

2.5.1 Nanoindentation

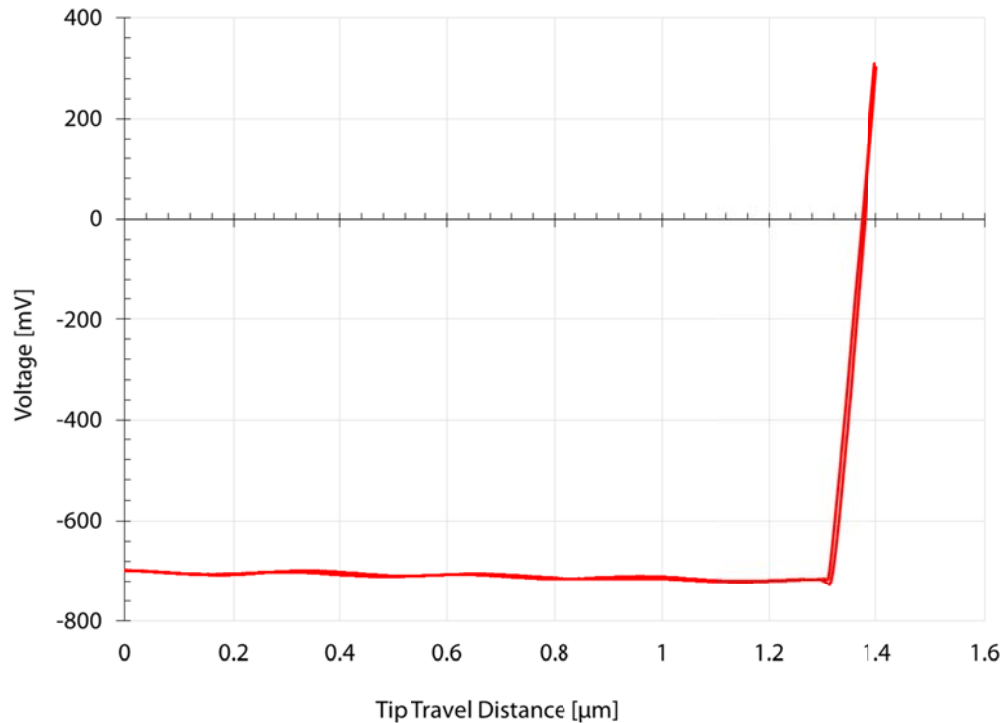


Figure 2.9. Unprocessed nanoindentation curves (loading, unloading). Data produced from nanoindentation of sputtered, 223 nm thick fluorocarbon film on silicon substrate (50 W sputtering power and deposition temperature of 36 °C used in film preparation).

A sample “raw” indentation curve is given in Figure 2.9. Hardness and elastic modulus were calculated from a number of voltage vs. piezo displacement curves that were generated from each indentation. Five indentations per sample were carried out at points spaced along the centerline of each wafer. In order to generate values for these physical properties, several calculations were required, which are outlined in the following steps:

1. First, an indentation was carried out on a blank silicon wafer; this deformation response serves as the ‘background’ for measurements of the

coatings. The background measurement yields the detector sensitivity constant, S (units: [V/nm]), which, along with the manufacturer specified cantilever stiffness, k_c (units: [nN/nm]), enables a relation of detector voltage and pre-calibrated piezo displacement into applied force and indentation depth. These relations are expressed as Eqn. 2.2.a and Eqn. 2.2.b:

$$F_i = V_d * (k_c / S) \quad (2.2.a)$$

$$x_i = x_p - (V_d / S) \quad (2.2.b)$$

Where:

- F_i = indentation force (nN)
- V_d = detector voltage (V)
- k_c = cantilever stiffness (nN/nm)
- S = detector sensitivity (V/nm)
- x_i = indentation depth (nm)
- x_p = piezo displacement (nm)

2. Five indentations of the PTFE sample were made immediately afterwards, which yielded curves as shown in Figure 2.9.
3. Equations 2.2.a and 2.2.b were applied to the raw data, yielding the curves shown in Figure 2.10.

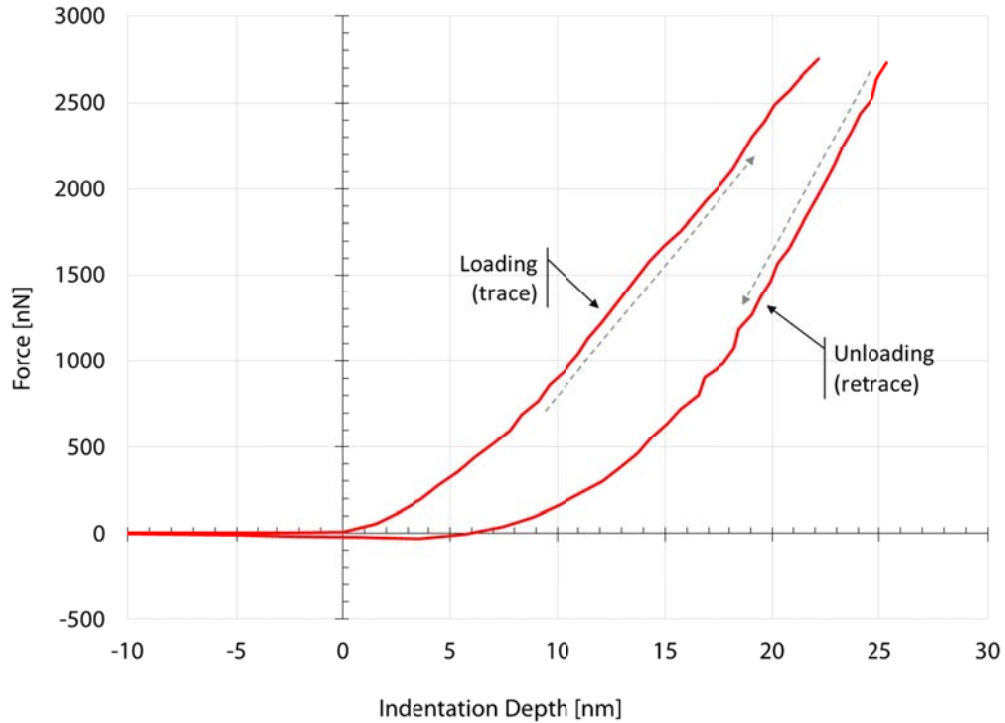


Figure 2.10. Processed nanoindentation curves (loading, unloading). Data produced from nanoindentation of sputtered, 223 nm thick fluorocarbon film on silicon substrate (50 W sputtering power and deposition temperature of 36 °C used in film preparation).

4. Both hardness and elastic modulus rely on the indented *cross-sectional area*, not simply the *depth*, so an indentation area function was assigned using the predetermined tip geometry.

$$A_i = A_t * (x_i / x_t) \quad (2.3)$$

Where:

- A_i = indentation area
- A_t = area of the tip at x_t
- x_i = indentation depth stiffness
- x_t = height of the tip

This area function makes the assumption of an ideally sharp tip, which in practice is typically not the case. Due to the relative sharpness of the (new) tip and the scales involved, tip deformation over time confounded the

measurement results. The resulting error introduced limited the analysis to comparing relative hardness and elastic modulus values between films.

5. Hardness values were calculated using the origin and peak of the loading (trace) curves of the processed data (shown in Figure 2.11, labeled in red) and Eqn. 2.4 below. Elastic modulus values were calculated using the linear portion of the unloading (retrace) curves (shown in Figure 2.11, labeled in blue) and Eqn. 2.5 below.

- a. Hardness values were calculated using Eqn. 2.4:

$$H = F_i / A_i \quad (2.4)$$

Where:

H = hardness

F_i = max indentation force on load (trace) curve

A_i = max indentation area on load (trace) curve

- b. Elastic modulus values were calculated using Eqn. 2.5:

$$E = (F_{i2} - F_{i1}) / (A_{i2} - A_{i1}) [44] \quad (2.5)$$

Where:

E = elastic modulus

F_{i1} = indentation force on the unloading (retrace) curve in the beginning of the linear section

F_{i2} = indentation force on the unloading (retrace) curve in the end of the linear section

A_{i1} = indentation area on the unloading (retrace) curve in the beginning of the linear section

A_{i2} = indentation area on the unloading (retrace) curve in the end of the linear section

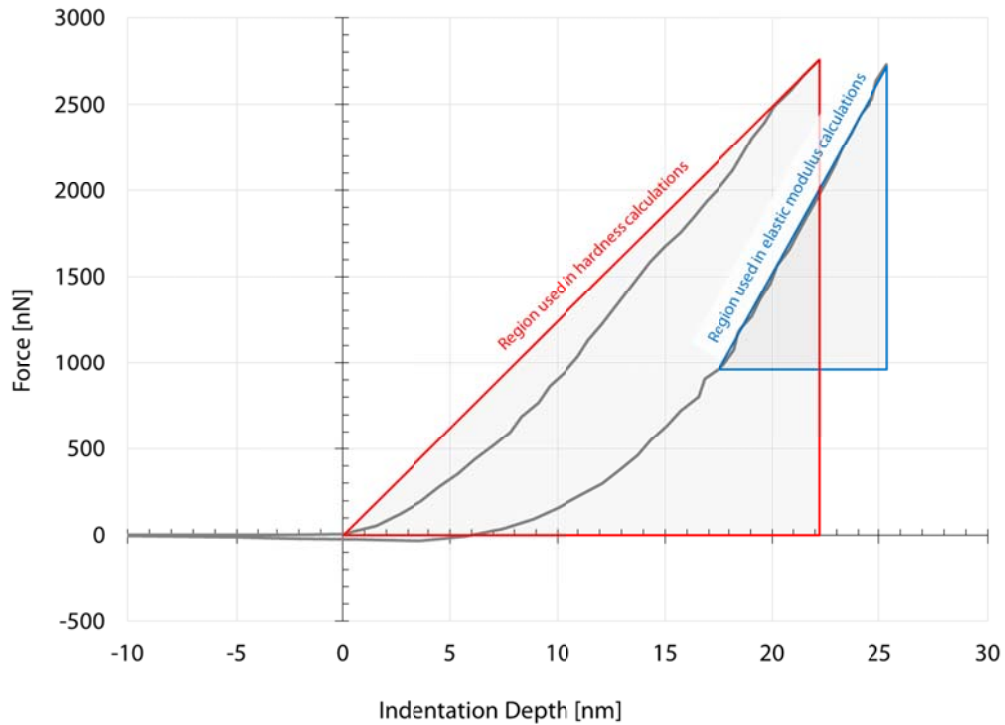


Figure 2.11. Regions used in calculating the hardness and elastic modulus of the films. Data produced from nanoindentation of sputtered, 223 nm thick fluorocarbon film on silicon substrate (50 W sputtering power and deposition temperature of 36 °C used in film preparation).

6. The mechanical property values from each indentation were then averaged.

The instrument used during the nanoindentation process was a Dimension 3100 AFM utilizing NanoMan-VS Nanolithography Software in contact mode. The resultant indentation depth was calculated using the indentation force, and this depth was kept below 10% of the total thickness of the film in order to minimize the potential substrate effects [15]. If films were produced in the same order of magnitude of thickness as the bulk target, bulk-likeness of the film could be established by comparing the resultant hardness and elastic modulus values of each film to the results measured from the bulk material. However, due to the drastic differences between the

bulk target (which was approximately 0.28 cm thick) and the sputtered fluorocarbon films (which were several orders of magnitude thinner than the target), bulk material indentations were performed only to establish the validity of the method, and values produced from the indentation of the films were compared relative to one another.

2.5.2 Contact Angle Measurements

To measure the hydrophobicity of the deposited films, water-surface contact angle was measured for every sample using a contact angle goniometer. A needle was used to place a drop of DI water on the surface of the sample from a height of 1 cm. The drop was allowed to settle for 30 seconds before a measurement was taken. Contact angle was determined through an optical scope with backlight illumination. Water was then wicked away from the un-wetted section of the wafer using a KimwipeTM to ensure additional measurements were unaffected. For each sample, contact angle was measured at three different locations along the diagonal of the wafer, and the results were then averaged. The standard triple-rinse was applied to each sample before measurements were taken to ensure a decontaminated surface. Bulk-likeness of the film was established by comparing the averaged film contact angles to the averaged bulk contact angles.

Chapter 3

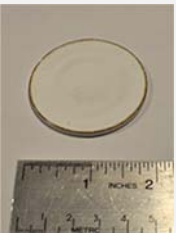
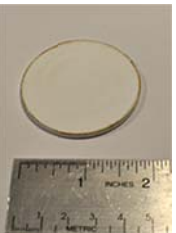
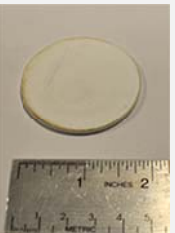
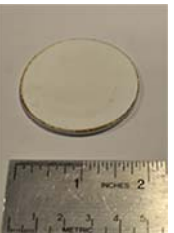
RESULTS

3.1 Sputtering Targets

Each compressed 7C PTFE sputtering target used in this study underwent similar mass loss and erosion ring formation. Post-deposition target pictures with initial and final masses for each target are presented in Table 3.1 below. The erosion ring on each of the targets is visible, and there was little-to-no warping of the target surface, indicating good contact with the copper backing plate. As mentioned in the previous chapter, targets were only used for a 2 hour, 50 W deposition and a 1 hour, 100 W deposition each. Average mass loss for each target was $1.882 \text{ g} \pm 0.332 \text{ g}$. In addition to the tabulated target data, an additional target was used for films prepared at sputtering powers of 150 W. Target integrity was nearly compromised, as the deepest points of the erosion ring were noticeably thinner than those of the other targets in Table 3.1 (see Figure 3.1 for comparison). The mass loss for this additional target (target #6) was 2.957 g from an initial 12.886 g.

Table 3.1. Post-deposition target pictures and initial / final masses for the targets used in the bulk of this study. Each target was used for a 2 hour, 50 W deposition and a 1 hour, 100 W deposition.

Target #	1	2	3	4	5
----------	---	---	---	---	---

Target (above)					
Target (profile)					
mass initial [g]	12.098	12.930	12.726	13.033	12.362
mass final [g]	10.153	11.341	10.298	11.266	10.681
mass loss [g]	1.945	1.589	2.428	1.767	1.681

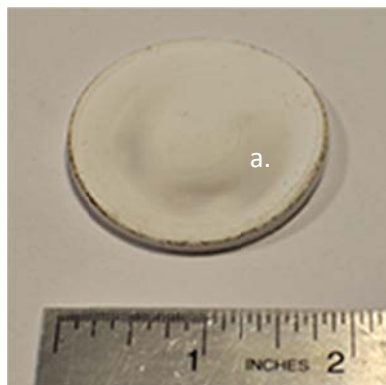


Figure 3.1. Target used for deposition of films using a sputtering power of 150 W. Dark areas on the target surface at a) are extremely thin and close to failure due to erosion through to the copper backing mesh.

3.2 Sputtering Deposition Rates

Film thickness variability across multiple depositions was established by depositing three different films on three different wafers each (three groups of three wafers, each group nominally identical). Deposition conditions for these three films were an RF sputtering power of 50 W and a sputtering temperature of 36 °C. Film thickness of the three wafers in each group was averaged and plotted against the other

two groups. Results of these three nominally identical depositions are given in Figure 3.2.

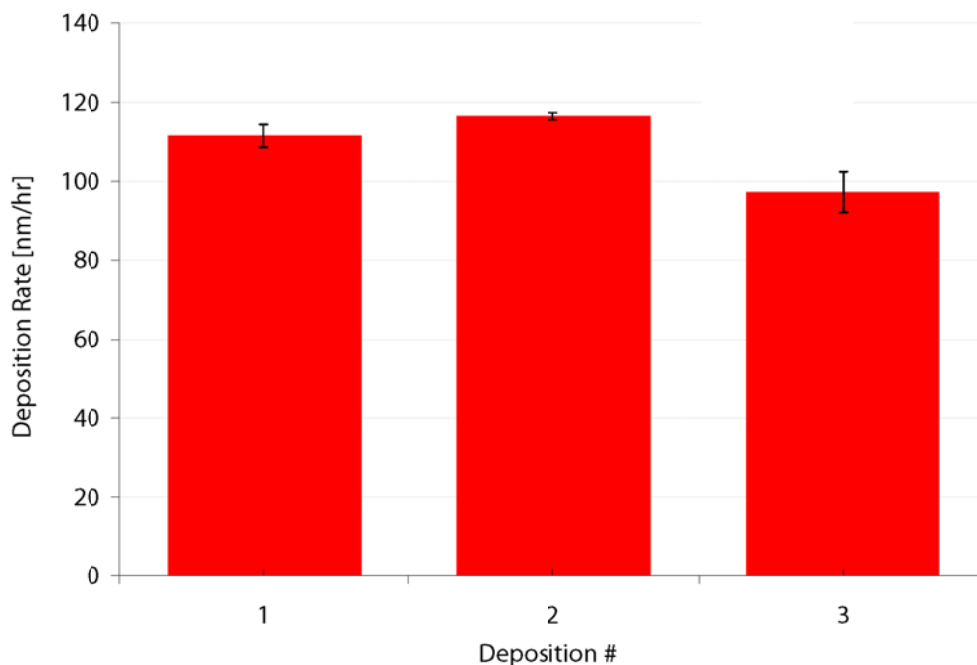


Figure 3.2. Deposition rate data measured from three films prepared under nominally identical sputtering and deposition conditions: sputtering power of 50 W and deposition temperature of 36 °C used. Error bars indicate the standard deviation calculated from averaging the film thickness over three samples within the same deposition, three measurements on three samples each.

Figure 3.3 shows the relationship between fluorocarbon film deposition rate and sputtering power. An unexpected, nonlinear relationship between deposition rate and sputtering power was observed. The maximum sputtering power used was 150 W; increasing sputtering power beyond 150 W, while possible in the sputtering system used, would cause the soft polymer targets to rapidly degrade, potentially damaging the sputtering system.

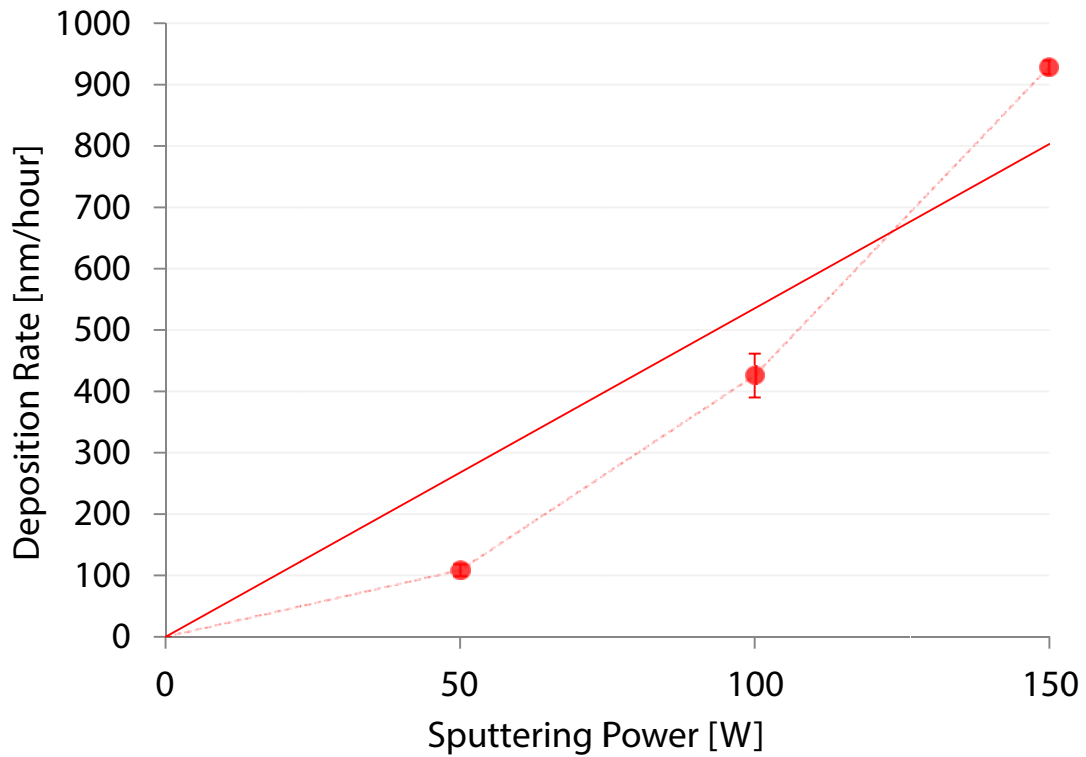


Figure 3.3. Deposition rate vs. RF sputtering power for sputtered fluorocarbon films. Deposition temperature for these films was 36 °C. Linear regression fit shown.

A nonlinear decrease in deposition rate was found for depositions performed at increasing deposition temperatures. Deposition rates for 50 W depositions and 100 W depositions at various deposition temperatures are plotted in Figure 3.4. The relative decrease in deposition rate was roughly the same for both sputtering powers, with an immediate and severe drop in deposition rate seen with a corresponding temperature increase of just 32 °C (from ≈ 36 °C to 68 °C). Across both sputtering powers, there were no films of measurable thickness ($>$ approx. 5 nm) formed at deposition temperatures of 200 °C. Similarly, no films of significant thickness were formed using deposition temperatures of 100 °C and sputtering powers of 50 W. All films deposited at similar deposition temperatures were prepared from the same sputtering

targets (i.e. 50 W and 100 W films deposited at 68 °C were prepared from the same target).

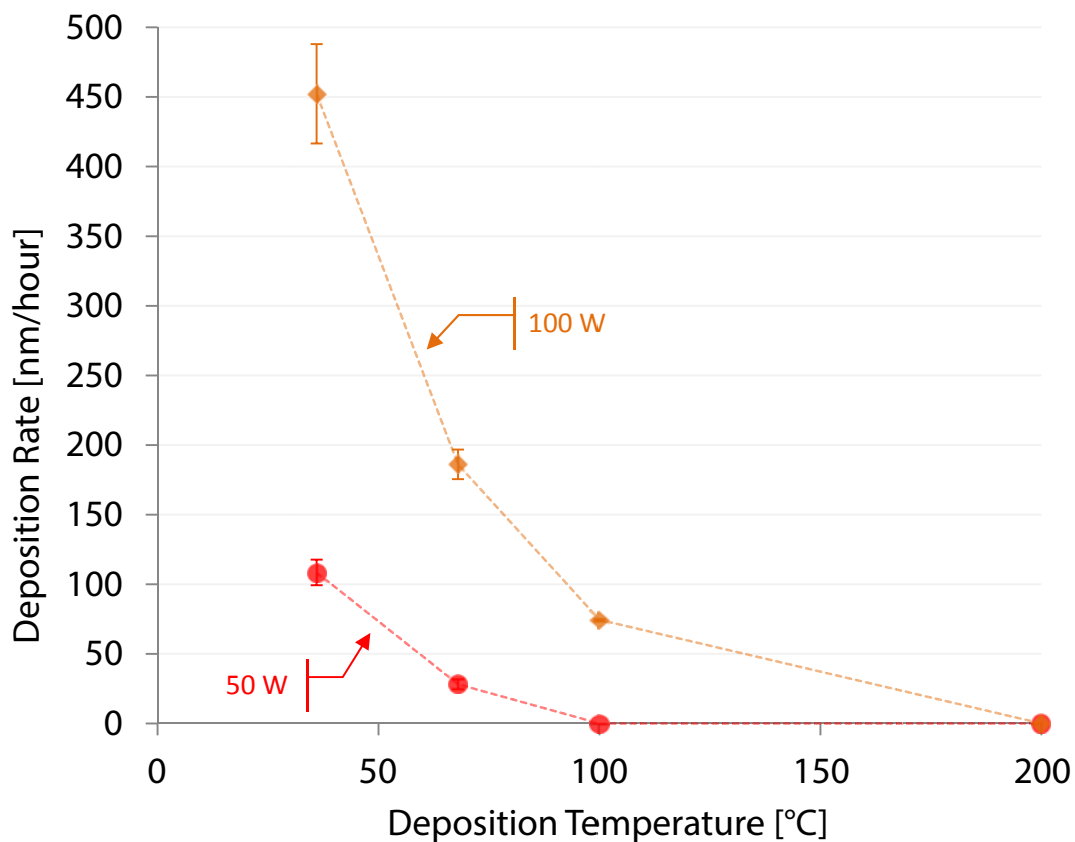


Figure 3.4. Deposition rate vs. RF sputtering power for sputtered fluorocarbon films. Films sputtered at similar temperature were prepared from the same sputtered targets. Connecting lines are not from curve fitting and are meant only as a visual guide.

The change in film thickness upon post-deposition annealing was also measured for each film. These results for the same three sample sets shown in Figure 3.2 are given in Figure 3.5. It is important to note that the data shown in Figure 3.2 and Figure 3.5 are not from the exact same films pre and post-anneal, but rather different films from the same sample/deposition sets. Inconsistencies in film thickness

within the same sample set thus complicate these measurements, as the assumption is made that the thickness is uniform over all wafers within one deposition. Post-deposition annealing ultimately caused film thickness to change an average of -9.7% (with a standard deviation of 5.8%).

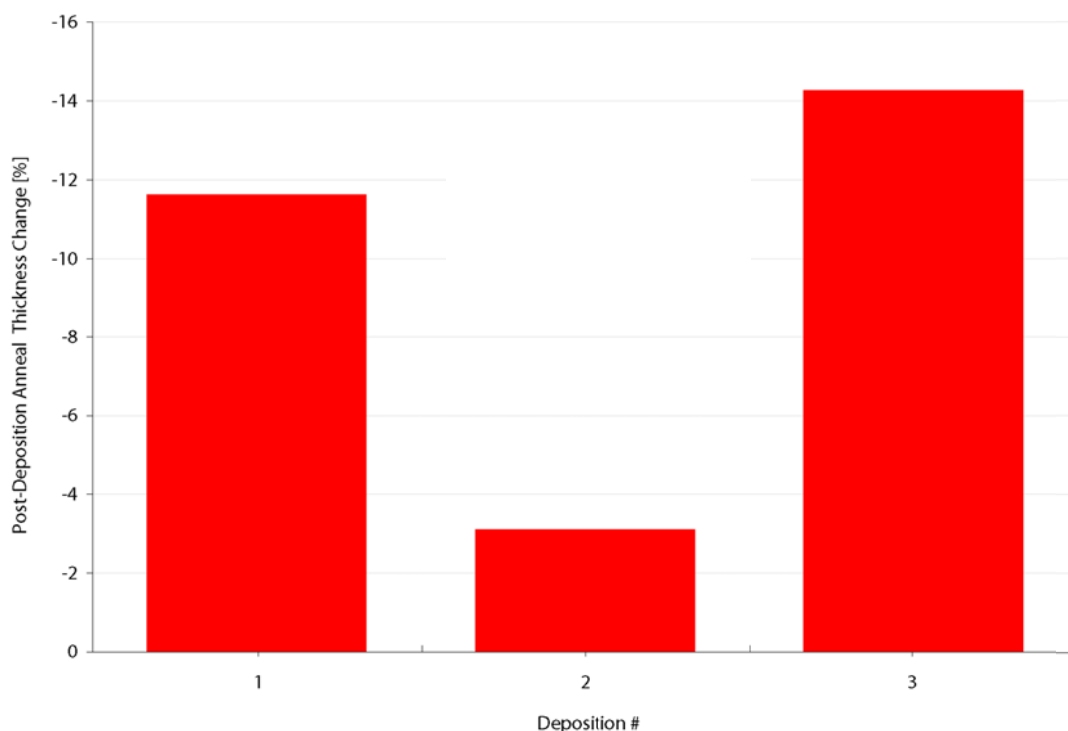


Figure 3.5. Percent change in thickness for three films prepared under nominally identical deposition conditions (50 W sputtering power at 36 °C) after post-deposition annealing.

3.3 Chemical Characterization

3.3.1 Fourier Transform Infrared Spectroscopy

A FTIR spectrum was recorded for the bulk target material in order to have a baseline for comparison with sputtered film spectra. The resultant spectrum (Figure 3.6) is similar to the results found in the literature for bulk PTFE [7, 12, 21, 45–49].

The prominent two peaks located at approximately 1150 cm^{-1} – 1205 cm^{-1} are indicative of the vibrational modes of linear CF_2 chain structures [50]. The peak located at 1150 cm^{-1} is associated with symmetric stretching of CF_2 and the peak located at 1205 cm^{-1} is associated with asymmetric stretching of CF_2 ; both are characteristic of (crystalline) bulk PTFE.

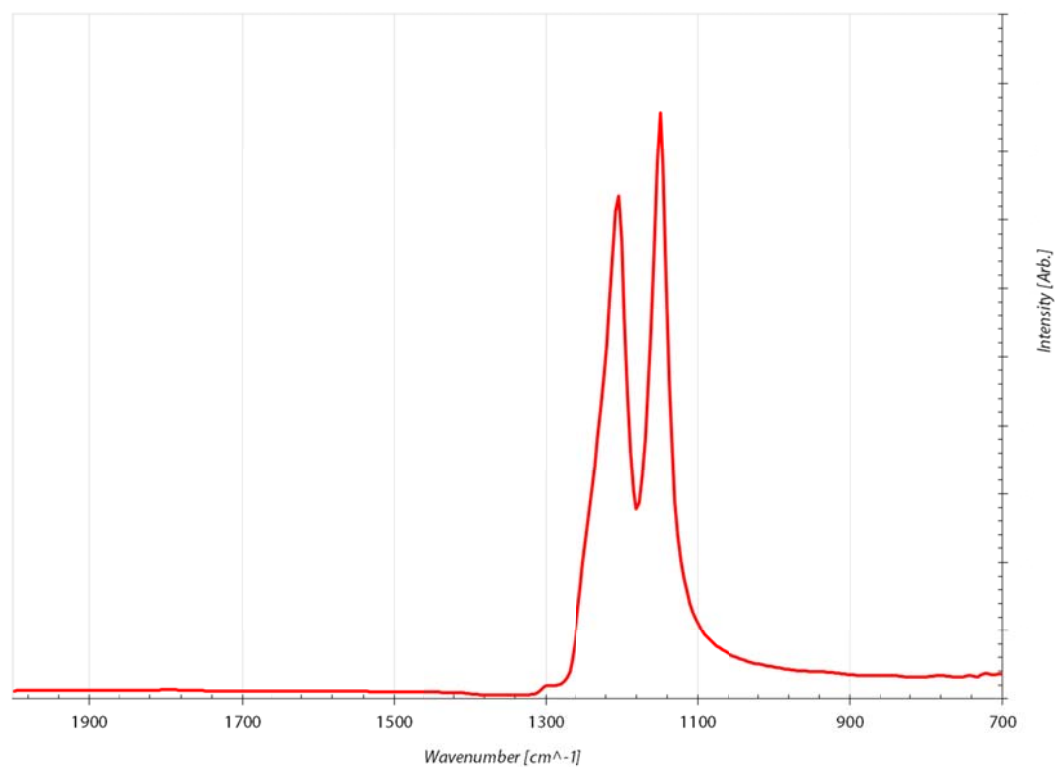


Figure 3.6. An FTIR spectrum generated from a sample of bulk 7C PTFE.

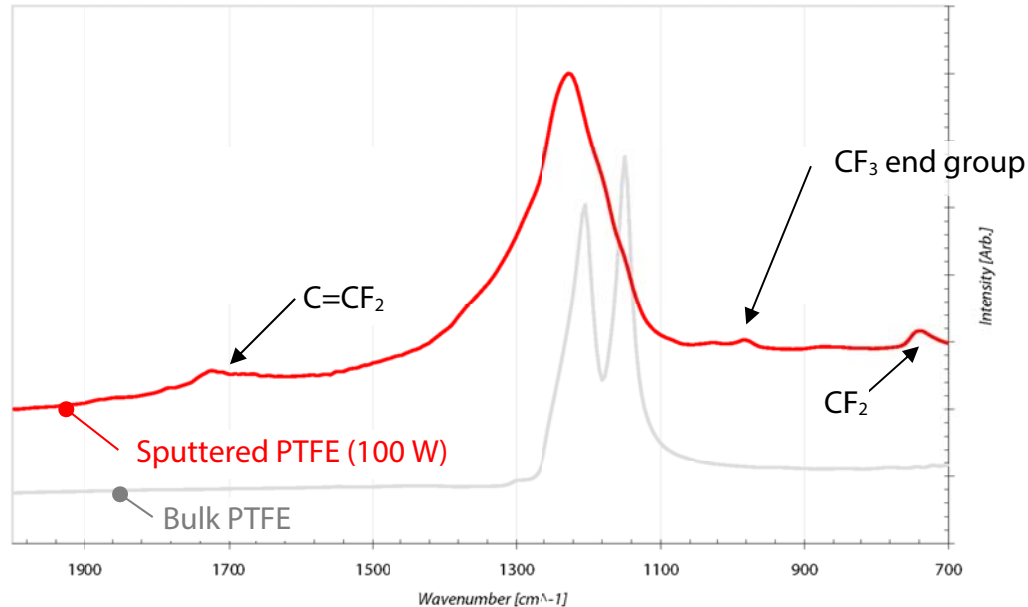


Figure 3.7. A representative FTIR spectrum from a sputtered (100 W at 36 °C) PTFE film. Spectrum from corresponding bulk parent target material (see Figure 3.6, above) underlaid for comparison.

Spectra from the sputtered fluorocarbon films have similar characteristics, though differ significantly from that acquired from the bulk target. A representative spectrum is given in Figure 3.7, produced from a film prepared at 100 W and 36 °C. Of note in the complete fluorocarbon film spectra are several peaks present outside of the CF₂ stretching region (roughly 1100 cm⁻¹ to 1300 cm⁻¹) that do not appear in the spectrum of the bulk PTFE. Assignments for these peaks were made according to the data in Table A.1 using values established from the literature, and are overlaid on Figure 3.7, and tabulated in Table 3.2. None of these extraneous peaks are present in the IR spectrum of the bulk PTFE, and their appearance is therefore taken to indicate non-bulk-likeness. However, two peaks (at 625 cm⁻¹ and 630 cm⁻¹) are associated with the presence of CF₂ bonds of different configurations; because CF₂ acts the backbone of PTFE, it is unclear whether appearance of these peaks indicates a shift in sputtered

film bulk-likeness. The modulation of sputtering power, post-deposition annealing, and film thickness seem to have little effect on the appearance of these extraneous peaks. Increasing the deposition temperature to 100 °C appears to cause the disappearance of peaks associated with CF₃ terminating bonds and amorphous fluorocarbon, which would indicate an increase in film bulk-likeness. Unfortunately the signal / noise ratio of films produced at those higher temperatures is low due to a dramatic decrease in film thickness.

Table 3.2. Peak appearances and associations found in the IR spectra outside of the CF₂ stretching region produced from sputtered fluorocarbon films. “(Noisy)” indicates a region where the signal / noise ratio was too low to clearly indicate the presence or absence of a peak in that region.

Wavenumber	1729 cm ⁻¹	985 cm ⁻¹	700-800 cm ⁻¹	630 cm ⁻¹	625 cm ⁻¹
Bond Association	-(CF = CF)- [51]	CF ₃ [8, 52]	Amorphous CF [51, 52]	CF ₂ Symmetric Deformation [53]	CF ₂ [8]
Sputtered Fluorocarbon Film, 50 W	(Noisy)	Peak Appears	Peak Appears	None	None
Sputtered Fluorocarbon Film, 100 W	Peak Appears	Peak Appears	Peak Appears	None	None
Sputtered Fluorocarbon Film, 150 W	Peak Appears	Peak Appears	Peak Appears	None	None
Sputtered Fluorocarbon Film, 50 W 36 °C	(Noisy)	Peak Appears	Peak Appears	None	None
Sputtered Fluorocarbon Film, 50 W 68 °C	None	Peak Appears	Peak Appears	None	Peak Appears
Sputtered Fluorocarbon Film, 50 W 100 °C	(Noisy)	None	None	None	Peak Appears
Sputtered Fluorocarbon Film, 100 W	Peak Appears	Peak Appears	Peak Appears	None	None

Sputtered Fluorocarbon Film, 100 W with Post-Deposition Anneal	Peak Appears	Peak Appears	Peak Appears	None	None
Sputtered Fluorocarbon Film, 100 W 452 nm	Peak Appears	Peak Appears	Peak Appears	None	None
Sputtered Fluorocarbon Film, 100 W 3545 nm	Peak Appears	Peak Appears	Peak Appears	Peak Appears	None

The CF₂ stretching region in FTIR lies between roughly 1300 cm⁻¹ and 1100 cm⁻¹. With the sputtered fluorocarbon films, there is a strong, broad peak present in that region, however it is difficult to differentiate between specific bond types (namely between CF₃ and CF₂ groups) [54]. CF₃ has a larger infrared absorbance spectrum than that of CF₂, and there is a large amount of overlap between the two [55]. With this in mind, the metric of bulk-likeness of each film was measured any shift in the fit-Gaussian curves towards that of those found in bulk PTFE, as well as the emergence of a two-peak spectrum.

A comparison of FTIR spectra (in the CF₂ stretching region) for films prepared using increasing sputtering powers is given in Figure 3.8. FTIR spectra of the sputtered films were not strongly variant with sputtering power, however curves fit to the spectrum of the 50 W sputtered film (peaks at 1233 cm⁻¹ and 1203 cm⁻¹) appear to shift towards those peaks found in the spectrum of the bulk PTFE (peaks at 1204 cm⁻¹ and 1150 cm⁻¹) as sputtering power is increased. This result would indicate that the bulk-likeness of the resulting fluorocarbon film is increased as sputtering power is increased during film deposition.

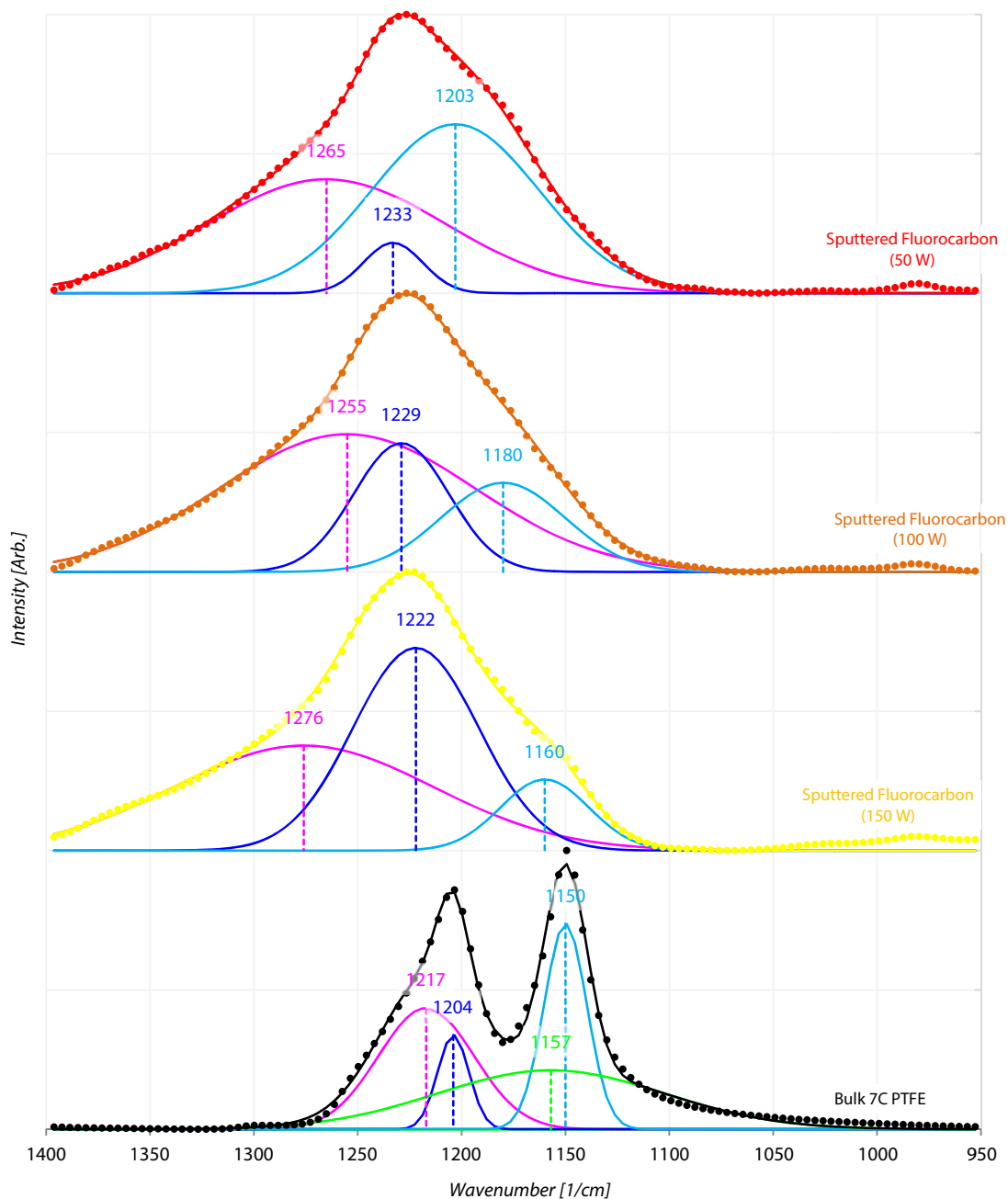


Figure 3.8. FTIR spectra in the CF₂ stretching region for films sputtered at increasing RF sputtering powers. Spectra of 50 W, 100 W, and 150 W power levels are shown; all produced at a deposition temperature of 36 °C. Spectrum produced from bulk PTFE given as a reference (bottom). The location of the fit peak maxima [1/cm] are indicated above each peak.

FTIR spectra for films prepared using a sputtering power of 50 W and at various deposition temperatures are given in Figure 3.9. When the deposition temperature is increased from 36 °C to 68 °C there is a slight decrease in the area and slight increase in height of the fit curve located at 1180 cm^{-1} , however no shift in peak center is observed. The fit curve located at 1229 cm^{-1} shows a decrease in both height and area, but likewise no shift in peak center. The drastic decrease in film thickness with increasing sputtering temperatures severely affects the resultant FTIR spectra – the signal / noise ratio decreases noticeably in films prepared using temperatures at or above 100 °C. At higher temperatures, film thickness diminishes such that the signal / noise ratio renders spectral analysis meaningless (the 200 °C deposition spectra is not shown because of this).

There is a drastic difference between spectra as deposition temperature is increased from 68 °C to 100 °C. Surprisingly, even though little / no film thickness was detected via interferometry (see Figure 3.4), and even though the signal / noise ratio was very low, the spectrum for the film prepared at 100 °C nonetheless shows peaks associated with a crystalline, CF_2 chain structure. Once background interference is corrected for (the fit curve located at 1183 cm^{-1} is needed due to the lack of signal), two distinct peaks emerge: one located at 1211 cm^{-1} and the other at 1156 cm^{-1} , similar to those found at 1204 cm^{-1} and 1150 cm^{-1} in the bulk spectrum. These peaks indicate that as deposition temperature is increased, although film thickness decreases drastically, there is an increase in the bulk-likeness of the sputtered fluorocarbon film structure.

Additionally, comparison of film spectra pre- and post-anneal is given in Figure 3.10. FTIR revealed little change in film structure through this process.

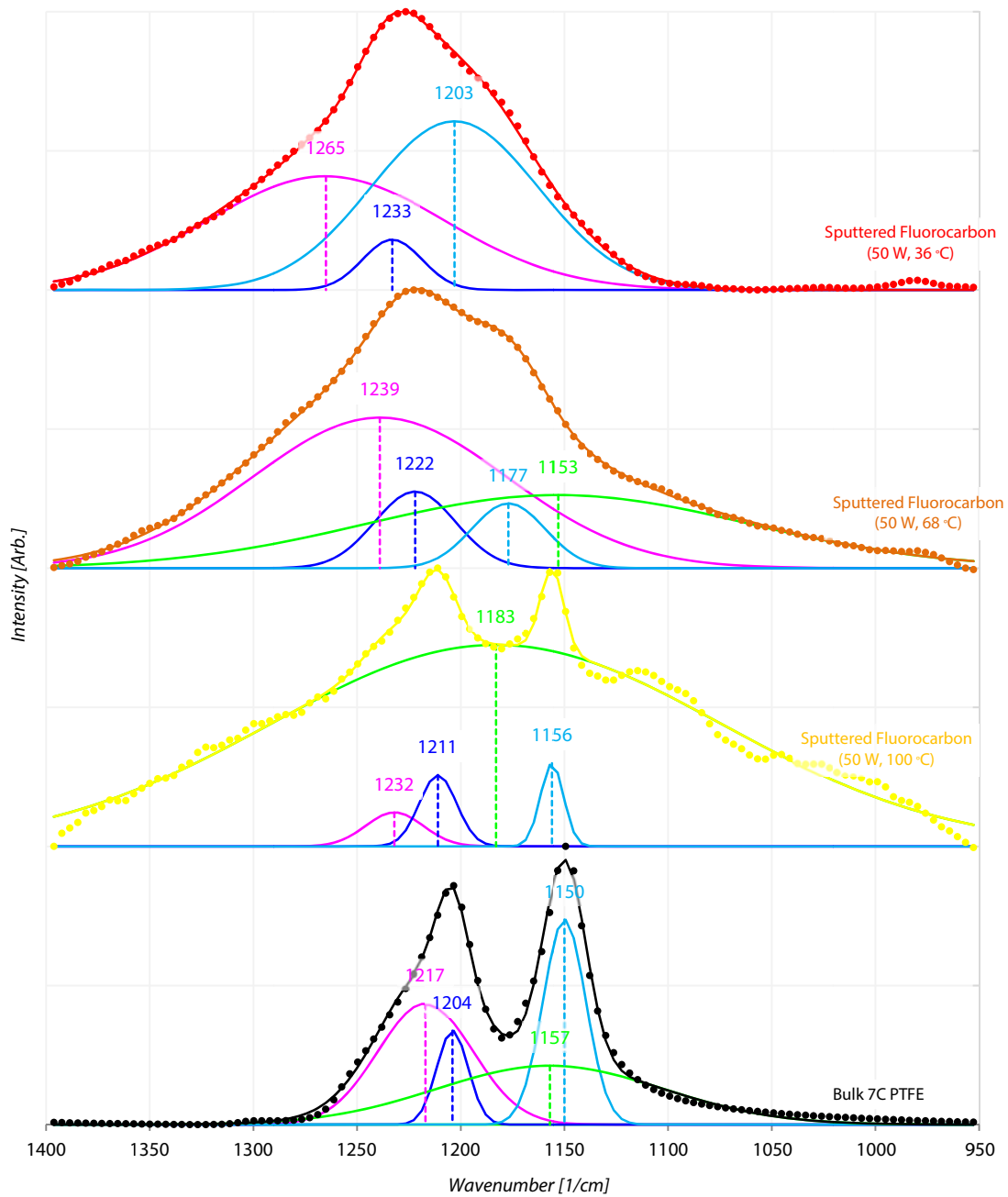


Figure 3.9. FTIR spectra in the CF₂ stretching region for films sputtered at increasing deposition temperatures. Spectra for film prepared at temperatures of 36 °C, 68 °C, and 100 °C are shown; all produced using a sputtering power of 50 W. Spectrum produced from bulk PTFE given as a reference (bottom). The location of the fit peak maxima [cm⁻¹] are indicated above each peak.

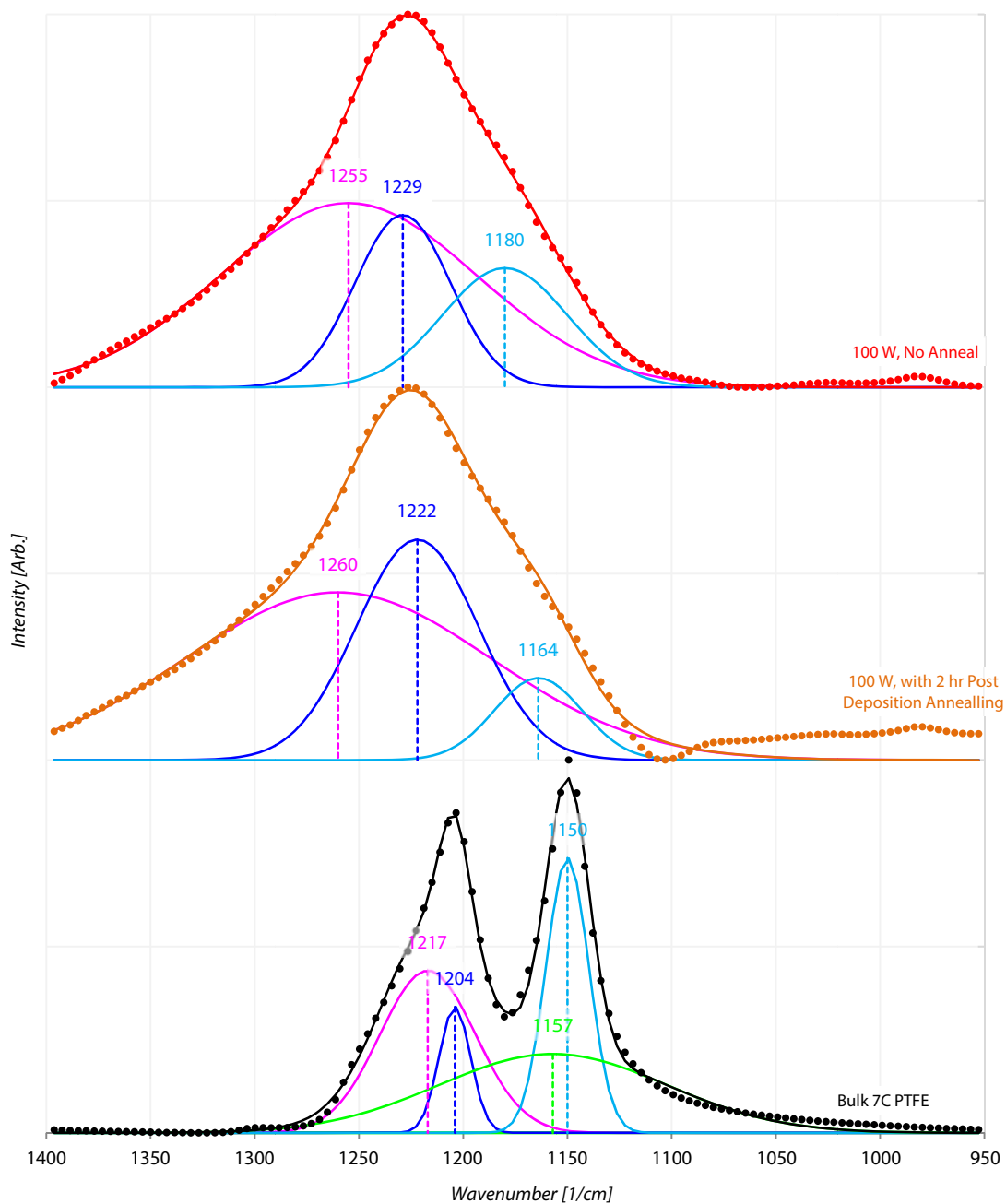


Figure 3.10. FTIR spectra in the CF₂ stretching region for pre-anneal and post-anneal films; both produced using deposition temperature of 36 °C. Spectrum produced from bulk PTFE given as a reference (bottom). The location of the fit peak maxima [cm⁻¹] are indicated above each peak.

The use of transmission-mode FTIR means that the spectra presented here take into account the fluorocarbon structure throughout the thickness of the film. Changes in spectral qualities due to changes in film thickness have to be considered. Figure 3.11 demonstrates how film thickness can affect the FTIR results, with one film prepared at 100 W and 36°C with a resulting film thickness of 452 nm, and the other film prepared under identical deposition conditions having a thickness of 3545 nm. The emergence of a prominent shoulder peak in Figure 3.11.a, resembling the two-peak spectra found in the bulk PTFE, suggests increasing spectral similarity to that of bulk PTFE and therefore an increase in bulk-likeness as film thickness increases. Curve fitting reveals a shift in peak center from 1180 cm^{-1} to 1157 cm^{-1} (compared to a peak located 1150 cm^{-1} in the bulk spectrum). This may be due to improved PTFE bulk-likeness in chemistry and structure with decreased substrate effects. Alternatively, these changes could be due to an increase in signal inherent in the FTIR process (i.e., the thicker films caused more infrared absorption in the spectrometer, and thus created spectra with greater accuracy in structural representation).

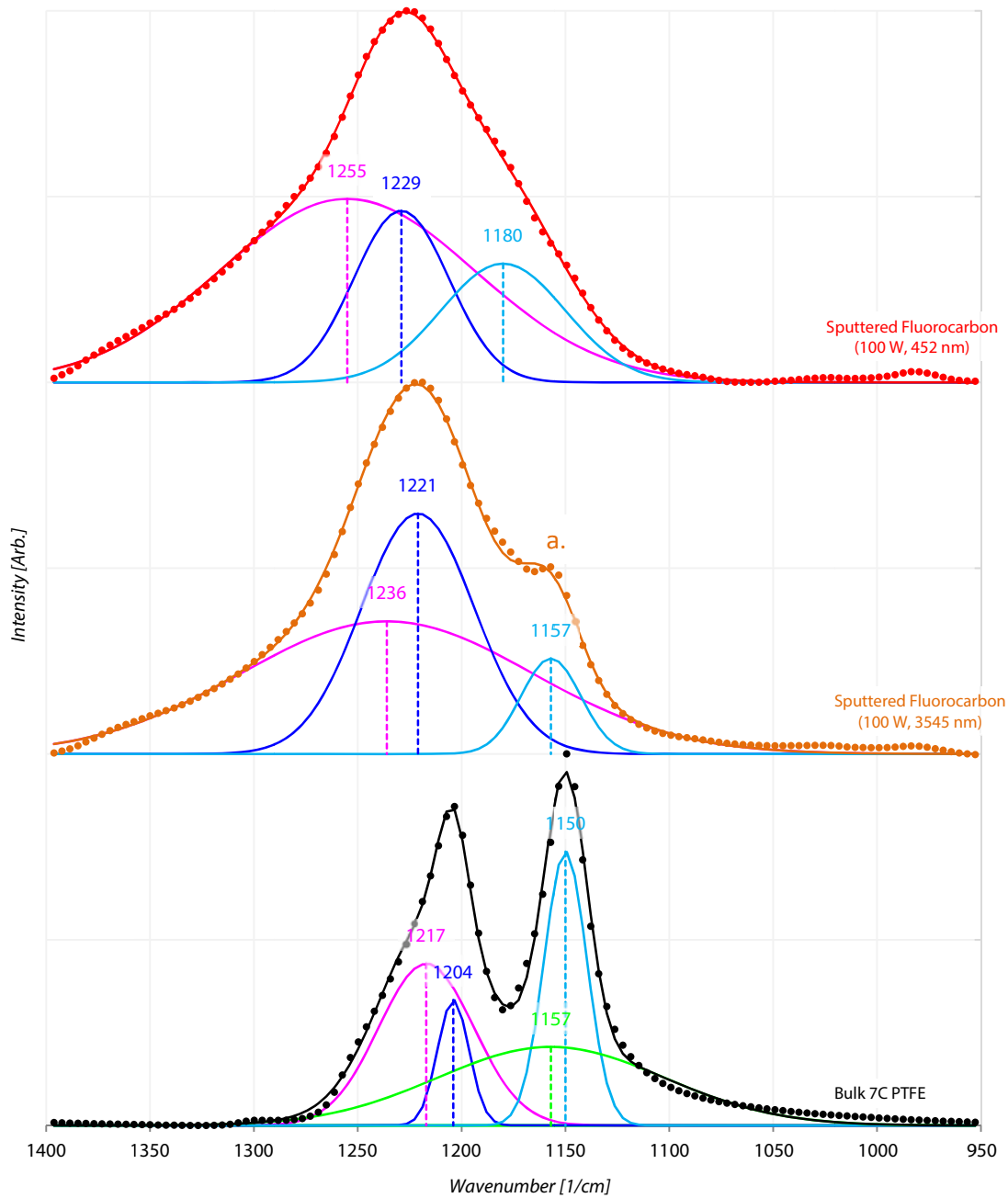


Figure 3.11. FTIR spectra of thick and thin fluorocarbon films prepared using the same deposition conditions (deposition temperature measured at approximately 36 °C). Spectrum produced from bulk PTFE given as a reference (bottom). The location of the fit peak maxima [cm^{-1}] are indicated above each peak. Emergence of secondary peak at 'a.' is noted (middle).

3.3.2 X-Ray Photoelectron Spectroscopy

Bond-peak assignment of XPS spectra of PTFE typically begins with the assignment of $-\text{CF}_2\text{-CF}_2\text{-}_n$ to the most prominent peak in the C1s region, which is found at approximately 292 eV. This assignment serves as an energy level calibration for the XPS instrument across studies and trials. As seen in Figure 1.9, the $-\text{CF}_2\text{-CF}_2\text{-}_n$ bond type is the primary peak found in XPS spectra obtained from long-chain bulk PTFE, as the “chain” is formed from linked CF_2 bonds (Figure 1.2), with CF_3 end groups terminating each of the long chains. In sufficiently thick (>10 nm) sputtered amorphous fluorocarbon films prepared from PTFE targets, this peak is typically also the most common bond type found in the XPS spectra [10, 13, 15, 26]. Peaks in the XPS spectra in this study were assigned bond groups, based on assignments compiled from the literature, the sources of which are presented in Table A.2. Gaussian fitting parameters for the C1s bond spectra are shown for increasing power (Figure 3.12), and for increasing deposition temperature (Figure 3.13), with each spectra annotated with the ranges of binding energies as suggested in the literature for particular bond assignments. For XPS spectra in this study, five peaks were assigned bond types, given in Table 3.3, and the area under each peak was associated with the relative presence of each bond type.

Table 3.3. Bond types assigned to Gaussian curves fit to XPS spectra.

Bond Assignment	Approximate Binding Energy [eV]	Peak found in bulk PTFE?
CF_3	293.5	Yes – terminating bond
$-\text{CF}_2\text{-CF}_2\text{-}_n$	292.5	Yes – primary bond found
CF	287	No
C-CF_x	291.5	No

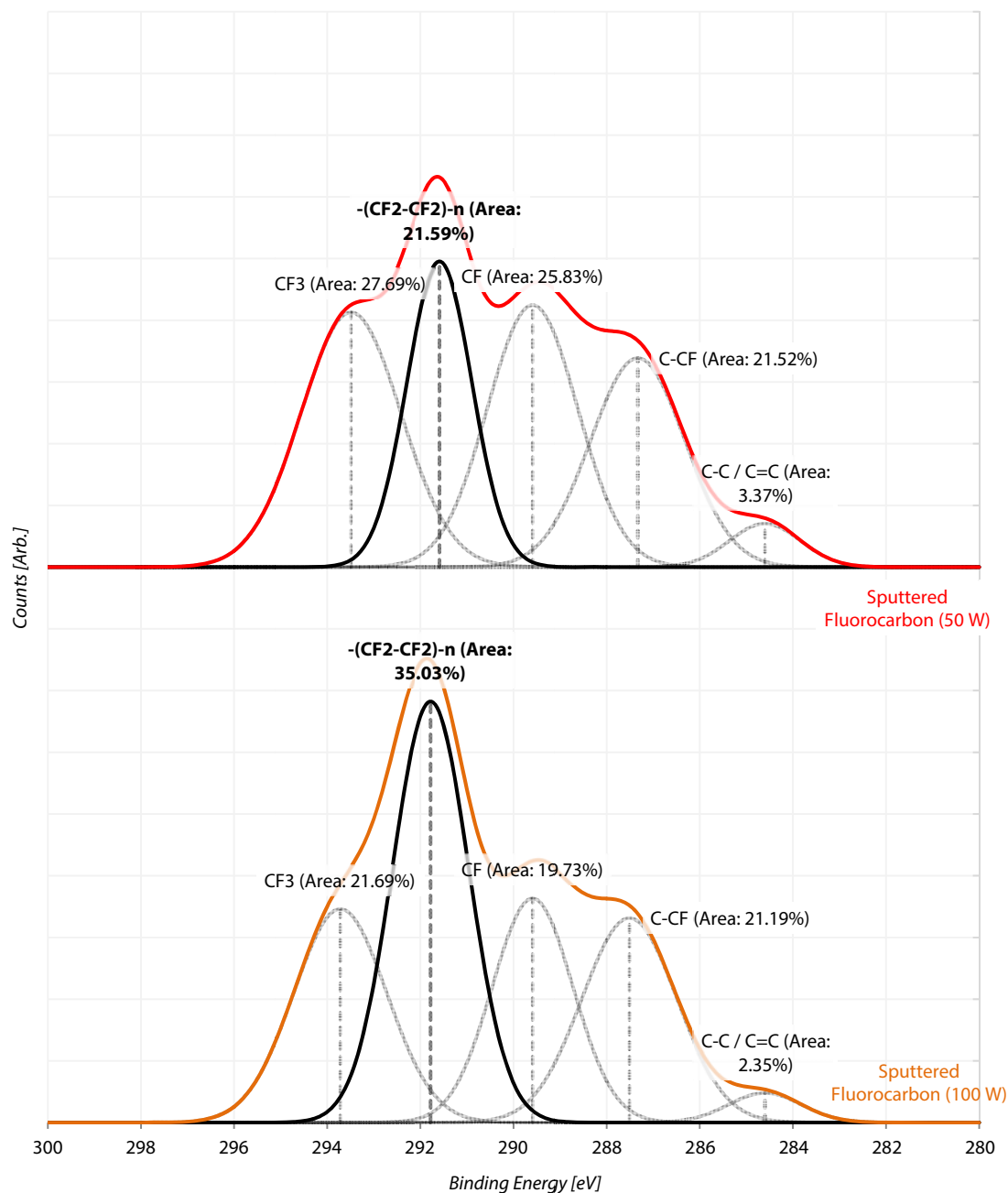


Figure 3.12. XPS spectra and curve fitting for sputtered PTFE films prepared using 50 W sputtering power (top) and 100 W sputtering power (bottom). Both films prepared using deposition temperature of 36 °C.

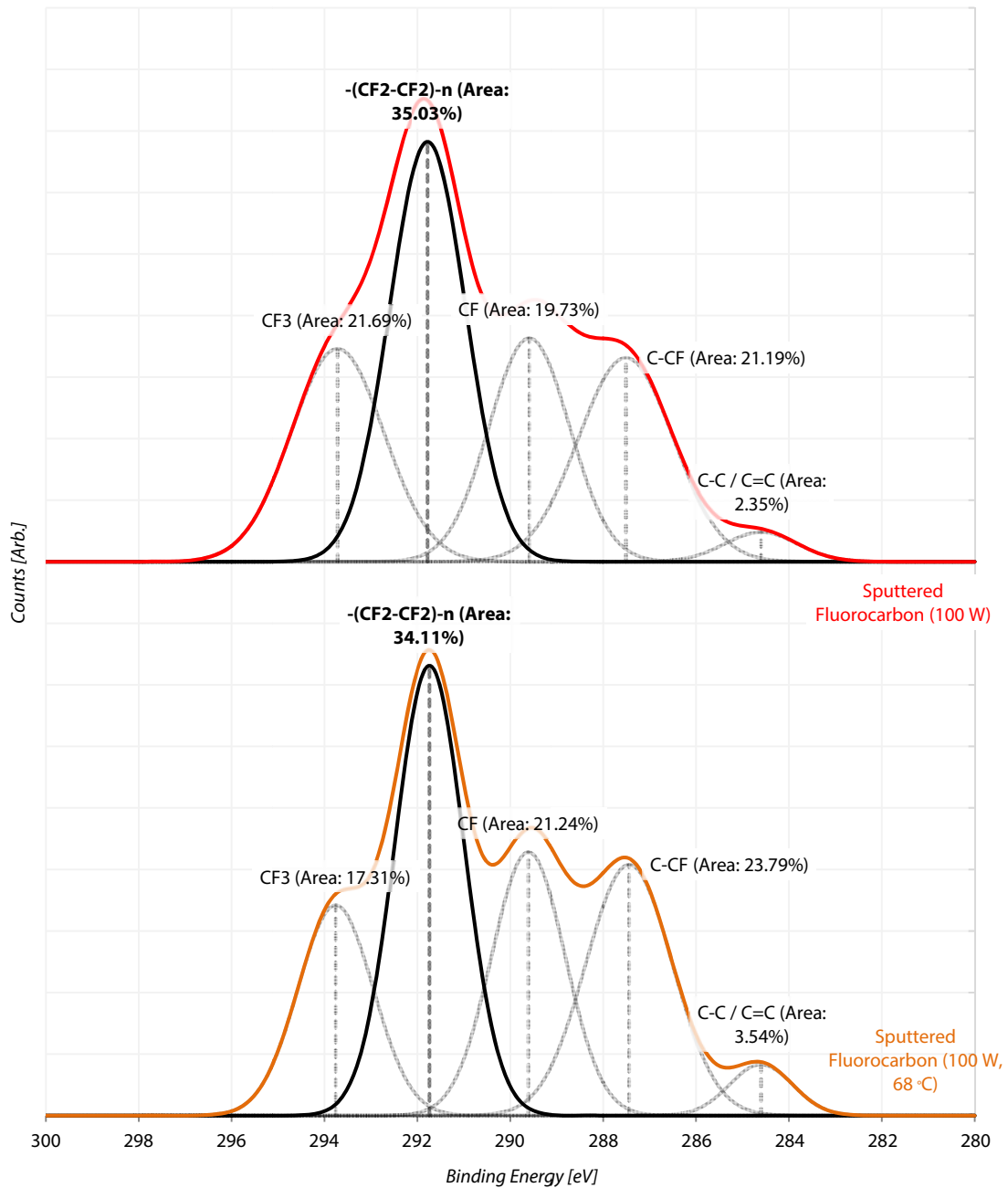


Figure 3.13. XPS spectra and curve fitting for sputtered PTFE films prepared using deposition temperatures of 36 °C (top) 68 °C (bottom). Both films prepared using sputtering powers of 100 W.

The two bond types found in the structure of the bulk PTFE are CF_3 and $-\text{[CF}_2\text{-CF}_2\text{]}_n-$. These two bonds combine to make long fluorocarbon chains, with the $-\text{[CF}_2\text{-CF}_2\text{]}_n-$ bonds consisting of the bulk of the chain and the CF_3 bonds serving as the terminating end bonds. Since each spectra contains both of these bond types, the ratio of $-\text{[CF}_2\text{-CF}_2\text{]}_n-$ to CF_3 bond types is taken as a measure of fluorocarbon chain quality (this metric is explained visually in Figure 2.6). For bulk PTFE, the $-\text{[CF}_2\text{-CF}_2\text{]}_n-$ to CF_3 ratio has been reported to be approximately 22.5 [21]. This ratio is shown for all three spectra in Figure 3.14. When using this metric, by increasing the sputtering power from 50 W to 100 W the ratio of bonds more than doubles from 0.78 to 1.62 (a 107.7% increase). The increase is less dramatic when increasing in deposition temperature from 36 °C to 68 °C, with the ratio rising from 1.62 to 1.97 (a 21.60% increase). These results are consistent with data produced from FTIR, which show a decrease in a peak associated with CF_3 as sputtering temperature is increased, as indicated in Table 3.2. If an increase in this bond ratio is taken as a measure of bulk-likeness, it is shown that an increase in either sputtering power or sputtering temperature increases the bulk-likeness of the film.

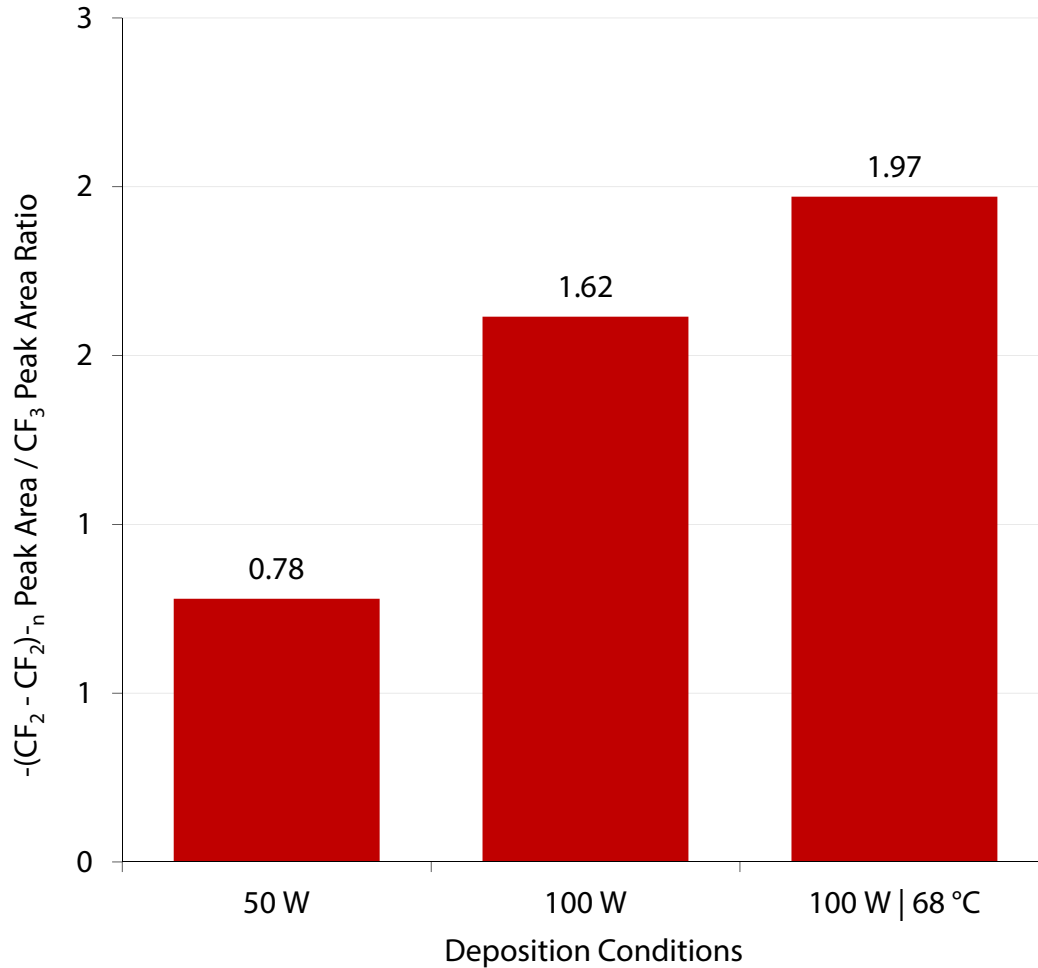


Figure 3.14. $-\text{[CF}_2\text{-CF}_2\text{]}_n$ peak area / CF_3 peak area ratio of the C1s spectrum for sputtered fluorocarbon films prepared at two different sputtering powers (50 W, 100 W, both at 36 °C), and using like sputtering powers (100 W) with two different deposition temperatures (36 °C and 68 °C).

The peak areas for the non-bulk-like C=C, CF and C-CF_x bond types are of the same order of magnitude the $-\text{[CF}_2\text{-CF}_2\text{]}_n$ and CF_3 bond types for all three spectra. These bond types have not been shown to be present in significant quantities in the spectra for the bulk PTFE material [13, 21]. The percentage of the C1s spectrum taken up by the $-\text{[CF}_2\text{-CF}_2\text{]}_n$ bonds indicate how much of the film consists of

fluorocarbon chains. Therefore, for the purposes of XPS data interpretation in this study, the percentage of the C1s spectrum taken up by the $-\text{[CF}_2\text{-CF}_2\text{]}_n$ bond peak area is quantified as a metric indicative of sputtered film bulk-likeness (this metric is represented visually in Figure 2.7). This percentage is shown for all three spectra in Figure 3.15. By increasing the sputtering power from 50 W to 100 W $-\text{[CF}_2\text{-CF}_2\text{]}_n$ peak area as a percentage of the total C1s area increases from 21.59% to 35.03%. When increasing in deposition temperature from 36 °C to 68 °C, the percentage decreases from 35.03% to 34.11%. Using this metric it is shown that an increase in sputtering power increases the bulk-likeness of the film, but an increase in deposition temperature marks, if anything, a slight decrease in the-bulk likeness of the film.

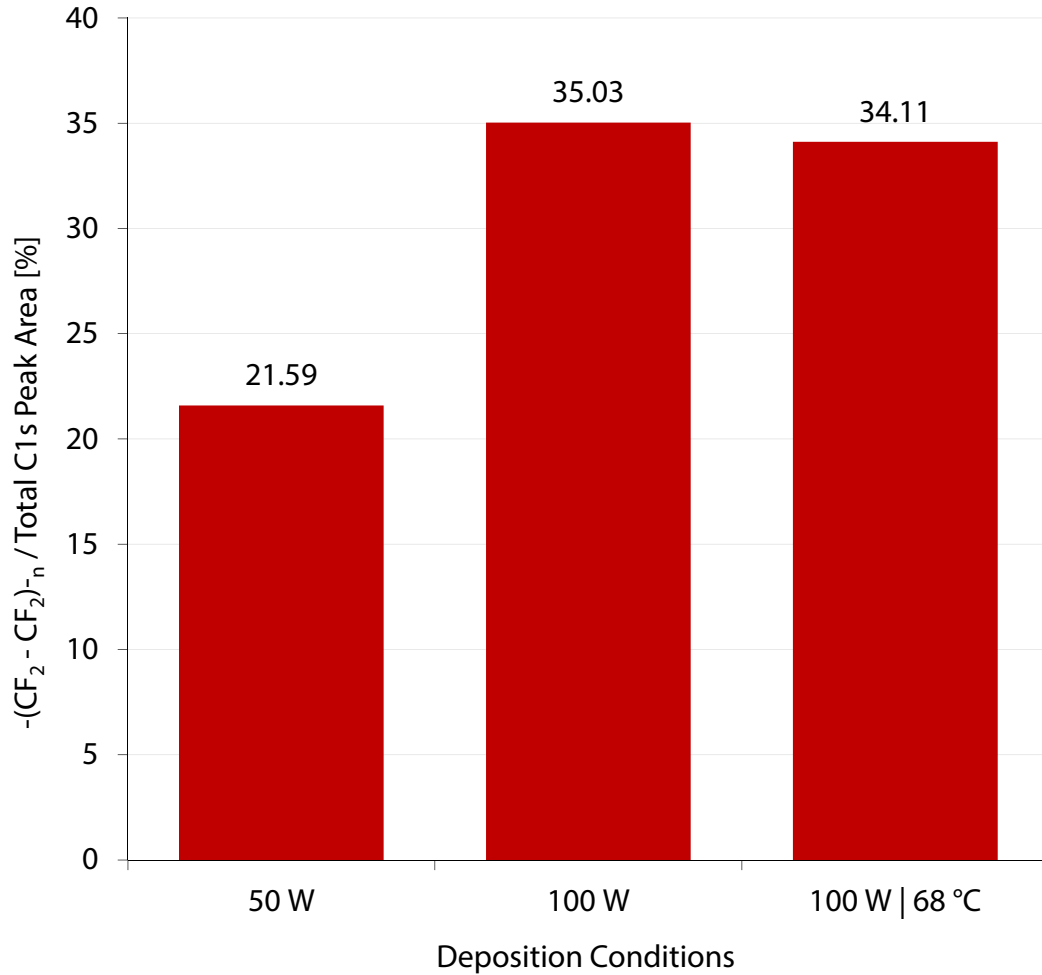


Figure 3.15. $-\text{[CF}_2\text{-CF}_2\text{]}_n$ peak area percentage of total peak area of the C1s spectrum for sputtered fluorocarbon films prepared using two different sputtering powers (50 W and 100 W, both at 36 °C), and using like sputtering powers (100 W) with two different deposition temperatures (36 °C and 68 °C).

The total F1s peak area / C1s peak area ratio can also be utilized as a method of structural quantification when using XPS on fluorocarbon films (the values for this ratio are shown in Figure 2.8). The ratio of F1s and C1s peak areas roughly correlates to the atomic percentage (at.%) of the fluorine and carbon in the films, with the bulk value for this ratio reported as 2.03 by Chen et. al. [21]. The F1s total area vs. C1s

total area ratio measured in the films from this study are given in Figure 3.16. Some difference was observed between F1s / C1s ratios of the various measured samples, with an increase in sputtering power from 50 W to 100 W yielding a slight increase from 5.71 to 6.13 (7.36%), and an increase in deposition temperature from 36 °C to 68 °C yielding a slight decrease from 6.13 to 5.87 (-4.24%), suggesting that an increase in power is weakly associated with a structure containing more fluorine, while an increase in deposition temperature is weakly associated with a structure containing less fluorine. F1s/C1s ratios reported in the literature typically fall below the reported values found for the bulk material [12, 21, 26], however results in this study are found to be 3X greater than those of the bulk PTFE.

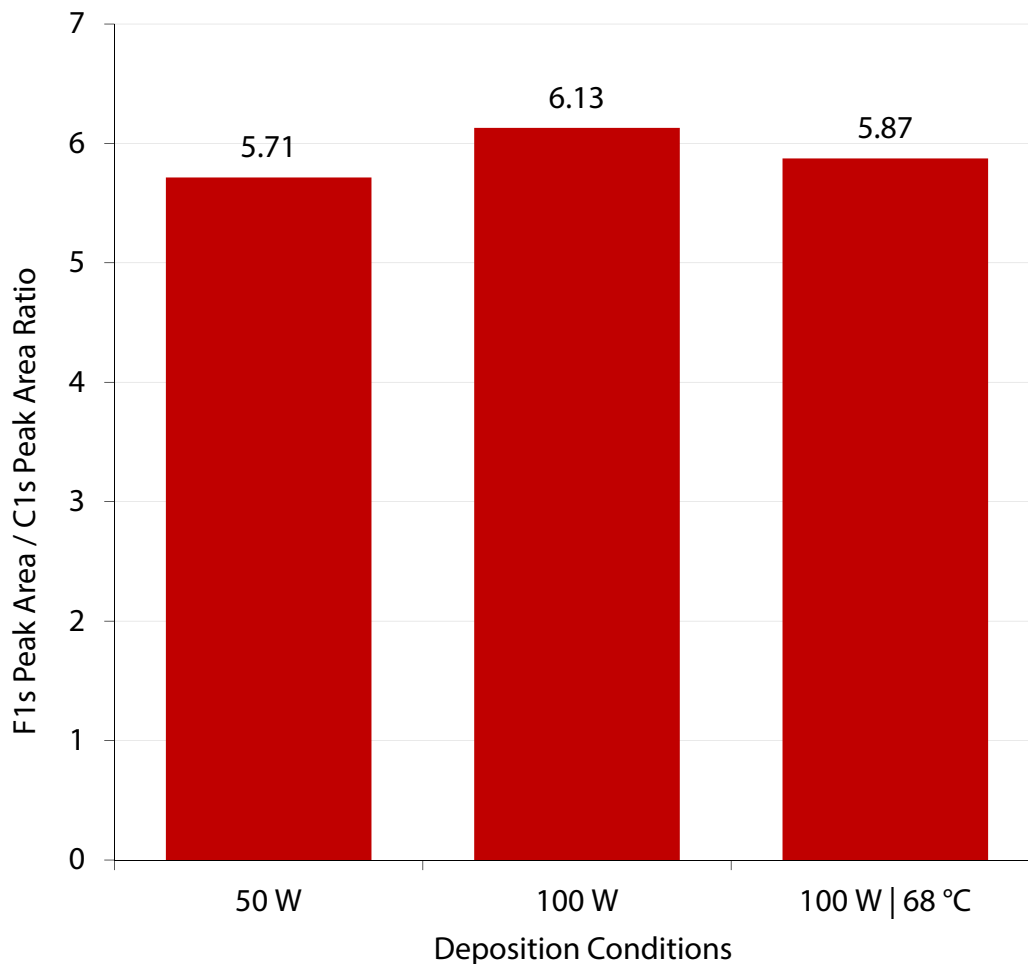


Figure 3.16. F1s / C1s ratio for sputtered fluorocarbon films prepared using two different sputtering powers (50 W and 100 W, both at 36 °C), and using like sputtering powers (100 W) with two different deposition temperatures (36 °C and 68 °C).

3.4 Mechanical Characterization

3.4.1 Nanoindentation

The hardness values and elastic moduli measured from nanoindentation on the sputtered fluorocarbon films and bulk PTFE are given in Figure 3.17. The bulk PTFE target was tested along with the sputtered fluorocarbon films under the same indentation conditions and using the same AFM tip. The thin sputtered films

exhibited much larger elastic modulus and hardness values than those of the bulk target, in agreement with values reported in the literature [11]. An increase in sputtering power from 50 W to 100 W increased both the elastic modulus and hardness values of the sputtered films, decreasing the bulk-likeness of the films using both metrics. This would indicate that the physical performance of the fluorocarbon films improves with increased sputtering power, conflicting with the results reported by Li et. al. [12, 15], which show a decrease in both hardness and elastic modulus values with increasing sputtering powers. However, the large amount of error present in the data for both tested samples limits the strength of any conclusions made about the physical performance of the films.

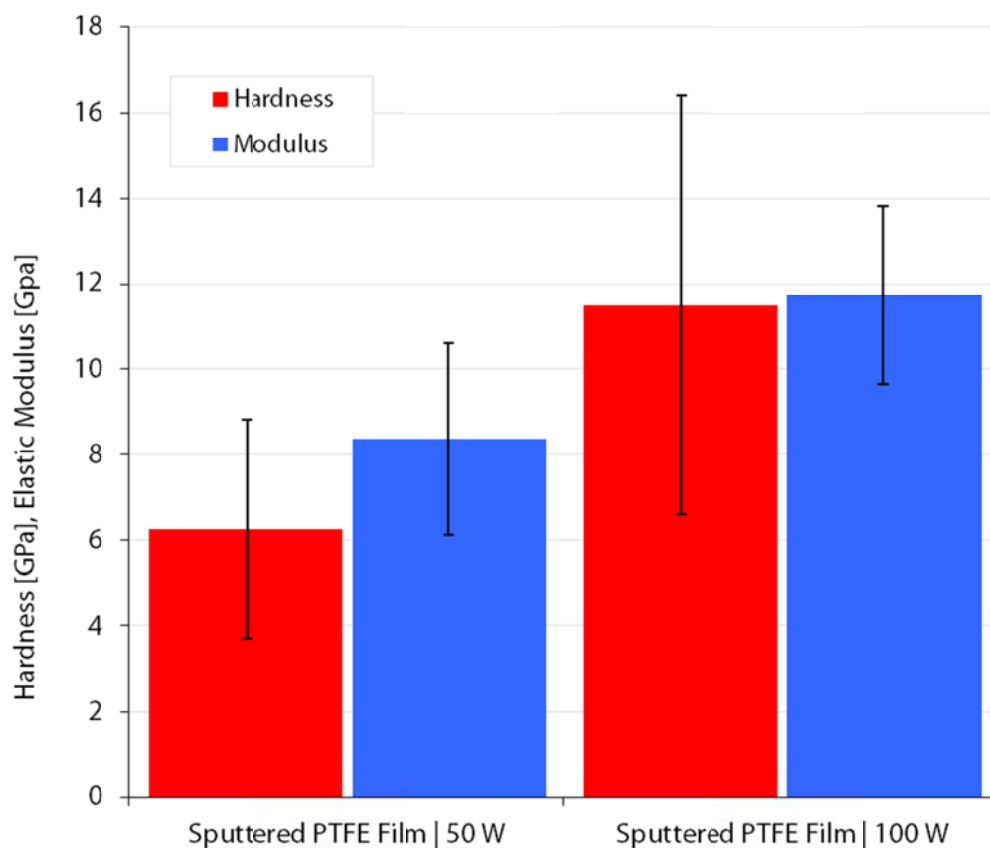


Figure 3.17. Hardness and elastic modulus values produced from nanoindentation on the fluorocarbon thin films prepared using differing sputtering powers. Film thicknesses were 223 nm for the film prepared using a sputtering power of 50 W and 452 nm for the film prepared using 100 W. Error bars represent standard deviation produced from an average of five indentations across the surface of each of the films.

3.4.2 Contact Angle Measurements

Contact angle measurements were performed on all sputtered fluorocarbon films, in addition to the bulk PTFE material and the unspattered silicon substrate. Contact angle of the bulk PTFE material was approximately 119°, while contact angle of the unspattered silicon was approximately 28°. All sputtered fluorocarbon films exhibited hydrophobicity, with a water / sample contact angle (γ) larger than 90°,

however all film contact angles fell below the contact angle of the bulk material. Sputtering power appeared to play little role in the contact angle exhibited by the fluorocarbon films (Figure 3.18) – contact angles were approximately 106° regardless of the sputtering power used.

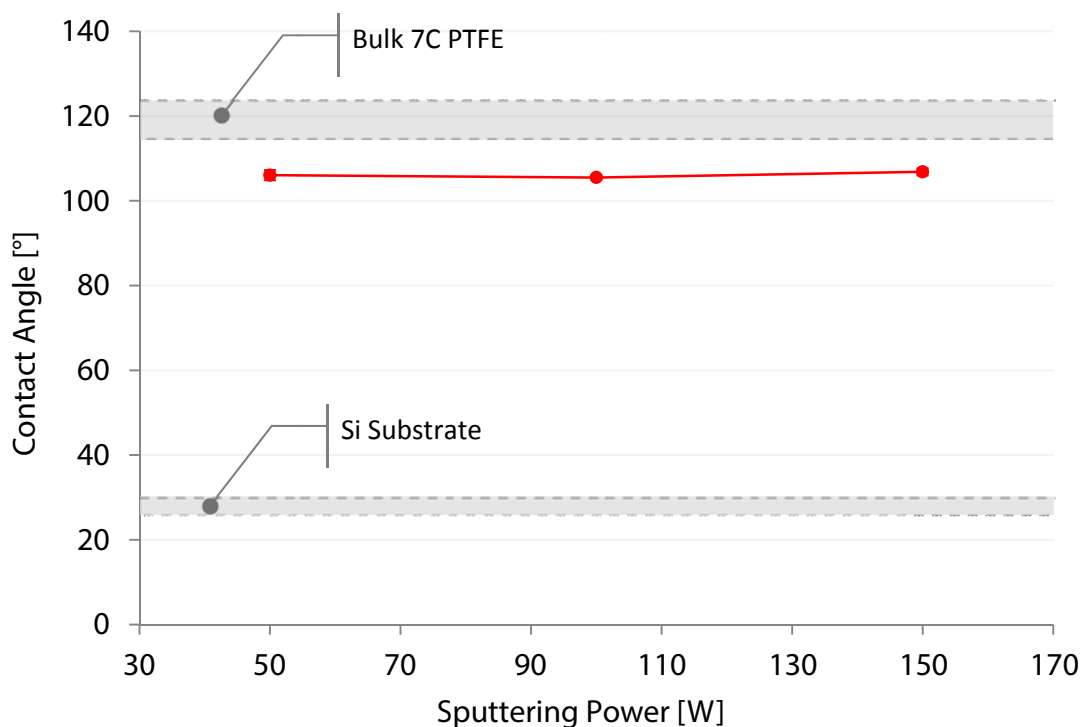


Figure 3.18. Contact angle of DI water droplets on sputtered fluorocarbon films prepared under increasing RF sputtering powers at a deposition temperature of 36 °C. Contact angle range for unsputtered silicon wafer substrate and bulk PTFE material included for reference.

Figure 3.19 plots the contact angles of the films vs. the deposition temperature used. An increase in deposition temperature from 36 °C to 68 °C resulted in an increase in contact angle from 105.3° to 106.8° (1.42%) for the films deposited using at sputtering power of 50 W, and an increase from 105.0° to 109.3° (4.1%) for the films deposited using 100 W. When the deposition temperature was increased from

68 °C to 100 °C, the contact angle of the film deposited using 50 W decreased back to approximately 105° (error increased significantly at this point). This decrease in contact angle with increasing temperature could be due to the lack of deposited film at elevated deposition temperatures, shown in Figure 3.4. This explanation is reinforced by the increasing contact angle/increasing deposition temperature relationship continuing for the films prepared at 100 W, as these films (100 °C, 100 W) have a detectable thickness, also shown in Figure 3.4.

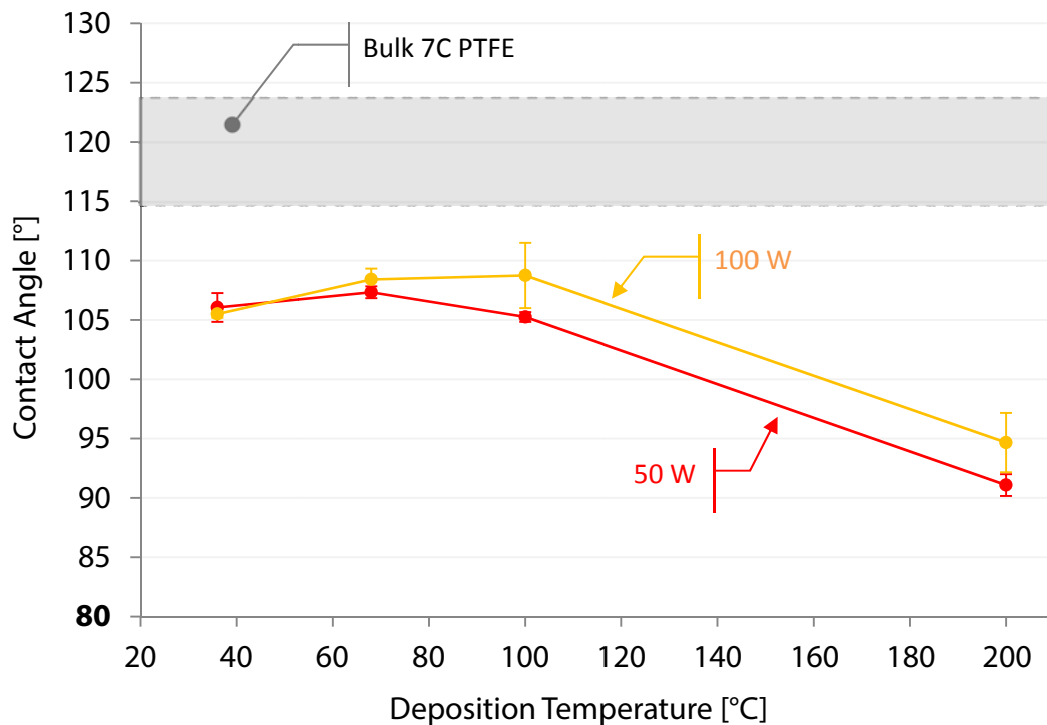


Figure 3.19. Contact angle of DI water droplets on sputtered fluorocarbon films prepared under increasing deposition temperatures for RF sputtering powers of 50 W and 100 W. Contact angle range for bulk PTFE material included for reference. Y-axis is truncated for clarity.

Though no significant film thickness was able to be measured for the films prepared at 200 °C (see Figure 3.4), contact angle decreased from those films prepared

at lower temperatures but remained above 90° for both power levels, significantly higher than the measured contact angle of 28° for an untreated silicon substrate. This suggests the presence of some form of fluorination on the substrate surface, which increases with increased sputtering power. The results suggest that, while increasing deposition temperature results in significantly lower deposition rates and thinner films, the surface of what little film remains is more hydrophobic than those films prepared at lower deposition temperatures. If the increased hydrophobicity is associated with an increased level of fluorination on the surface of the film, then increasing deposition temperature increases the fluorine content of the film.

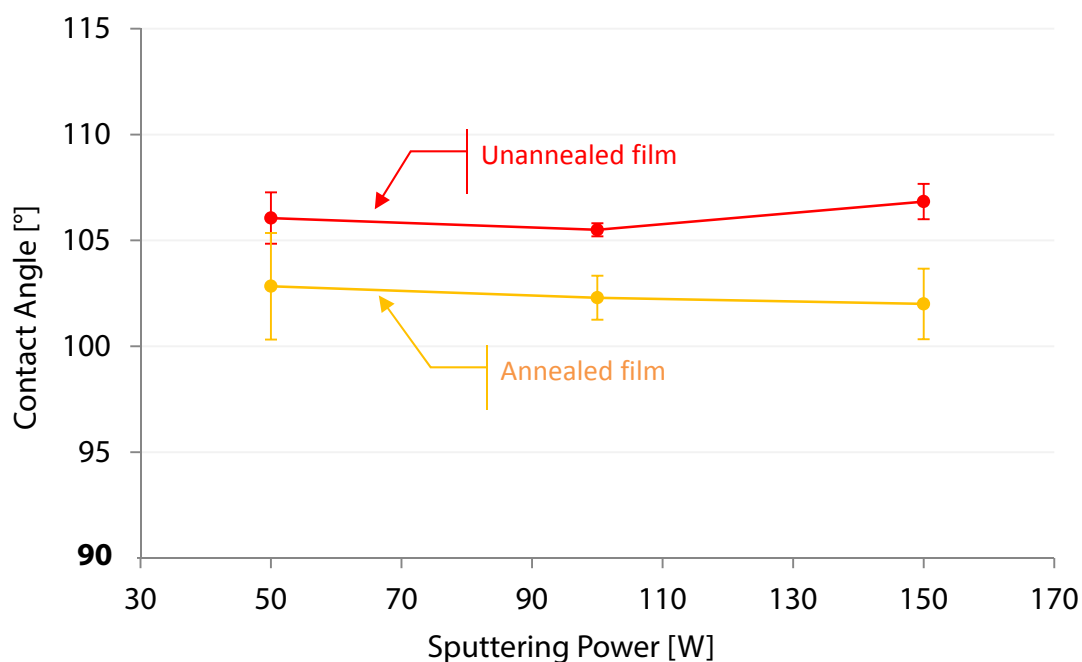


Figure 3.20. Contact angle of DI water droplets on sputtered fluorocarbon films prepared under increasing RF sputtering powers for both unannealed and annealed films. Deposition temperature remained 36°C . Y-axis is truncated for clarity.

Figure 3.20 and Figure 3.21 plots the contact angle data from Figure 3.18 and Figure 3.19 with the addition of the data acquired from the equivalent annealed films. Contact angles for the annealed films are consistently lower than those of the unannealed films in both cases (increasing sputtering power and increasing deposition temperature); the difference remains steady at approximately 3.5° as sputtering power is increased. As deposition temperature is increased, the difference in contact angle between the unannealed and annealed films appears to become more exaggerated, approaching 7° as deposition temperature reaches 100°C (error also increases with temperature, somewhat weakening the trend).

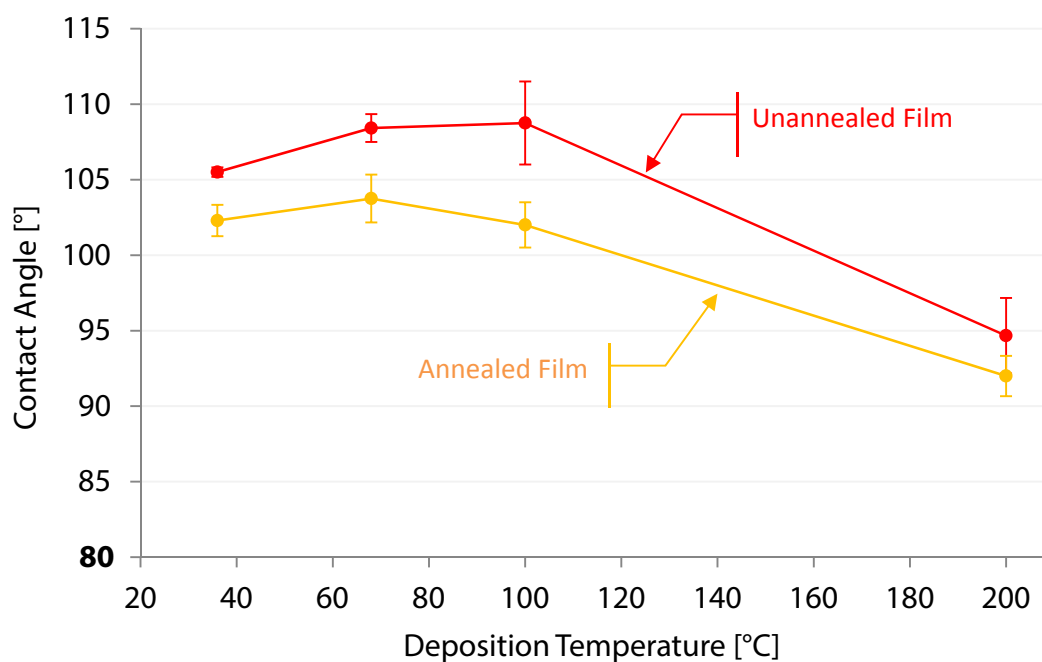


Figure 3.21. Contact angle of DI water droplets on sputtered fluorocarbon films prepared under increasing deposition temperatures for both unannealed and annealed films. Data shown is from depositions using sputtering powers of 100 W. Y-axis is truncated for clarity.

Chapter 4

DISCUSSION

4.1 The Effects of Changing Film Preparation Parameters

In the course of this study, the effects of changing two primary film preparation parameters were examined with the intent of understanding sputtered fluorocarbon film structure: increasing sputtering power and increasing deposition temperature. The effects of changing two other parameters were also examined: post-deposition annealing of the sputtered fluorocarbon films, and film thickness. The effects were quantified using five characterization techniques; interferometry measuring film thickness, FTIR, XPS, nanoindentation via AFM, and the contact angle of water-on-film.

4.1.1 The Effects of Sputtering Power

When examining the effects of sputtering power on fluorocarbon film deposition rate (proportional to film thickness), an increase in sputtering power has been shown to result in a nonlinear increase in film thickness (see Figure 3.3). Increasing deposition rate with increasing sputtering power is consistent across similar studies [33, 56], however the nonlinearity of the results in this study appear to be unusual – results from other studies exhibit more-or-less linear deposition rate vs. sputtering power relationships. It is possible that this nonlinearity is only present when using lower sputtering powers (0 – 100 W), and that when increasing sputtering

powers to 200 W, 250 W, and beyond the deposition rates vs. power relationship will become more linear.

When examining the results produced from FTIR as sputtering power is increased, there is a shift in the centers of the Gaussian curves fit to the data towards those fit to the spectrum of bulk PTFE (Figure 3.8). Such a shift is indicative of an increase in fluorocarbon film bulk-likeness. Examining the results produced from XPS, as power is increased there is a marked increase in both the ratio of $-\text{[CF}_2\text{-CF}_2\text{]}_n$ bonds to CF_3 bonds, and the percentage of the total C1s spectrum consisting of $-\text{[CF}_2\text{-CF}_2\text{]}_n$ bonds. Both of these metrics imply that as sputtering power is increased, the spectra more closely resembles that of bulk PTFE and there is an increase in film bulk-likeness.

Sputter yield is linked to deposition rate and is driven by sputtering power. As sputtering power is increased, there is an increase in the energy of the argon ions that impact the surface of the target, increasing the sputter yield and subsequently the deposition rate. Other important factors influencing the sputter yield are chamber geometry (which remained fixed for all films prepared in this study), the arrival angle of the impacting argon ions (linked closely with the chamber geometry), and the mass and binding energy (bond strength) of the atoms in the target material. Atomic mass is 12.011 amu for carbon, 18.998 amu for fluorine, and 39.948 amu for argon [57]. Bonds found in bulk PTFE are C–C and C–F; binding energy for C–C is reported to be 618.3 ± 15.4 kJ/mol, while binding energy for C–F is reported to be 513.8 ± 10.0 kJ/mol [57]. Bulk PTFE is formed of long chains of CF_2 , and in order to eject a section of the chain two C–C bonds with a combined binding energy of approximately 1236 kJ/mol must be broken. This is opposed to a much lower binding energy of

513 kJ/mol for the ejection of a single fluorine atom from the CF₂ chain. Further complicating matters, as the energy of the impacting argon ions increase, the energy of the sputtered off PTFE increases. This increase in energy could potentially play a role in both the sticking coefficient for the fluorocarbon deposition and the temperature of the substrate [28], both of which are underreported in the literature.

One explanation for the nonlinearity found in the deposition rate vs. sputtering power relationship is that initially (50 W sputtering power) only single fluorine and carbon atoms are sputtered from the target surface; that the impacting argon ions lack the energy needed to break the stronger CF₂–CF₂ bonds and lift off their combined atomic masses (50.007 amu for CF₂). As sputtering power is increased (100 W), impacting argon ion energy increases to the point where ejecting larger sections of the PTFE chain with each strike is possible. This explanation is supported by the aforementioned results from FTIR and the relative increase in CF₂ bonds found in the XPS spectra when increasing the sputtering power from 50 W 100 W (see Figure 3.15). Continuing nonlinearity would be tested with additional films prepared at sputtering powers beyond 150 W, however the increased sputtering rate could rapidly degrade the PTFE target, eroding through to the copper backing plate and potentially damaging the sputtering system. Thicker targets, and an assembly to fit them into the target guns, would have to be utilized.

Contact angle measurements taken on each sample show no relationship with sputtering power used in film preparation (Figure 3.18), with the contact angle remaining at approximately 106°. If hydrophobicity is correlated with the fluorination present at the surface of the films, then this result would suggest that the fluorination of the film is independent of sputtering power. This is supported by XPS results (see

Figure 3.16) that show little change in fluorine content relative to carbon content when power is increased. It is possible that if sputtering power is decreased to powers below 50 W there would be an increase in film fluorine content as impacting argon ion energy decreases to the point of only ejecting single atoms of fluorine from the bulk PTFE chain. Such a decrease could potentially increase the fluorination of the film surface and result in an increase in the hydrophobicity.

Nanoindentation results show a negative relationship between sputtering power and both elastic modulus and hardness of the films, with both increasing away from the values found in the bulk material as sputtering power is increased. However, as mentioned previously, comparison between the hardness and elastic modulus values calculated from the bulk material and the sputtered fluorocarbon film are difficult to make due to the drastically different thicknesses of the two materials, as well as the potential for substrate effects found when indenting the fluorocarbon films. When comparing the films prepared at the two power levels (50 W and 100 W), both hardness and elastic modulus increase at the higher power level, a behavior which conflicts with the results reported in the literature [12, 15] (although film thickness for those studies cited are either unreported or much thinner than those films prepared for this study). When film thickness is increased, as it does in Figure 3.17 with increasing power levels, substrate effects should decrease. The increases in hardness and elastic modulus when sputtering power is increased are likely attributable to changes in the film properties. The results of this study suggest that increasing the sputtering power is a potentially underreported method of improving the physical durability of the fluorocarbon films, however the error present in the nanoindentation results weaken any conclusion that can be reached.

Something to consider (unrelated to fluorocarbon film quality but still relevant) is the effect of increasing sputtering power on the integrity of the targets themselves. As sputtering power is increased, sputter yield increases, causing the targets to erode. When this erosion reaches the back surface of the target the deposition must be stopped or the results will be invalidated and the system could suffer (sometimes catastrophic) damage. If sputtering yield (target mass loss) increased linearly with sputtering power, then the mass loss experienced by the target in Figure 3.1 (150 W for 1 hour and a mass loss of 2.957 g) should match those targets in Table 3.1 (50 W for 2 hours, 100 W for 1 hour, and an average mass loss of $1.882 \text{ g} \pm 0.332 \text{ g}$), which is obviously not the case. Unfortunately, those targets tabulated in Table 3.1 were used for successive 50 W and 100 W depositions, and were not weighed between sputtering sessions. This obfuscates the relationship somewhat, but it is evident that, for the sputtering arrangement used in this study, the nonlinear increases in the deposition rate are also present in the sputter yield. If, as sputtering power is increased, the increases in the target mass loss are correlated to the increases in deposition rate, then target mass loss per hour of sputtering at 50 W and 100 W can be estimated using the data collected from the target in Figure 3.1. Using these estimates, predicted target mass loss for 2 hours of sputtering at 50 W and 1 hour of sputtering at 100 W is 2.15 g, which is within the average loss of $1.882 \text{ g} \pm 0.332 \text{ g}$ range measured from the actual sputtering targets. Estimated mass loss rates for increasing sputtering powers are plotted in Figure 4.1 below. These results suggest that when maximizing film thickness, sputtering power is independent of target longevity.

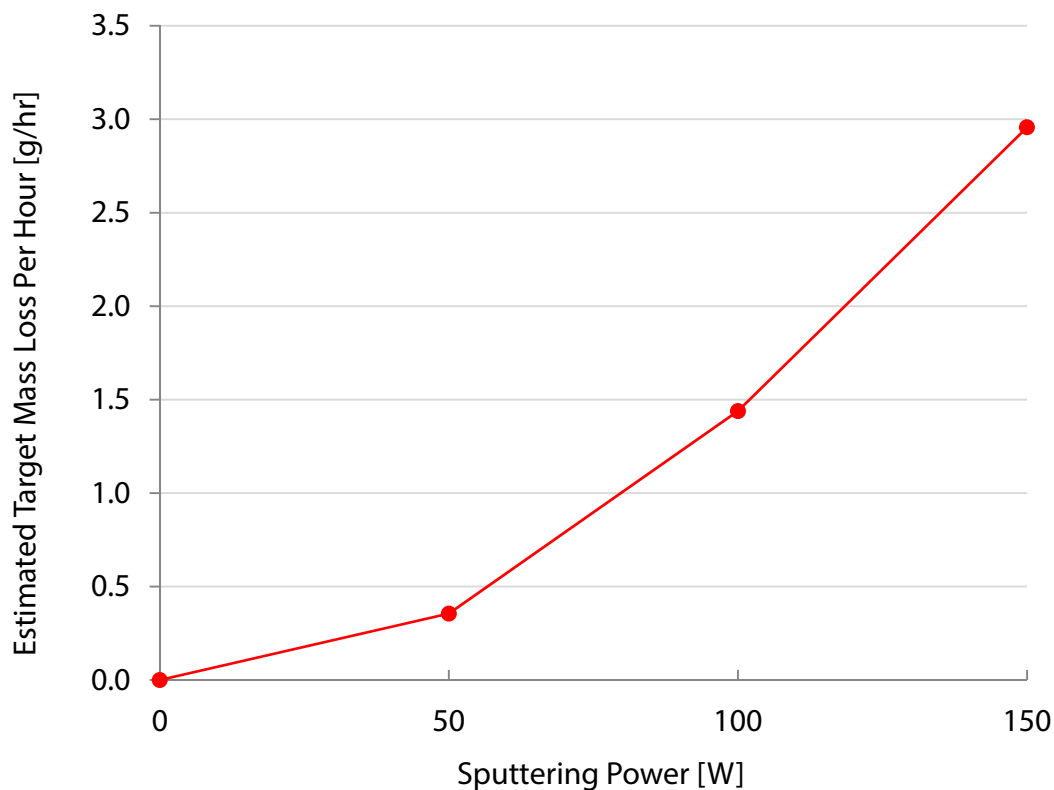


Figure 4.1. Estimated 7C PTFE powder target mass loss as a function of sputtering power. Data point at 150 W is measured directly from target weights before and after sputtering. Data points at 50 W and 100 W are estimated using deposition rates compiled from 50 W, 100 W, and 150 W fluorocarbon film depositions. Connecting lines are not generated from curve fitting and are intended to serve as a visual guide.

4.1.2 The Effects of Deposition Temperature

While the fluctuation of sputtering power affected the quality and quantity of the deposited sputtered target material, substrate deposition temperature is one variable that can directly affect how sputtered fluorocarbon molecules recombine onto the surface of the substrate. The effects of increasing substrate deposition temperature from 36 °C to 68 °C, 100 °C, and 200 °C had drastic effects on film deposition rate (Figure 3.4). No detectable film was found at deposition temperatures of 200 °C for either power level, and for temperatures of 100 °C only films prepared using 100 W

sputtering powers were detectable. The only variable changing in these depositions was substrate temperature, and temperatures were held at well below (more than 100 °C) the melting point of the bulk PTFE material (327 °C [42]). Although film densification may occur due to an increase in substrate temperature, the primary mechanism causing extremely thin films is more likely a significant decrease in the sticking coefficient. This mechanism can apparently be overcome by increasing sputtering powers: for films prepared at 100 °C using higher power levels (100 W) there was still a significant amount of film deposited upon the substrate. It is possible that the decrease of the sticking coefficient to near-zero for elevated temperatures is offset by either the increasing size or energy of the sputtered fluorocarbon molecules that result from increasing the sputtering power.

When taking contact angle measurements of the films deposited at the higher temperature levels used (100 °C and 200 °C), contact angle remained well above the unsputtered substrate contact angle of $\approx 27^\circ$, exhibiting hydrophobic contact angles between 90° and 100° when using either 50 W or 100 W sputtering powers. If contact angle is again correlated to the degree of film surface fluorination, then the results suggest that, though film thickness is less than 5 nm when using deposition temperatures at or above 100 °C, those films exhibit fluorination similar to those of the films deposited using lower deposition temperature. Whatever mechanism is preventing the deposition of significant amounts film at these higher temperatures is allowing some minimum amount of fluorocarbon to be deposited. It is then possible that the sticking coefficient for fluorocarbon molecules on silicon is significantly higher than on a fluorocarbon substrate; the sputtered off fluorocarbon coats the silicon substrate but fails to adhere to the already deposited fluorocarbon film. This

theory could be tested by an increase in the deposition time in order to rule out any slow-film growth past the initial, minimum coating of fluorocarbon film on the silicon substrate.

When examining the spectra generated from FTIR using films prepared under increasing deposition temperatures (Figure 3.9), there is an increase in bulk-like spectral qualities. Fit Gaussian curves shift towards the lower wavenumbers seen in the bulk spectra, and there is a development of a distinct two-peak system as deposition temperatures reach 100 °C in the 50 W film. A film containing larger fragments of sputtered off PTFE would explain this increase in bulk likeness. It is possible that as deposition temperature increases the sticking coefficient of the sputtered off fluorocarbon decreases as a whole, but that the sticking coefficient of the larger sputtered molecules increases relative to the smaller / single atom fragments. This would explain both the decrease in film deposition rate and the increase in the bulk-likeness seen in the FTIR spectra, however it would be expected to be reflected in the XPS spectra as an increase in CF₂ bonds. XPS data shows an increase in the – [CF₂–CF₂]_n bonds / CF₃ bonds ratio (Figure 3.14) and a slight decrease in the F1s area / C1s area ratio (Figure 3.16), both metrics suggesting an increased bulk-likeness of the film. There is, however, no corresponding increase in CF₂ bonds as a percentage of the C1s spectrum.

While increasing deposition temperature results in significantly thinner deposited films, FTIR results strongly suggest that whatever film remains is more bulk-like structurally, while XPS results are inconclusive. This suggests that if whatever mechanism that causes practically no film to be deposited at higher temperatures can be compensated for, films deposited at higher temperatures of

100 °C and beyond might continue the trend of being more bulk-like than those films deposited at 36 °C. It is also possible that there is some optimal deposition temperature between 68 °C and 100 °C that would yield the most bulk-like sputtered fluorocarbon film. More depositions at temperatures of 76 °C, 84 °C, and 92 °C would test this possibility.

4.1.3 The Effects of Post-Deposition Annealing

The role of post-deposition annealing on sputtered fluorocarbon film properties was examined using film thickness, FTIR, and contact angle measurements. There was a detectable decrease in film thickness after annealing, seen in Figure 3.5. These results at anneal temperatures below PTFE melting point (327 °C) suggest some degree of film densification with post-deposition annealing, however the results produced using FTIR could detect little, if any, difference between the un-annealed and annealed films structurally, and their spectra and the associated Gaussian curve fittings are similar (Figure 3.10 presents an example spectral pair). Likewise, little change could be detected when examining the appearance of extraneous peaks on the spectra outside of the CF₂ stretching region. Because the FTIR spectra were generated using transmission, structure of the fluorocarbon through the thickness of the film was represented in the spectra; structural changes at the top surface of the film would be ‘lost’ in the signal from the rest of the film. As the annealing process was performed at a temperature of 200 °C, below the melting point of PTFE, based on the work by Sun et al. [42] there is reason to think that hotter anneals could cause more dramatic changes to the interior structure of the fluorocarbon films. Contact angle measurements present evidence that the surface of the fluorocarbon films is changing

to some degree after undergoing the anneal process. There is a consistent decrease in the contact angles seen on the films once annealing is performed. If contact angle is again correlated film fluorination, then the data suggests that when post-deposition annealing is performed, the fluorination at the top surface of the film decreases. XPS, which could provide data specifically about the top 10 nm of the film surface, was unfortunately not performed on annealed films, limiting the conclusions that can be made about the annealing process.

4.1.4 The Effects of Film Thickness

The role of increasing film thickness on measurable film structure has been shown in Figure 3.11. Two films prepared under nominally identical conditions (100 W at 36 °C) were examined using FTIR. The only difference between the films was thickness (time spent in the chamber, presumably with the same deposition rate), with one film measuring 452 nm thick and the other film measuring 3545 nm thick. The emergence of a prominent shoulder peak could mean that the increased thickness of the film increases the FTIR signal / noise ratio, or that as the film thickness increases there is a significant increase in the bulk-likeness of the structure. In either case, this result, combined with an obvious desirability to maximize signal strength and enable more dependable mechanical testing, creates an incentive to produce as thick a film as possible within practical limits.

Chapter 5

CONCLUSION

5.1 Summary and Conclusions

The goal of this study was to establish a procedure for producing the most bulk-like fluorocarbon film possible, bearing in mind the ultimate objective of co-sputtering PTFE nanocomposite blends. Four film parameters were modified: sputtering power, deposition temperature, post-deposition annealing, and sputter deposition duration. The findings of this study were:

- Fluorocarbon films prepared from the sputtering of PTFE were largely different from the parent bulk material. Differences included a much more amorphous fluorocarbon structure, a higher fluorine to carbon ratio, and a less hydrophobic surface.
- Increasing sputtering power resulted in disproportionate increases in fluorocarbon film deposition rate and an increase in the bulk-likeness of the structure of the resultant films.
- Increasing the deposition temperature resulted in disproportionate decreases in fluorocarbon film deposition rate and an increase in the bulk-likeness of the structure of the resultant films.
- Annealing of sputtered fluorocarbon films at below PTFE melting temperature is an ineffectual method of changing the film interior structure. More data is needed for conclusions to be made about the top surface of the

films, which, as indicated by contact angle data, clearly undergoes some structural change.

The sputtered fluorocarbon films appear more bulk-like as sputtering power and deposition temperatures are increased, as indicated by results from FTIR and XPS characterization. The decreasing deposition rates caused by the increase in deposition temperature indicate that some optimization of the two parameters (temperature and bulk-likeness of the film) will be necessary before proceeding with co-sputtering of PTFE and the nanofiller material of choice, as the characterization techniques used will most likely be limited by film thickness.

5.2 Recommendations

Mechanical testing and certain methods of structural characterization are severely limited by the thickness of the fluorocarbon films, and depositions should be optimized for maximum film thickness wherever possible. Sputtering power should be maximized in order to increase both the deposition rate and the bulk-likeness of the fluorocarbon films. A deposition time of 2 hours is recommended to ensure target integrity throughout the deposition. Because substrate temperature has been shown to clearly have an effect on the bulk likeness of the films, deposition temperatures for future film preparations should be set in the range of 70 – 100 °C. Any deposition temperatures above this level yield deposition rates that are unacceptable to film characterization. Additionally, because it was found that post-deposition annealing, as carried out using the methods in this study, was an ineffective method of significantly modifying fluorocarbon film interior structure, anneal conditions should either be drastically altered by increasing the temperature or anneal time, or abandoned entirely.

XPS (as opposed to transmission-mode FTIR) should be carried out on annealed films for more relevant data concerning the film structure.

REFERENCES

- [1] “Atlas V and Delta IV Technical Summary.” United Launch Alliance, LLC, 2013.
- [2] “Pegasus® Fact Sheet.” Orbital Sciences Corporation, 2013.
- [3] “Taurus® Fact Sheet.” Orbital Sciences Corporation, 2013.
- [4] B. Bhushan, “Friction,” in *Principles and Applications of Tribology*, 2nd ed., John Wiley & Sons, 2013, p. 1008.
- [5] M. R. Johnson, “The Galileo High Gain Antenna Deployment Anomaly,” in *Aerospace Mechanisms Symposium Lewis Research Center, USA*, 1994.
- [6] R. J. Plunkett, “Tetrafluoroethylene Polymers,” 1941.
- [7] J. L. He, W. Z. Li, L. D. Wang, J. Wang, and H. D. Li, “Deposition of PTFE thin films by ion beam sputtering and a study of the ion bombardment effect,” *Nucl. Instruments Methods Phys. Res.*, vol. 135, pp. 512–516, 1998.
- [8] N. Sprang, D. Theirich, and J. Engemann, “Surface modification of fluoropolymers by microwave plasmas: FTIR investigations,” *Surf. Coatings Technol.*, vol. 98, no. 1–3, pp. 865–871, Jan. 1998.
- [9] R. W. Jaszewski, H. Schiff, B. Schnyder, a. Schneuwly, and P. Gröning, “The deposition of anti-adhesive ultra-thin teflon-like films and their interaction with polymers during hot embossing,” *Appl. Surf. Sci.*, vol. 143, no. 1–4, pp. 301–308, Apr. 1999.
- [10] H. Jung and H. Park, “Structural and electrical properties of co-sputtered fluorinated amorphous carbon film,” *Thin Solid Films*, vol. 420–421, pp. 248–252, Dec. 2002.
- [11] G. Tang, X. Ma, M. Sun, and X. Li, “Mechanical characterization of ultra-thin fluorocarbon films deposited by R.F. magnetron sputtering,” *Carbon N. Y.*, vol. 43, no. 2, pp. 345–350, Jan. 2005.

- [12] L. Li, F. Zi, and Y. Zheng, "The characterization of fluorocarbon films on NiTi alloy by magnetron sputtering," *Appl. Surf. Sci.*, vol. 255, no. 2, pp. 432–434, Nov. 2008.
- [13] T. Oya and E. Kusano, "Characterization of organic polymer thin films deposited.pdf," *Vacuum*, 2009.
- [14] R. Jafari, R. Menini, and M. Farzaneh, "Superhydrophobic and icephobic surfaces prepared by RF-sputtered polytetrafluoroethylene coatings," *Appl. Surf. Sci.*, vol. 257, no. 5, pp. 1540–1543, Dec. 2010.
- [15] L. Li, P. M. Jones, and Y.-T. Hsi, "Characterization of a nanometer-thick sputtered polytetrafluoroethylene film.pdf," *Appl. Surf. Sci.*, 2011.
- [16] K. R. Makinson and D. Tabor, "The friction and transfer of polytetrafluoroethylene," vol. 281, no. 1384, pp. 49–61, 1964.
- [17] M. Suzuki and P. Prat, "Synergism of an MoS₂ sputtered film and a transfer film of a PTFE composite," *Aerospace*, pp. 995–1003, 1999.
- [18] J. Khedkar, I. Negulescu, and E. I. Meletis, "Sliding wear behavior of PTFE composites," *Wear*, vol. 252, no. 5–6, pp. 361–369, Mar. 2002.
- [19] J. K. Lancaster, "The effect of carbon fibre reinforcement on the friction and wear of polymers," *J. Phys. D. Appl. Phys.*, vol. 1, no. 5, pp. 549–559, May 1968.
- [20] S. T. Li, E. Arenholz, J. Heitz, and D. Bkerle, "Pulsed-laser deposition of crystalline Teflon (PTFE) films," vol. 4332, no. 97, 1998.
- [21] Q. Chen, "Investigation of corona charge stability mechanisms in polytetrafluoroethylene (PTFE) teflon films after plasma treatment," *J. Electrostat.*, vol. 59, no. 1, pp. 3–13, Jul. 2003.
- [22] W. G. Sawyer, K. D. Freudenberg, P. Bhimaraj, and L. S. Schadler, "A study on the friction and wear behavior of PTFE filled with alumina nanoparticles," *Wear*, vol. 254, no. 5–6, pp. 573–580, Mar. 2003.
- [23] D. L. Burris and W. G. Sawyer, "Improved wear resistance in alumina-PTFE nanocomposites with irregular shaped nanoparticles," *Wear*, vol. 260, no. 7–8, pp. 915–918, Apr. 2006.

- [24] P. B. Mozhaev, P. V. Komissinski, N. P. Kukhta, A. Kühle, G. A. Ovsyannikov, and J. L. Skov, "Comparison of High-Pressure dc-Sputtering and Pulsed Laser Deposition of Superconducting YBa₂Cu₃O_x Thin Films," *J. Supercond.*, 1997.
- [25] H. Biederman, P. Bfikovfi, J. Je, P. Hffdek, and D. Slavinsk, "RF magnetron sputtering of polymers," *J. Non. Cryst. Solids*, vol. 218, pp. 44–49, 1997.
- [26] V. Stelmashuk, H. Biederman, D. Slavinska, J. Zemek, and M. Trchova, "Plasma polymer films rf sputtered from PTFE under various argon pressures," *Vacuum*, vol. 77, no. 2, pp. 131–137, Jan. 2004.
- [27] J. D. Plummer, *Silicon VLSI Technology: Fundamentals, Practice, and Modeling*. Prentice Hall, 2000, p. 817.
- [28] S. Mahieu, K. Van Aeken, D. Depla, D. Smeets, and a Vantomme, "Dependence of the sticking coefficient of sputtered atoms on the target–substrate distance," *J. Phys. D. Appl. Phys.*, vol. 41, no. 15, p. 152005, Aug. 2008.
- [29] S. D. Ekpe and S. K. Dew, "Measurement of energy flux at the substrate in a magnetron sputter system using an integrated sensor," *J. Vac. Sci. Technol. A Vacuum, Surfaces, Film.*, vol. 22, no. 4, p. 1420, 2004.
- [30] J. H. Park, "Deposition-Temperature Effects on AZO Thin Films Prepared by RF Magnetron Sputtering and Their Physical Properties," vol. 49, no. December, pp. 584–588, 2006.
- [31] N. Ariel, M. Eizenberg, Y. Wang, and S. P. Murarka, "Deposition temperature effect on thermal stability of fluorinated amorphous carbon films utilized as low-K dielectrics," *Mater. Sci. Semicond. Process.*, vol. 4, no. 4, pp. 383–391, Aug. 2001.
- [32] L. Combadiere and J. Machet, "Reactive magnetron sputtering deposition of TIN films . II . Influence of substrate temperature on the mechanical properties of the films," vol. 88, pp. 28–37, 1996.
- [33] K. J. Lawson and J. R. Nicholls, "Ultrathin PTFE, PVDF, and FEP Coatings Deposited Using Plasma-assisted Physical Vapor Deposition," in *Fluoropolymers 1*, Springer, 2002, pp. 313–320.

- [34] D. Lin-Vien, N. B. Colthup, W. G. Fateley, and J. G. Grasselli, *The Handbook of Infrared and Raman Characteristic Frequencies of Organic Molecules*, 1st ed. Academic Press, 1991, p. 503.
- [35] D. Briggs, *Surface Analysis of Polymers by XPS and Static SIMS*. Cambridge University Press, 1998, p. 198.
- [36] N. Vandencastele and F. Reniers, "Plasma-modified polymer surfaces: Characterization using XPS," *J. Electron Spectros. Relat. Phenomena*, vol. 178–179, pp. 394–408, May 2010.
- [37] B. H. Park, M.-H. Lee, S. B. Kim, and Y. M. Jo, "Evaluation of the surface properties of PTFE foam coating filter media using XPS and contact angle measurements," *Appl. Surf. Sci.*, vol. 257, no. 8, pp. 3709–3716, Feb. 2011.
- [38] D. S. Bodas, A. B. M. Mandale, and S. A. Gangal, "Deposition of PTFE thin films by RF plasma sputtering on <1 0 0> Si substrates.pdf," *Appl. Surf. Sci.*, 2005.
- [39] R. Harrop and P. J. Harrop, "Friction of sputtered PTFE films," *Polymer (Guildf.)*, vol. 3, no. 1969, pp. 109–117, 1968.
- [40] S. Küster, N. Ludwig, G. Willers, J. Hoffmann, H. B. Deising, and A. Kiesow, "Thin PTFE-like membranes allow characterizing germination and mechanical penetration competence of pathogenic fungi.," *Acta Biomater.*, vol. 4, no. 6, pp. 1809–18, Nov. 2008.
- [41] Y. Suzuki, H. Fu, Y. Abe, and M. Kawamura, "Effects of substrate temperature on structure and mechanical properties of sputter deposited fluorocarbon thin films," *Vacuum*, pp. 5–8, May 2012.
- [42] H. Sun, R. S. Cooke, W. D. Bates, and K. J. Wynne, "Supercritical CO₂ processing and annealing of polytetrafluoroethylene (PTFE) and modified PTFE for enhancement of crystallinity and creep resistance," *Polymer (Guildf.)*, vol. 46, no. 20, pp. 8872–8882, Sep. 2005.
- [43] J. L. Koenig, *Spectroscopy of Polymers*. American Chemical Society, 1991.
- [44] W. C. Oliver and G. M. Pharr, "An improved technique for determining hardness and elastic modulus using load and displacement sensing indentation experiments," *J. Mater. Res.*, vol. 7, no. 06, pp. 1564–1583, Jan. 2011.

- [45] G. Masetti, F. Cabassi, G. Morelli, and G. Zerbi, "Conformational Order and Disorder in Poly (tetrafluoroethylene) from the Infrared Spectrum," vol. 465, no. 10, 1973.
- [46] H. W. Starkweather, R. C. Ferguson, D. B. Chase, and J. M. Minor, "Infrared Spectra of Amorphous and Crystalline Poly(tetrafluoroethylene)," pp. 1684–1686, 1985.
- [47] T. C. Nason and T.-M. Lu, "Thermoplastic and spectroscopic properties of amorphous fluoropolymer thin films," vol. 239, pp. 27–30, 1994.
- [48] M. Schott, "Preparation and properties of highly oriented polytetrafluoroethylene films," *Synth. Met.*, vol. 67, pp. 55–61, 1994.
- [49] V. G. Kuryavyi, A. K. Tsvetnikov, and V. M. Buznik, "EFFECTS OF PRESSURE AND PULSED MECHANICAL ACTION ON THE IR AND ESR SPECTRA OF ULTRAFINE POLYTETRAFLUOROETHYLENE," *Text*, vol. 43, no. 5, pp. 761–765, 2002.
- [50] K. K. S. Lau, J. A. Caulfield, and K. K. Gleason, "Structure and Morphology of Fluorocarbon Films Grown by Hot Filament Chemical Vapor Deposition," *Mater. Res.*, no. 14, pp. 3032–3037, 2000.
- [51] W. K. Fisher and J. C. Corelli, "Effect of ionizing radiation on the chemical composition, crystalline content and structure, and flow properties of polytetrafluoroethylene," *J. Polym. Sci. Polym. Chem. Ed.*, vol. 19, no. 10, pp. 2465–2493, Oct. 1981.
- [52] S. J. Limb, K. K. S. Lau, D. J. Edell, E. F. Gleason, and K. K. Gleason, "Molecular Design of Fluorocarbon Film Architecture by Pulsed Plasma Enhanced and Pyrolytic Chemical Vapor Deposition 1," vol. 4, no. 1, 1999.
- [53] J. Mihály, S. Sterkel, H. M. Ortner, L. Kocsis, and L. Hajba, "FTIR and FT-Raman Spectroscopic Study on Polymer Based High Pressure Digestion Vessels," vol. 79, no. 3, pp. 497–501, 2006.
- [54] H. W. Thompson and R. B. Temple, "Infra-red spectra of fluorinated hydrocarbons. Part II. ?Methyl fluoroform?(1 : 1 : 1-trifluoroethane)," *J. Chem. Soc.*, p. 1428, 1948.
- [55] G. Socrates, *Infrared and Raman Characteristic Group Frequencies: Tables and Charts*, 3rd ed. Wiley, 2004, p. 366.

- [56] C. Becker, J. Petersen, G. Mertz, D. Ruch, and A. Dinia, "Ultrathin Fluoropolymer Coatings Deposited by Innovative PVD Process, Based on Laser-Assisted Magnetron Sputtering, on Flexible Poly(Ethylene Terephthalate) for Superhydrophobic Properties." 2010.
- [57] D. R. Lide, Ed., *Handbook of Chemistry and Physics*, 90th ed., vol. 15, no. 3. Boca Raton: CRC Press, 2009.

Appendix A

SUPPLEMENTAL CHEMICAL CHARACTERIZATION DATA

A.1 FTIR Bond Group Assignment References

The following group assignments were compiled from various papers. Note some degree of assignment overlap between studies.

Table A.1. Bond group / binding energy assignments compiled from the literature. Sorted by wavenumber.

Assigned Group	Wavenumber [cm ⁻¹]	Reference	Year
-(CF = CF)-	1733.00	Fisher et al.	1981
CF ₂ Asymmetric Stretch	1545.00	Sprang et al.	1998
CF ₂ Asymmetric Stretch	1450.00	Sprang et al.	1998
CF Stretch	1340.00	Limb et al.	1999
CF	1340.00	Sprang et al.	1998
CF ₂ Asymmetric Stretching	1299.00	Mihály et al.	2006
C-C Stretching	1299.00	Mihály et al.	2006
CF ₂ Parallel Asymmetric Stretch	1242.00	Sprang et al.	1998
<i>CF₂ Parallel Asymmetric Stretch</i>	<i>1242.00</i>	<i>Chen</i>	<i>2003</i>
CF ₂ Symmetric Stretch	1220.00	Limb et al.	1999
CF ₂ Parallel Symmetric Stretch	1207.00	Sprang et al.	1998
CF ₂ Perpendicular Asymmetric Stretch	1207.00	Chen	2003

CF ₂ Symmetric Stretching	1199.00	Mihály et al.	2006
CF ₂ Asymmetric Stretch	1160.00	Limb et al.	1999
CF ₂ Parallel Asymmetric Stretch	1152.00	Sprang et al.	1998
CF ₂ Parallel Asymmetric Stretch	1152.00	Chen	2003
CF ₂ Symmetric Stretching	1146.00	Mihály et al.	2006
CF ₃ End Group	985.00	Sprang et al.	1998
CF ₃	980.00	Limb et al.	1999
Amorphous Phase PTFE	780.00	Sprang et al.	1998
Amorphous CF	740.00	Limb et al.	1999
CF ₂ Scissoring	729.00	Mihály et al.	2006
CF ₂ Wagging	650.00	Limb et al.	1999
CF Deformation	640.00	Mihály et al.	2006
CF ₂	638.00	Sprang et al.	1998
CF ₃ Symmetric Deformation	630.00	Mihály et al.	2006
CF ₂	625.00	Sprang et al.	1998
CF ₂ Bending	553.00	Mihály et al.	2006
CF ₂	553.00	Sprang et al.	1998
CF ₂ Twisting	507.00	Mihály et al.	2006
CF ₂ Wagging	507.00	Mihály et al.	2006
CF ₂ Rocking	507.00	Mihály et al.	2006

A.2 XPS Bond Group Assignment References

The following group assignments were compiled from various papers covering a wide variety of topics, although a majority studied sputtered films. Note some degree of assignment overlap between studies.

Table A.2. Bond group / binding energy assignments compiled from the literature. Sorted by binding energy.

Assigned Bond Group	Binding Energy [eV]	Reference	Year
C–C or C=C	283.3 - 284.2	Li et al.	2011
C–C or C=C	284.2	Tang et al.	2005
C–C or C=C	284.5	Jung & Park	2002
C–C or C=C	284.6 - 284.7	Vandencastele & Reniers	2009
C–C or C=C	284.6 - 284.7	Park et al.	2011
C–C or C=C	284.8	Jazewski et al.	1999
C–C or C=C	284.8	Li et al.	2008
C–C or C=C	285	Stelmashuk et al.	2005
C–C or C=C	285.1	Jafari et al.	2010
C–CF _x	286	Jung & Park	2002
C–CF _x	286.2 - 286.7	Li et al.	2011
C–CF _x	286.5	Vandencastele & Reniers	2009
C–CF _x	286.9	Jazewski et al.	1999
C–CF _x	287.4	Stelmashuk et al.	2005
C–CF _x	287.4	He et al.	1998
C–CF _x	287.5	Jafari et al.	2010
C–CF _x	289.2	Park et al.	2011

CF	288, 288.3, 289.8	Vandencastele & Reniers	2009
CF	288.8 - 289.5	Li et al.	2011
CF	289	Jazewski et al.	1999
CF	289	Jung & Park	2002
CF	289.5	He et al.	1998
CF	289.6	Jafari et al.	2010
CF	289.8	Park et al.	2011
CF	290	Stelmashuk et al.	2005
$-\text{[CF}_2\text{-CF}_2\text{]}_n$	290.6	Li et al.	2008
$-\text{[CF}_2\text{-CF}_2\text{]}_n$	290.7 - 291.6	Li et al.	2011
$-\text{[CF}_2\text{-CF}_2\text{]}_n$	291	Jung & Park	2002
$-\text{[CF}_2\text{-CF}_2\text{]}_n$	291.4	Jazewski et al.	1999
$-\text{[CF}_2\text{-CF}_2\text{]}_n$	291.44 - 292.5	Chen	2003
$-\text{[CF}_2\text{-CF}_2\text{]}_n$	291.8	Jafari et al.	2010
$-\text{[CF}_2\text{-CF}_2\text{]}_n$	291.8	Oya & Kusano	2009
$-\text{[CF}_2\text{-CF}_2\text{]}_n$	292	He et al.	1998
$-\text{[CF}_2\text{-CF}_2\text{]}_n$	292	Stelmashuk et al.	2005
$-\text{[CF}_2\text{-CF}_2\text{]}_n$	292.5	Vandencastele & Reniers	2009
$-\text{[CF}_2\text{-CF}_2\text{]}_n$	292.5	Park et al.	2011
$-\text{[CF}_2\text{-CF}_2\text{]}_n$	292.8 - 293.6	Li et al.	2011
CF ₃	293	Jung & Park	2002
CF ₃	293	Li et al.	2008
CF ₃	293.2	Jazewski et al.	1999

CF ₃	293.5	Chen	2003
CF ₃	293.9	Jafari et al.	2010
CF ₃	293.9	Oya & Kusano	2009
CF ₃	294	He et al.	1998
CF ₃	294.1	Stelmashuk et al.	2005
CF ₃	294.1, 294.6	Vandencastele & Reniers	2009
CF ₃	294.6	Park et al.	2011

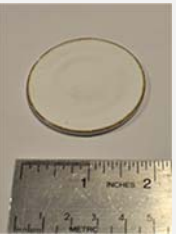
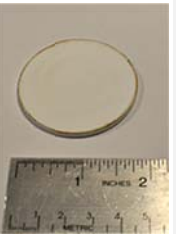
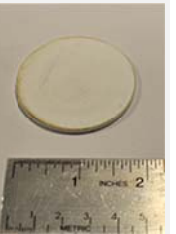
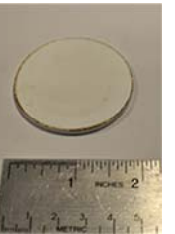
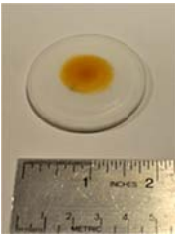
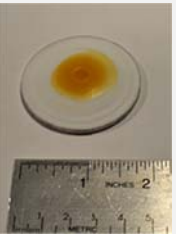
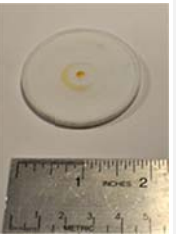
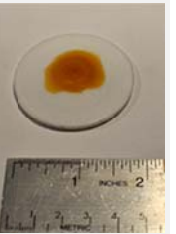
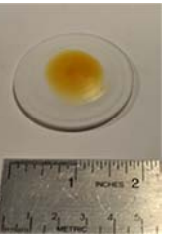
Appendix B

PTFE TARGET SOURCES

B.1 Compressed Powder vs. Extruded Stock Targets

Mostly unreported in the literature, the processing of the initial PTFE sputtering targets can have a significant impact on both the sputtering process and the resulting film properties. In addition to the films discussed up to this point in this study, a duplicate set of films were prepared using targets machined from extruded rods of PTFE. These films underwent all of the same characterizations as those films sputter-prepared from the compressed, 7C PTFE powder. To differentiate between the two target types in this section, targets prepared from compressed, 7C PTFE powder (all previously mentioned depositions) are simply referred to as “compressed targets”, and all targets machined from the extruded rods of PTFE are referred to as “extruded targets”. The target size, mass, and appearance for both materials were recorded for all targets used in the study, both before and after sputtering – half of those results were presented in Table 3.1, the full set of data is given below in Table B.1.

Table B.1. Post-deposition target pictures and initial / final masses for both compressed, 7C PTFE powder targets and extruded PTFE targets used in the bulk of this study. Each target was used for a 2 hour, 50 W deposition and a 1 hour, 100 W deposition

Compressed Target #	1	2	3	4	5
Target (above)					
Target (profile)					
mass initial [g]	12.098	12.726	13.033	12.362	12.930
mass final [g]	10.153	10.298	11.266	10.681	11.341
mass loss [g]	-1.945	-2.428	-1.767	-1.681	-1.589
Extruded Target #	1	2	3	4	5
Target (above)					
Target (profile)					
mass initial [g]	13.007	12.557	13.060	11.927	11.992
mass final [g]	12.168	11.956	11.339	11.254	11.452
mass loss [g]	-0.839	-0.601	-1.721	-0.673	-0.540

As can be seen in the table, behavior of the extruded targets varies significantly compared to the compressed targets. There is a browning of the sputtering side of the extruded target, associated with de-fluorination of the target surface. As seen in the

profile pictures of the targets, significant bowing is observed in the extruded targets, away from the surface of the sputtering gun. There is also a difference in mass loss (proportional to the sputter yield) between the two target types, with the extruded targets losing less mass than the compressed targets. This difference in target mass loss is reflected in the difference between the deposition rates of films prepared from both targets, seen in Figure B.1. Additionally, all but one of the extruded targets exhibited a significant amount of warping during deposition. This warping is thought to be due to a heating up of the target during deposition, causing the detachment of the back surface of the target from the copper cooling mesh, further driving the warping of the target. The deposition rates for films produced at 50 W are similar between target types. It is possible that the warping mechanism for the extruded targets occurs only at higher temperatures, and, when occurring, negatively affects the deposition rate. This theory is supported by the results from extruded target #3, which did not undergo the warping experienced by the other targets. Mass loss (again, proportional to the sputtering yield) for this target was much higher than those of the other extruded targets, and was comparable to that of the compressed powder targets. The surface of extruded target #3 also lacks most of the browning seen in the other extruded targets.

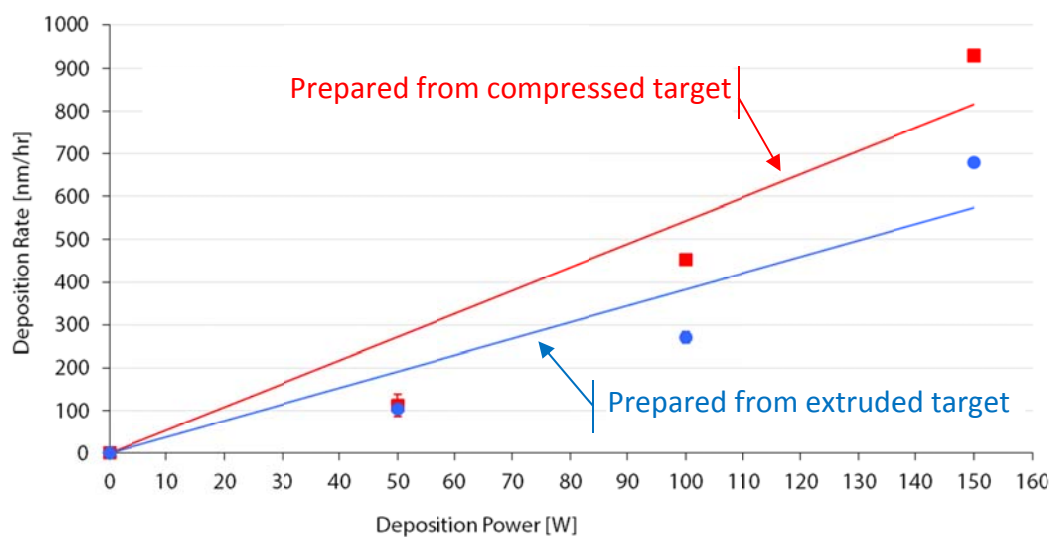


Figure B.1. Deposition rate vs. RF sputtering power for sputtered fluorocarbon films prepared from the compressed powder targets (red) and the extruded targets (blue). Deposition temperature for these films was 36°C. Linear regression fits shown for each set of data.

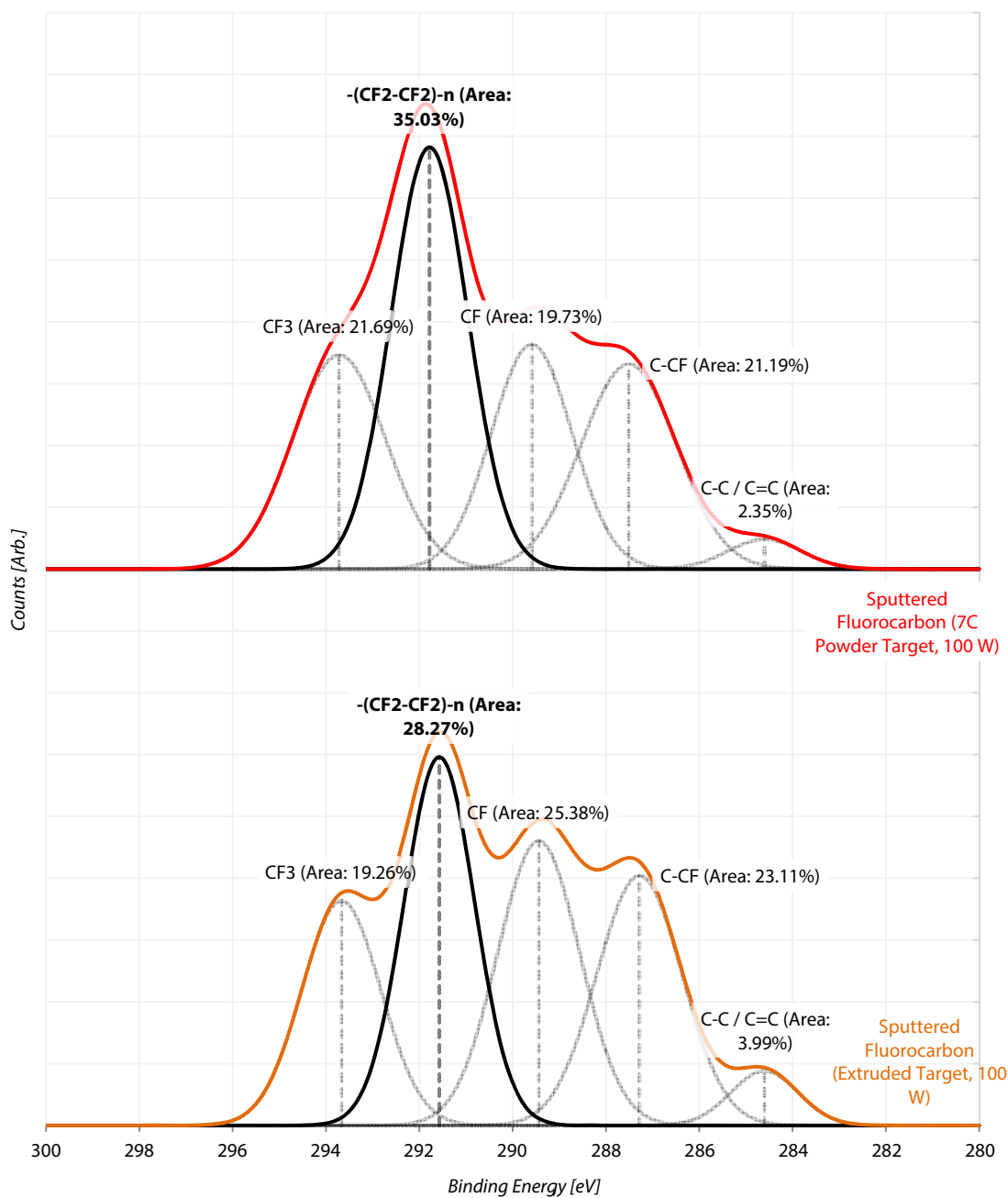


Figure B.2. XPS spectra of two films prepared under nominally identical depositions (100 W sputtering power, deposition temperature of 36 °C) using two different PTFE target sources: compressed powder (top), and extruded powder (bottom).

When examining results produced from XPS (Figure B.2 above), differences between films prepared from the two PTFE sources continue. There is an increase in Gaussian peak area associated with the $-\text{[CF}_2\text{-CF}_2\text{]}_n$ bond type when comparing across targets: 35.05% of the total C1s area for the compressed target film compared to only 28.27% of the total C1s area for the extruded target film. These differences in the structure and deposition rate of the films when changing PTFE are one example of how unreported differences in sputtering system setup can result in much larger differences in the resultant films.

Appendix C
PERMISSION LETTERS

C.1 Permission Letters

Table C.1. Permission letters obtained by the author for usage of select figures.

Supplier	Elsevier Limited, The Boulevard, Langford Lane, Kidlington, Oxford, OX5 1GB, UK
Registered Company Number	1982084
Customer Name	Philip Zandona
Customer Address	821 Carrie Ct, McLean, VA 22101
License Number	3435390919135
License Date	Jul 24, 2014
Licensed Content Publisher	Elsevier
Licensed Content Publication	Carbon
Licensed Content Title	Mechanical characterization of ultra-thin fluorocarbon films deposited by R.F. magnetron sputtering
Licensed Content Author	Guangze Tang, Xinxin Ma, Mingren Sun, Xiaodong Li
Licensed Content Date	2005
Licensed Content Volume Number	43

Licensed Content Issue Number	2
Number of Pages	6
Start Page	345
End Page	350
Type of Use	Reuse in a Thesis/Dissertation
Intended Publisher of New Work	Other
Portion	Figures/Tables/Illustrations
Number of Figures/Tables/Illustrations	1
Format	Both Print and Electronic
Are You The Author of This Elsevier Article?	No
Will You Be Translating?	No
Title of Thesis/Dissertation	The Effects of Changing Deposition Conditions on the Similarity of Sputter-Deposited Fluorocarbon Thin Films to Bulk PTFE
Expected Completion Date	Jul 2014
Number of Pages	112
Elsevier VAT Number	GB 494 6272 12

Supplier	Elsevier Limited, The Boulevard, Langford Lane, Kidlington, Oxford, OX5 1GB, UK
----------	--

Registered Company Number	1982084
---------------------------	---------

Customer Name	Philip Zandona
Customer Address	821 Carrie Ct, McLean, VA 22101
License Number	3435390419148
License Date	Jul 24, 2015
Licensed Content Publisher	Elsevier
Licensed Content Publication	Applied Surface Science
Licensed Content Title	The characterization of fluorocarbon films on NiTi alloy by
Licensed Content Author	L. Li,F.T. Zi,Y.F. Zheng
Licensed Content Date	15 November 2008
Licensed Content Volume Number	255
Licensed Content Issue Number	2
Number of Pages	3
Start Page	432
End Page	434
Type of Use	Reuse in a Thesis/Dissertation
Intended Publisher of New Work	Other
Portion	Figures/Tables/Illustrations
Number of Figures/Tables/Illustrations	1
Format	Both Print and Electronic

Are You The Author of This Elsevier Article?	No
Will You Be Translating?	No
Title of Thesis/Dissertation	The Effects of Changing Deposition Conditions on the Similarity of Sputter-Deposited Fluorocarbon Thin Films to Bulk PTFE
Expected Completion Date	Jul 2014
Number of Pages	112
Elsevier VAT Number	GB 494 6272 12
<hr/>	
Supplier	Elsevier Limited, The Boulevard, Langford Lane, Kidlington, Oxford, OX5 1GB, UK
Registered Company Number	1982084
Customer Name	Philip Zandona
Customer Address	821 Carrie Ct, McLean, VA 22101
License Number	3435391007163
License Date	Jul 24, 2016
Licensed Content Publisher	Elsevier
Licensed Content Publication	Applied Surface Science
Licensed Content Title	Characterization of a nanometer-thick sputtered polytetrafluoroethylene film
Licensed Content Author	Lei Li,Paul M. Jones,Yiao-Tee Hsia
Licensed Content Date	15 February 2011

Licensed Content Volume Number	257
Licensed Content Issue Number	9
Number of Pages	8
Start Page	4478
End Page	4485
Type of Use	Reuse in a Thesis/Dissertation
Intended Publisher of New Work	Other
Portion	Figures/Tables/Illustrations
Number of Figures/Tables/Illustrations	1
Format	Both Print and Electronic
Are You The Author of This Elsevier Article?	No
Will You Be Translating?	No
Title of Thesis/Dissertation	The Effects of Changing Deposition Conditions on the Similarity of Sputter-Deposited Fluorocarbon Thin Films to Bulk PTFE
Expected Completion Date	Jul 2014
Number of Pages	112
Elsevier VAT Number	GB 494 6272 12
<hr/>	
Supplier	Elsevier Limited, The Boulevard, Langford Lane, Kidlington, Oxford, OX5 1GB, UK

Registered Company Number	1982084
Customer Name	Philip Zandona
Customer Address	821 Carrie Ct, McLean, VA 22101
License Number	3435390261991
License Date	Jul 24, 2017
Licensed Content Publisher	Elsevier
Licensed Content Publication	Journal of Electrostatics
Licensed Content Title	Investigation of corona charge stability mechanisms in polytetrafluoroethylene (PTFE) teflon films after plasma treatment
Licensed Content Author	Qiang Chen
Licensed Content Date	July 2003
Licensed Content Volume Number	59
Licensed Content Issue Number	1
Number of Pages	11
Start Page	3
End Page	13
Type of Use	Reuse in a Thesis/Dissertation
Intended Publisher of New Work	Other
Portion	Figures/Tables/Illustrations
Number of Figures/Tables/Illustrations	1

Format	Both Print and Electronic
Are You The Author of This Elsevier Article?	No
Will You Be Translating?	No
Title of Thesis/Dissertation	The Effects of Changing Deposition Conditions on the Similarity of Sputter-Deposited Fluorocarbon Thin Films to Bulk PTFE
Expected Completion Date	Jul 2014
Number of Pages	112
Elsevier VAT Number	GB 494 6272 12

Supplier	Elsevier Limited, The Boulevard, Langford Lane, Kidlington, Oxford, OX5 1GB, UK
Registered Company Number	1982084
Customer Name	Philip Zandona
Customer Address	821 Carrie Ct, McLean, VA 22101
License Number	3435381124741
License Date	Jul 24, 2018
Licensed Content Publisher	Elsevier
Licensed Content Publication	Journal of Non-Crystalline Solids
Licensed Content Title	RF magnetron sputtering of polymers
Licensed Content Author	H. Biederman,P. Bílková,J. Ježek,P. Hlídaek,D. Slavínská

Licensed Content Date	2 September 1997
Licensed Content Volume Number	218
Licensed Content Issue Number	None
Number of Pages	6
Start Page	44
End Page	49
Type of Use	Reuse in a Thesis/Dissertation
Intended Publisher of New Work	Other
Portion	Figures/Tables/Illustrations
Number of Figures/Tables/Illustrations	1
Format	Both Print and Electronic
Are You The Author of This Elsevier Article?	No
Will You Be Translating?	No
Title of Thesis/Dissertation	The Effects of Changing Deposition Conditions on the Similarity of Sputter-Deposited Fluorocarbon Thin Films to Bulk PTFE
Expected Completion Date	Jul 2014
Number of Pages	112
Elsevier VAT Number	GB 494 6272 12

Supplier	Elsevier Limited, The Boulevard, Langford Lane, Kidlington, Oxford, OX5 1GB, UK
Registered Company Number	1982084
Customer Name	Philip Zandona
Customer Address	821 Carrie Ct, McLean, VA 22101
License Number	3435390768289
License Date	Jul 24, 2019
Licensed Content Publisher	Elsevier
Licensed Content Publication	Vacuum
Licensed Content Title	Plasma polymer films rf sputtered from PTFE under various argon pressures
Licensed Content Author	V. Stelmashuk,H. Biederman,D. Slavínská,J. Zemek,M. Trchová
Licensed Content Date	17 January 2005
Licensed Content Volume Number	77
Licensed Content Issue Number	2
Number of Pages	7
Start Page	131
End Page	137
Type of Use	Reuse in a Thesis/Dissertation
Intended Publisher of New Work	Other
Portion	Figures/Tables/Illustrations

Number of Figures/Tables/Illustrations	1
Format	Both Print and Electronic
Are You The Author of This Elsevier Article?	No
Will You Be Translating?	No
Title of Thesis/Dissertation	The Effects of Changing Deposition Conditions on the Similarity of Sputter-Deposited Fluorocarbon Thin Films to Bulk PTFE
Expected Completion Date	Jul 2014
Number of Pages	112
Elsevier VAT Number	GB 494 6272 12

Supplier	Elsevier Limited, The Boulevard, Langford Lane, Kidlington, Oxford, OX5 1GB, UK
Registered Company Number	1982084
Customer Name	Philip Zandona
Customer Address	821 Carrie Ct, McLean, VA 22101
License Number	3435390677582
License Date	Jul 24, 2020
Licensed Content Publisher	Elsevier
Licensed Content Publication	Applied Surface Science
Licensed Content Title	Deposition of PTFE thin films by RF plasma sputtering on <1 0 0> silicon substrates

Licensed Content Author	Dhananjay S. Bodas,A.B. Mandale,S.A. Gangal
Licensed Content Date	30 May 2005
Licensed Content Volume Number	245
Licensed Content Issue Number	1-4
Number of Pages	6
Start Page	202
End Page	207
Type of Use	Reuse in a Thesis/Dissertation
Intended Publisher of New Work	Other
Portion	Figures/Tables/Illustrations
Number of Figures/Tables/Illustrations	1
Format	Both Print and Electronic
Are You The Author of This Elsevier Article?	No
Will You Be Translating?	No
Title of Thesis/Dissertation	The Effects of Changing Deposition Conditions on the Similarity of Sputter-Deposited Fluorocarbon Thin Films to Bulk PTFE
Expected Completion Date	Jul 2014
Number of Pages	112
Elsevier VAT Number	GB 494 6272 12

Supplier	Elsevier Limited, The Boulevard, Langford Lane, Kidlington, Oxford, OX5 1GB, UK
Registered Company Number	1982084
Customer Name	Philip Zandona
Customer Address	821 Carrie Ct, McLean, VA 22101
License Number	3435391091623
License Date	Jul 24, 2021
Licensed Content Publisher	Elsevier
Licensed Content Publication	Vacuum
Licensed Content Title	Effects of substrate temperature on structure and mechanical properties of sputter deposited fluorocarbon thin films
Licensed Content Author	Yuta Suzuki,Haojie Fu,Yoshio Abe,Midori Kawamura
Licensed Content Date	January 2013
Licensed Content Volume Number	87
Licensed Content Issue Number	None
Number of Pages	4
Start Page	218
End Page	221
Type of Use	Reuse in a Thesis/Dissertation

Intended Publisher of New Work	Other
Portion	Figures/Tables/Illustrations
Number of Figures/Tables/Illustrations	1
Format	Both Print and Electronic
Are You The Author of This Elsevier Article?	No
Will You Be Translating?	No
Title of Thesis/Dissertation	The Effects of Changing Deposition Conditions on the Similarity of Sputter-Deposited Fluorocarbon Thin Films to Bulk PTFE
Expected Completion Date	Jul 2014
Number of Pages	112
Elsevier VAT Number	GB 494 6272 12
